
Flooding at Fort Simpson, afternoon of 14 May 2021 (Kevin Corrigan).


Liard River (NHC 2024 Survey)


Mackenzie River (NHC 2024 Survey)

Fort Simpson Flood Hazard Mapping Study

Summary Report

Prepared by:

Northwest Hydraulic Consultants Ltd.
9819 – 12 Avenue SW
Edmonton, AB T6X 0E3
Tel: 780.436.5868
www.nhcwater.com

Prepared for:

Government of Northwest Territories
Environment and Climate Change
Yellowknife, NT X1A 2L9

May 18, 2025
Summary Report

NHC Reference No. 1008469

Report prepared by:

2025-05-23

Dan Healy, PhD, PEng
Principal

Kevin Emmelkamp
Engineer-in-Training

Report reviewed by:

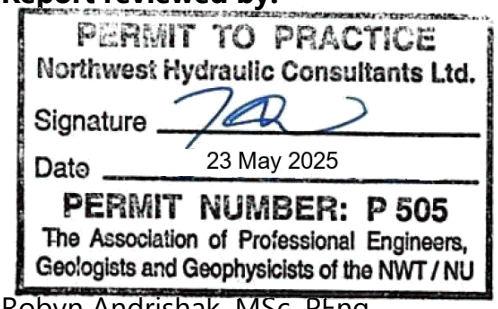

Robyn Andrishak, MSc, PEng
Principal
Branch Manager

DISCLAIMER

This report has been prepared by Northwest Hydraulic Consultants Ltd. for the benefit of Government of Northwest Territories for specific application to the Fort Simpson Flood Hazard Mapping Study. The information and data contained herein represent **Northwest Hydraulic Consultants Ltd.'s** professional judgment in light of the knowledge and information available to **Northwest Hydraulic Consultants Ltd.** at the time of preparation and were prepared in accordance with generally accepted engineering and geoscience practices.

Except as required by law, this report and the information and data contained herein are to be treated as confidential and may be used and relied upon only by Government of Northwest Territories, its officers, and employees. **Northwest Hydraulic Consultants Ltd.** denies any liability whatsoever to other parties who may obtain access to this report for any injury, loss, or damage suffered by such parties arising from their use of or reliance upon this report or any of its contents.

CREDITS AND ACKNOWLEDGEMENTS

The authors would like to thank the Government of Northwest Territories for initiating this study as well as the Government of Canada for funding through the Flood Hazard Identification and Mapping Program.

The following agencies were key contributors of information supporting this work.

- Government of Northwest Territories (GNWT)
- Natural Resources Canada (NRCan)
- Environment and Climate Change Canada (ECCC)
- Water Survey of Canada, ECCC (WSC)
- Village of Fort Simpson (Fort Simpson)

We are grateful for the support provided during the project, in particular:

- Anna Coles – GNWT
- Ryan Connon – GNWT
- Michèle Culhane – GNWT
- Melanie Desjardins – GNWT
- Christy Fung – GNWT
- Shawne Kokelj – GNWT
- Kyle Little – GNWT
- Jad Saade – GNWT
- Brian Perry – NRCan
- Sarah Karam - NRCan
- Marcena Croizier – WSC
- Joshua Wiebe – ECCC
- Apurba Das - ECCC
- Mitchell Gast – Fort Simpson
- Roger Pilling – WSC (retired) / Fort Simpson
- Tyler Pilling – Fort Simpson

The primary author of this report was Dan Healy of Northwest Hydraulic Consultants. Kevin Emmelkamp provided significant contributions to report writing and figures. Mariza Costa-Cabral provided expert review and most of the documentation pertaining to climate change assessment.

TABLE OF CONTENTS

TABLES

FIGURES

APPENDICES

1 INTRODUCTION

1.1 Project Overview

Northwest Hydraulic Consultants Ltd. (NHC) was retained by the Government of the Northwest Territories (GNWT) Department of Environment and Climate Change to develop flood hazard maps for the communities of Hay River, K'atl'odeeche First Nation, Fort Simpson, and Aklavik. This project was funded in part by Natural Resource Canada's Flood Hazard Identification and Mapping Program (FHIMP) with additional support from the GNWT. The intended use of these flood hazard maps is for community infrastructure planning and other flood mitigation measures, and emergency preparedness, in particular, community planning.

This report provides the results of the flood hazard mapping study for Fort Simpson and includes the following: a summary of the data collection and review; results of the 2024 river cross section survey; ice jam flood hydrology; hydraulic modelling; and, the development of flood inundation and flood hazard maps. Potential impacts of climate change are also discussed.

1.2 Study Area

The village of Fort Simpson is located directly downstream of the confluence of the Liard River with the Mackenzie River, approximately 400 km west of Yellowknife (**Figure 1**). The Liard River drains an area of approximately 275,000 km^2 and is one of the largest tributaries to the Mackenzie River. The headwaters of the Liard River are in the Yukon, and the river flows southeast into northern British Columbina and then follows a north-easterly path into the Northwest Territories.

The Village of Fort Simpson (**Figure 2**) is situated predominantly on an alluvial island along the left (southwest) bank of the Mackenzie River. The island measures approximately 4 km in length and 1 km in width. The island is connected to the mainland by a causeway located at the upstream (southeast) end. This causeway disconnects flow through the back channel (commonly referred to as the *Snye*) along the southwest side of the island. Much of the community resides along the east side of the island next to the main stem of the Mackenzie River.

1.3 Study Basin

The study basin is comprised of the Mackenzie River basin above the Liard River confluence and Liard River basin, as depicted on **Figure 1**. Flows reporting to the study area from the Mackenzie River include outflows from Great Slave Lake and tributary inflows between the lake and confluence with the Liard River, including: the Kakisa River (outflows from Kakisa Lake), Trout River, Jean Marie River, Horn River, and Rabbitskin River. Flows reporting to the study area on the Liard River include runoff from the entirety of the Liard River basin. The Liard River drains

about 21% (275,000 km^2) of the total area draining to the study site (1,300,000 km^2). The Liard River is the largest tributary below Great Slave Lake. The incremental increase in flows at spring breakup are mostly attributed to the Liard River.

Total inflows reporting to the Mackenzie River, upstream of the Liard River, are recorded at the Water Survey of Canada (WSC) gauge near Strong Point (10FB006). Inflows on the Liard River study reach are recorded at the WSC gauge located at the Liard River ferry crossing (10ED002). The combined Mackenzie River and Liard River flows are recorded at the WSC gauge at Fort Simpson (10GC001). The locations of these gauges are depicted on **Figure 2**.

2 DATA COLLECTION AND REVIEW

The following describes the relevant information and data sets collected and reviewed during this study. Much of the information and data were used to support understanding of the river ice regime, document the flood history, and inform our methodology for estimating ice jam flood frequencies. Available geospatial data and historical flood elevation data were used to inform planning of our cross section survey program, and the surveyed data were used to develop the hydraulic model.

2.1 Studies, Reports, and Accounts Specific to Study Site

Relevant studies, reports, and accounts, specific to the study site, are listed below (chronologically). Items are annotated with a description of information relevant to the study. These documents informed our understanding of the river ice regime and flood history. Some of the documents provide historical flood information and data that will be used for model calibration.

1974. Fort Simpson Water Intake Mackenzie River. Northwest Hydraulic Consultants Ltd.

- Historic river cross section survey data in the vicinity of the confluence.
- Description of bed material, overview of hydrology and river ice.
- Ice jam highwater level, reported as El. 418 feet (datum or highwater date unknown).

1976. River Bed Investigation Fort Simpson Water Intake and Sewerage Outfall. Northwest Hydraulic Consultants Ltd.

- Historic river cross section survey data on Mackenzie River along the Village for Fort Simpson.
- Borehole data.

1981. Mackenzie River Basin Study Report. Mackenzie River Basin Committee.

- Basin spring breakup regime summary for the Liard River and Mackenzie River basins.

1982. Liard and Mackenzie River Ice Break-up, Fort Simpson region, NWT, 1982. Anderson, J.C.

- 1982 local ice jam breakup chronology (characterized as "typical"), with river ice characterization maps.
- Description of Liard River basin breakup.
- Ice thickness data.
- Historic river station convention (in kilometers).

1983. Historical Flood Review: Fort Simpson, Fort Norman, Fort Good Hope, Fort McPherson, Aklavik, Fort Liard, Nahanni Butte. Kriwoken, L.A.

- Suggests key factors contributing to ice jam floods are
    - (1) the sudden release of ice runs from the Liard into a stable Mackenzie ice cover,
    - (2) constrictions to the passage of ice on the Mackenzie River (shoals on left bank just downstream of Fort Simpson and
    - (3) abrupt bend about 19 km downstream of Fort Simpson).
- Documents historic flood levels (including estimates of flood magnitudes from Hudson Bay records and long-term resident recollections)
- 1963 peak flood level estimates.

1984. Liard and Mackenzie River Ice Break-up, Fort Simpson Region, NWT, 1983. Prowse, T.D.

- 1983 local ice jam breakup chronology (a significant event), with river ice characterization maps.
- Overview of general river ice breakup conditions in the Liard River and Mackenzie River basins.
- Analytical assessment of breakup conditions including flow assessments and potential ice jam locations.
- Historical breakup data review.
- Climate information review.

1985. Hydrometeorologic Conditions Prevailing During the 1984 River Ice Breakup, Fort Simpson Region. Prowse, T.D.

- 1984 breakup chronology of the Liard River and Mackenzie River near Fort Simpson (breakup was uneventful).

1986. Ice Jam Characteristics, Liard-Mackenzie rivers confluence. Prowse, T.D.

- Descriptions of typical breakup chronology and river ice regime.
- Summary of climate and breakup flood level data (1978 to 1984).
- Breakup "type" classification.

1992. An Historic NWT Flood: 1988 Flooding in the Liard and Mackenzie River Basins. Jasper, J.N. and Kerr, J.A.

- Documents a major open water flood which may provide context for ice jam flooding severity.

2019. Application of a Hydrologic Model for Predicting River Ice Breakup. Brown, G.

- Descriptions of basin ice regime.
- Describes hydrological model calibration for the Liard River basin.
- Limited information on historic breakup floods at Fort Simpson.
- Summaries from Canadian River Ice Database (CRID) and WSC hydrometric database (HYDAT).
- Characterization of breakup type or severity.

2020. NWT Flood Events. Coles, A.

- Summary information on ice jam flooding for nine communities in Northwest Territories including Hay River, Fort Simpson, and Aklavik. With reference to site specific ice jam chronology, extent, and classification.

2020. Flood Maps of the Northwest Territories. Coles, A.

- History of the existing Flood Damage Reduction Program maps.
- Provides flood levels and sources for major historic floods.

2.2 Hydrometric Data

2.2.1 National Water Data Archive

Hydrometric data were extracted from National Water Data Archive HYDAT database (Version 1.0 April 16, 2024) for WSC stations 10GC001 Mackenzie River at Fort Simpson, 10ED002 Liard River near the mouth, and 10FB006 Mackenzie River at Strong Point. The HYDAT data includes annual maxima and daily data. The daily data was supplemented with continuous unpublished data (e.g. 15-minute to 1-hour interval) provided by WSC staff during this project. **Table 1** lists the WSC hydrometric stations for which HYDAT data collected and reviewed for this study. The

period of record for which flow and level is available is also listed. Locations of these stations are depicted on **Figure 2**.

Table 1 WSC Hydrometric Stations

Station ID	Station Name	Period of Record
10FB006	MACKENZIE RIVER AT STRONG POINT	Flow: 1991 – 2021 [31 years] Level: 2002 – 2021 [20 years]
10GC001	MACKENZIE RIVER AT FORT SIMPSON	Flow: 1938 – 2021 [84 years] Level: 2001 – 2021 [21 years]
10ED002	LIARD RIVER NEAR THE MOUTH	Flow: 1972 – 2021 [50 years] Level: 2002 – 2021 [20 years]

Supplementary Hydrometric Data

Water level is the parameter of primary interest for estimation of ice jam flood level frequencies. As the published record of water level data is limited, additional data were acquired. Unpublished, hydrometric data was provided by GNWT staff for the gauges listed in **Table 2**. These data included continuous, uncorrected, flow and level data. These data were used to supplement the published data from the HYDAT database. Daily data provide estimates of the average flows over a 24-hour period. Continuous level data (5 and 15 minute frequency) provide a time series of discrete point measurements – each with an associated time stamp.

Table 2 Supplementary Hydrometric Data

ID	Data Description	Period of Record
10FB006 MACKENZIE RIVER AT STRONG POINT		
	Preliminary WSC Data Unpublished Daily Level Unpublished Continuous Level	Flow: 2022– 2023 Level: 2021 – 2023 Daily Level: 1991 – 2001 15-min Level: 2000 – 2010 15-min Level: 2011 – 2020 5-min Level: 2021 – 2022
10GC001 MACKENZIE RIVER AT FORT SIMPSON		
	Preliminary WSC Data Unpublished Daily Level Unpublished Continuous Level	Flow: 2022– 2023 Level: 2021 – 2023 Daily Level: 1976 – 1995 15-min Level: 1996 – 2010 15-min Level: 2011 – 2020 5-min Level: 2021 – 2023
10ED002 LIARD RIVER NEAR THE MOUTH		
	Preliminary WSC Data	Flow: 2022– 2023

		Level: 2021 – 2023 Daily Level: 1976 – 1995 15-min Level: 1996 – 2010 15-min Level: 2011 – 2020 5-min Level: 2021 – 2022

Canadian River Ice Database

The Canadian River Ice Database (CRID) was initiated by the Water Science and Technology Directorate of Environment and Climate Change Canada as a *long-term effort to compile, archive and extract river ice related information from hydrometric records*. The information was accessed online (Canadian River Ice Database - ECCC Data Catalogue). The program and data are detailed by de Rham et. al (2020). Additional supporting information relating to the program was made available during this study by University of Alberta researcher, Jennifer Nafziger. Supplementary breakup water level data was available in the CRID datasets for WSC Stations 10GC001 Mackenze River at Fort Simpson, and 10ED002 Liard River near the Mouth. Station 10FB006 Mackenzie River at Strong Point is not included in the CRID dataset. This data set provided valuable information on break dates and the associated peak flood level and discharge at these gauge sites. **Table 3** provides a summary of the available CRID data used in this study.

Table 3 Available CRID Data Used for Study

ID	Data Description	Period of Record
10GC001 MACKENZIE RIVER AT FORT SIMPSON		
	Peak Breakup Datetime Peak Breakup Water Level Peak Breakup Discharge	1972-2015 1963, 1967, 1971-2015 1972-2015
10ED002 LIARD RIVER NEAR THE MOUTH		
	Peak Breakup Datetime Peak Breakup Water Level Peak Breakup Discharge	1974-1976, 1978-1980, 1982-1997, 1999-2015 1974-1976, 1978-1980, 1982-2015 1974-1976, 1978-1980, 1982-1997, 1999-2015

2.2.2 Other Project Specific Data

The following provides a brief description of other project specific data received from GNWT, including hydrometric and river ice data.

Peak Stage Data for Mackenzie River at Fort Simpson

Listing of peak stage measurements collected at the Mackenzie River at Fort Simpson WSC gauge (10GC001) with corresponding date and approximate time. Notes describing additional information are included. Additionally, a word file is provided which contains analysis by Roger Pilling (WSC) of highwater marks from Fort Simpson's flood of 1963.

10GC001 (Mackenzie River at Fort Simpson) Stage Data

Unpublished daily stage measurements collected at the WSC gauge ranging from copies of original records from 1938 through to preliminary data for 2022. These data are valuable because published WSC data is only available from 2002 onward.

10ED002 (Liard River near the Mouth) Stage Data

Unpublished daily stage measurements collected at the WSC gauge ranging from copies of original records from 1972 through to preliminary data for 2022. These data are valuable because published WSC data is only available from 2002 onward.

10FB006 (Mackenzie River at Strong Point) Stage Data

Unpublished daily stage measurements collected at the WSC gauge between 1991 through to preliminary data for 2022. These data are valuable because published WSC data is only available from 2002 onward.

Fort Simpson 2021 ENR Spring Breakup Reports (Dehcho Report). Environment and Natural Resources, GNWT.

Daily breakup monitoring reports including breakup description, sequence of events, provisional water level data and photographs at select hydrometric gauges.

2022 River Ice Classification Data

Collection of river ice classification products from May 2022 classified by C-CORE for the GNWT.

2021 and 2020 Ice Classification Data

Collection of river ice classification products from April, May, and June of 2021 and 2022 obtained by the GOC and classified by NRCan.

2.3 Geospatial Data

Various geospatial data was collected in support of model development and flood mapping. The following includes a description of the geospatial data received from GNWT in support of this study.

Base Data

Information accessed through the GNWT's ATLAS interactive web-based mapping service to support reporting maps and flood hazard mapping, including road network, hydrography, and administrative boundaries.

DTM data

The most recent 1 m resolution bare-earth DTM data for Fort Simpson was developed from LiDAR obtained by McElhanney Ltd. on July 14, 2020.

Coarse DEM data with 30 m point resolution was obtained from Northwest Territories Centre for Geomatics.

Water body data

Waterbody data available in shapefile format delineated as part of the National Hydro Network (NHN) depicting spatial extent of various water bodies within the study area.

Orthophotos

The most recent orthorectified imagery (20 cm) for Fort Simpson were collected by McElhanney Ltd. on July 14, 2020, and received as georeferenced tiff files and in ECW format.

Previous (existing) flood mapping (1984)

Scans of the existing 1:10,000 scale flood map and 1:2,000 scale flood maps for Fort Simpson (1984) were provided by GNWT. These provided reference information for flood hazard mapping updates.

2.4 Field Data

The following includes a description of the local hydrometric gauge stations and field data received from GNWT for Fort Simpson as part of the study. These documents are briefly described below and included in the database provided with this case study.

Station Descriptions

Detailed description of the location of the WSC gauge station which includes control benchmark elevations as well as accompanying maps, sketches, and photos for stations: 10GC001 Mackenzie River at Fort Simpson, 10ED002 Liard River near the Mouth; and 10FB006 Mackenzie River at Strong Point.

Fort Simpson 2021 Highwater Marks

Ollerhead and Associates Ltd. surveyed eight HWMs identified by silt markings left on structures and witness testimony. This data is documented in a report with accompanying raw data files.

Fort Simpson Hydrometric Gauge Photos

Timelapse photo series taken during the 2021 breakup at WSC gauge stations 10GC001 Mackenzie River at Fort Simpson and 10ED002 Liard River near the Mouth.

Fort Simpson 2021 Flood Photography

Photos taken from within an aircraft during the 2021 flooding event by local filmmaker Jonathan Antoine.

Photos taken from within an aircraft at approximately the peak of the flood event on May 14, 2021 (15:12 – 15:19 MST) and provided by Kevin Corrigan, Senior Administrative Officer of Fort Simpson. Also included are photos collected at the WSC hydrometric gauge station 10GC001 (Mackenzie River at Fort Simpson) on the same date and around the same time (15:16 and 16:15 MST).

2.5 Previous Flood Mapping

The highwater mark information collected by Kriwoken (1983) was used to produce FDRP flood maps for Fort Simpson. Consideration was made for the flood events that occurred in 1857 and 1963 which corresponded to flood levels of 126.1 m and 127.5 m, respectively. Discussion of an intermediate design level of 127.0 m was held with the Fort Simpson village council and later approved by government officials responsible for overseeing the mapping effort (Coles, 2020a). The resulting flood maps for Fort Simpson were designated in June 1985, under the FDRP. Electronic geospatial files (ESRI shapefile format) delineating floodway and flood fringe extents for these FDRP maps were provided by GNWT.

3 FIELD SURVEY

The survey program was completed between June 6th and 11th, 2024. The objective was to survey channel cross sections along the study reaches to support the development of a hydraulic model, capable of simulating both open water and ice jam flood scenarios. The following summarizes the field survey work and methodology employed to collect the data.

3.1 Survey Procedures and Methodology

Ground positioning for the survey was measured using Global Navigation Satellite Systems (GNSS) and Trimble R10 and R12 Real Time Kinetic (RTK) GNSS receivers. Bathymetric surveys were performed in water areas typically deeper than 0.3 meters, using a CeeEcho echo sounder mounted on a jet boat to measure water depth under the transducer. The position and height of the transducer were recorded with the RTK GNSS receiver mounted directly above it and paired through the Hypack software. Riverbed elevations were derived by subtracting sounding depths

from the transducer elevations. In shallower, wadable areas, elevations were obtained directly with the RTK GNSS receiver attached to a survey rod. The surveyed cross sections included the riverbanks and extended into the floodplain, overlapping with the DTM provided by GNWT.

3.1.1 Coordinate System and Datum

Horizontal positions were referenced to the Universal Transverse Mercator (UTM) Zone 10N projection. The UTM 10N projection is part of the Canadian Spatial Reference System (CSRS) North American Datum of 1983 (NAD83). Orthometric heights are based on the Canadian Geodetic Vertical Datum of 2013 (CGVD2013a) in the NAD83 CSRS reference system, Canadian Gravimetric Geoid Model of 2013 – Version A (CGG2013a), and the 2010.0 epoch.

3.1.2 Control Network

A control point network was established from local available WSC benchmarks and GNSS surveying to provide a spatial reference for the survey program. Two WSC benchmarks, and four NHC project survey control points were tied into the survey. A list of the control point coordinates is provided in **Table 4**.

Table 4 Control point summary

Name	Type	Easting (m)	Northing (m)	Elevation (m)	Measurement Type
NHC 1	Project Control Point	591,957.123	6,851,086.957	165.524	Long term static measurement with PPP (+4 hours).
NHC 2		592,951.148	6,858,915.438	118.149	
NHC 3		584,410.89	6,861,482.511	118.035	
NHC 4		573,383.095	6,867,924.423	122.366	
NHC 5		593,656.893	6,846,842.673	128.587	Shorter term, 30 to 300 second, RTK observation.
NT00-204	WSC Benchmark	593,595.705	6,846,791.259	132.895	
NT04-224		586,328.266	6,860,611.225	123.176	

Coordinates for four of the NHC control points (NHC 1 through NHC 4) were determined by running the GNSS receivers simultaneously in static mode for over fours at each of the four control points. This enabled high accuracy precise point positioning (PPP) results from the CSRS for these control points. The data were then post-processed using Trimble Business Center software to adjust the network by establishing baselines between these control points.

A free adjustment of the base control network was completed, and the error from the adjustment was distributed equally throughout the network. The horizontal and vertical errors at the four control points, after post-processing and adjustment to the reference CSRS-PPP values, are summarized in **Table 5**. The largest horizontal error was 0.0023 m, and the largest vertical error was 0.0048 m.

Table 5 Control network errors

Control Point	Horizontal		Vertical
	Easting (m)	Northing (m)	Elevation (m)
NHC 1	0.0014	0.0021	0.0043
NHC 2	0.0014	0.0022	0.0045
NHC 3	0.0011	0.0016	0.0033
NHC 4	0.0016	0.0023	0.0048

A comparison between the surveyed elevations (after post-processing and adjustment) and benchmark elevations (provided by WSC staff) are listed in **Table 6.** Comparisons are limited to elevations since horizontal coordinates were not available for WSC benchmarks.

Table 6 Comparison between surveyed and published WSC benchmark elevations

Name	Description	Elevation Difference in m (Surveyed Minus Published)
NT00-204	WSC 10ED002 Gauge Benchmark	2.657
NT04-224	WSC 10GC001 Gauge Benchmark	-0.911

The differences between surveyed and published elevations are significant and, unfortunately, no information was found to reconcile or explain the differences. Based on discussions with WSC staff, it was determined that the WSC published benchmark elevations (and corresponding datum conversions) were not reliably accurate. For this investigation, a project-specific datum conversion was used to convert water levels published at WSC gauge locations into the NHC survey datum. This conversion was taken as the difference between surveyed water elevation at the gauge sites and gauge height published by WSC at the time of the surveyed water levels. The project-specific datum conversions are summarized in **Table 7**.

Table 7 Project-specific gauge datum conversions

Gauge ID	Gauge Name	Survey Date and Time	Surveyed Elevation (m)			Published Gauge Height (m)	Datum Conversion (m)
			Left Bank	Right Bank	Average Elevation		
10ED002	LIARD RIVER NEAR THE MOUTH	June 8, 2024 16:41 to 16:52	118.517	118.541	118.529	3.729	114.800
10GC001	MACKENZIE RIVER AT FORT SIMPSON	June 7, 2024 13:46 to 13:58	114.538	114.492	115.038	4.892	109.623

3.2 Survey Accuracy and Error

The Trimble RTK GNSS receivers used in the survey are capable of accuracies of ±0.02 meters under optimal conditions, such as a stable mounting (e.g. tripod) with a clear view of the sky, clear communication with enough satellites, and long sample time over a static location. Under normal field conditions errors are introduced when the receiver is off-level or obstructed by trees and vegetation. Operator errors can be introduced such as an incorrectly entered receiver height (an error that can be corrected during data post processing). Much of the ground-based surveyed data was collected under favourable conditions, with good satellite coverage, and errors were expected to be about ±0.05 meters. Larger errors were experienced on a few occasions where satellite coverage was poor, such as, in dense vegetation or alongside very high steep banks. The digital echo sounder used for the boat-based surveys can achieve accuracies of ±0.01 meters under optimal conditions. The dominant source of error was due to pitch and roll of the boat during data collection. Errors associated with depth sounding was expected to be about 0.07 meters. Considering the various sources and range of possible accuracy errors of the surveyed elevation data was about 0.10 m to 0.15 m.

3.3 Digital Terrain Model

For this study, NHC acquired a hydro-flattened 1m-grid Digital Terrain Model (DTM), along with the corresponding LAS files, from GNWT. The data was constructed from airborne LiDAR data gathered by McElhanney (2020) in July 2020. The mean point density of these data is 17 pts/m^2 with variation depending on the canopy closure, understory density, and topographic features.

Elevations extracted from the DTM were compared with selected ground survey points collected by NHC on roads and other dry ground areas. A summary of the comparison is shown in **Table 8**. Ground survey point elevations were slightly lower than the elevations extracted from the DTM and the average difference was less than 0.10 m. The differences are small, and therefore, elevations of the project LiDAR DTM (provided by GNWT) was in a good agreement with NHC-surveyed ground elevations.

Table 8 Comparison between LiDAR DTM and surveyed LiDAR check points

Name	Point Description	Easting (m)	Northing (m)	NHC Survey Elevation (m)	DTM Elevation (m)	Surveyed minus DTM (m)
1000	LiDAR Check	588,868.883	6,851,997.973	167.900	167.930	-0.030
1001	LiDAR Check	593,808.087	6,849,009.956	167.829	167.938	-0.109
1002	LiDAR Check	593,507.266	6,846,842.934	132.916	133.047	-0.133
1003	LiDAR Check	590,497.228	6,854,199.824	128.377	128.484	-0.107
1004	LiDAR Check	588,949.197	6,856,330.482	135.522	135.632	-0.110

3.3.1 Supplementary Terrain Data

The survey conducted by NHC for the Mackenzie River extended significantly downstream from the project's DTM to accurately capture the geometry of a known ice jam initiation location that is important to the study area.. For areas beyond the scope of the project DTM, the publicly available ArcticDEM Digital Surface Model (DSM) was utilized. The ArcticDEM DSM is a 2-meter full-feature surface model created from thousands of individual elevation models and satellite images (University of Minnesota 2024). It is a full feature dataset that provides elevations of the features other than terrain, such as trees and buildings. Therefore, it is not suitable for flood mapping that requires terrain elevations. However, it proved useful in extrapolating survey data into the overbank areas of the downstream reaches, extending well beyond the flood mapping study's domain.

3.4 Orthophoto (Aerial Photograph)

Orthophotos were provided by GNWT for this project, which were acquired for GNWT by McElhanney in 2020.

3.5 Cross Section Data

Cross section locations were selected to ensure adequate representation of the channel geometry to be used in the hydraulic model. The alignments were identified by desktop analysis with the available DTM and Orthophotos. Some adjustments were made based on the conditions observed in the field during the survey. All cross sections were surveyed between June 6 and 10, 2024. A summary of the surveyed cross sections in the study reaches is provided in **Table 9**.

Table 9 Cross section survey summary

River	Number of Cross Sections	Average Spacing (m)	Minimum Spacing (m)	Maximum Spacing (m)
Mackenzie	34	1,062	577	1,825
Liard	17	996	555	1,203

A total of 51 cross sections were surveyed to provide geometry for the hydraulic model – 34 along the Mackenzie River and 17 along the Liard River. Locations of survey sections are provided in a subsequent section. The survey extended approximately 16 km beyond the study area to capture an area of the Mackenzie River where ice jamming is known to occur. Additionally, this extension, may help reduce uncertainties in the hydraulic modeling results that could arise from downstream boundary condition parameters. Each cross section was identified by reach and river station (RS), where RS corresponds to the streamwise distance from the most

downstream cross section on the Mackenzie River and the location of the estimated confluence with the Liard River. The river stationing also corresponds to cross section distances in the hydraulic model.

Cross section locations were selected to ensure adequate representation of the channel geometry in the hydraulic model. Cross sections were positioned to capture changes in channel pattern, widths, and slopes. Additional cross sections were placed at the upstream and downstream faces of bridges, inlet and outlet of culverts, and a few river widths upstream and downstream of the structures. The additional sections at hydraulic structures followed the geometry requirements for modelling bridges and culverts as recommended in the HEC-RAS documentation.

The survey data was provided electronically in an ESRI-formatted geodatabase file (**Appendix A**).

3.6 Additional Data

There was no hydraulic structure (e.g., bridge) or flood control structure (e.g., dike) within the study reach.

Additional data collected during the field survey included water level measurements, taking site photographs, and survey of existing benchmarks (northing, easting, elevation).

3.6.1 Water Level Measurements

NHC has surveyed water levels at each cross section on both the left and right banks. This provided a surveyed water surface elevation profile, which will aid in the calibration of the open water model. The surveyed water levels at the gauge locations were also used to estimate datum conversions at the gauge sites of the Liard River (10ED002) and the Mackenzie River (10GC001).

3.6.2 Site Photographs

Representative photographs of the reaches were captured during the site inspection and survey are included. Selected photos with annotations are provided in **Appendix B**. A complete set of site photographs, in their native image file format, has been submitted as separate digital files.

3.6.3 Existing Benchmarks

Existing benchmarks were surveyed at both WSC gauging stations, identified as 10ED002 and 10GC001, for comparison with published elevation data. The results of the comparisons are listed in **Table 3** and **Table 5**, respectively. Additionally, NHC surveyed an iron pin near the Liard River WSC Gauge (10ED002) which was later discovered to have been surveyed previously by Ollerhead and Associates (2021). Both surveys utilized the UTM Zone 10N CSRS NAD83

projection system with the vertical datum of CGVD2013a. Very small differences were observed between the values reported by Ollerhead and Associates and those from the NHC survey as indicated in **Table 10**.

Table 10 Ollerhead and Associates and NHC surveys of the Iron Bar near WSC Gauge 10ED002

Survey	Northing (m)	Easting (m)	Elevation (m)
Ollerhead and Associates (2021)	6,846,783.336	593,624.183	129.87
NHC (2024)	6,846,783.348	593,624.146	129.798
Difference	-0.012	0.037	0.072

4 FLOOD HYDROLOGY

4.1 Flood History

Floods experienced by the village have historically occurred during spring breakup. Often, the Liard River breaks before the Mackenzie River at the confluence, where broken ice arriving from the Liard is arrested by intact ice in the Mackenzie River. A jam typically forms in the lower reach of the Liard as the ice collects, consolidates and shoves into and breaks up the Mackenzie River. As ice continues to run from the Liard into the Mackenzie River, the running ice can slow and consolidate to form a jam alongside the village and flood the community. Severe flooding occurred in this manner during the recent 2021 ice jam flood which resulted in the shut down of the local power plant and evacuation of some 700 people.

Flooding in Fort Simpson is dominated by ice jam floods during breakup. **Table 11** contains a list of the documented flooding events experienced throughout the Fort Simpson area resulting from an ice jam occurring during breakup in May. Context is provided about the impact of each flood event on the surrounding area, along with a list of reference documents. Kriwoken (1983) provides information from Hudson's Bay Company (HBC) archives and Royal Canadian Mounted Police (RCMP) records about ice jam flood events since 1828. The levels reported in Kriwoken's historical flood review are reported as a range of possible maximum flood levels. Most of the historic elevations were estimated from the authors' estimates on elevations of island terrace features as indicated on **Figure 3**.

Table 11 Documented flood events resulting from ice jams during breakup: 1828 – 2021

Year	Description	Estimated Flood Level[1]	Reference
1828	Ice jam downstream; Lower part of island inundated	124 – 125 m	Kriwoken (1983)
1830	Liard ice impeded by intact Mackenzie ice; Lower part of island inundated	124 – 125 m	Kriwoken (1983)
1832	Ice jam downstream; Lower part of island inundated	124 – 125 m	Kriwoken (1983)
1855	Ice jam downstream; Most parts of island inundated	126 – 127 m	Kriwoken (1983)
1857	Ice jam at mouth of Liard; Entire island inundated, except for the ridge on which the Fort stands; maximum flood level is delineated by upper terrace	127-127.5 m	Kriwoken (1983)
1875	Sudden breakup; Half of island inundated	126 – 127 m	Kriwoken (1983)
1882	Ice jam downstream; Water covered old causeway, over bank at barn	125 m	Kriwoken (1983)
1883	Liard ice impeded by intact Mackenzie ice and ice jam downstream; Water covered old causeway, over bank at barn	125 m	Kriwoken (1983)
1888	Sudden breakup; Ice jam below island; Water over bank at barn	125 m	Kriwoken (1983)
1892	Ice jam downstream; Water over bank at Roman Catholic mission	126 – 127 m	Kriwoken (1983)
1909	Ice impeded in front of Fort Simpson by intact Mackenzie ice; Flats flooded; water running through middle of island, within 6’ of top of bank at mission.	124 – 125 m	Kriwoken (1983)
1918	Ice jam at lower end of island; Lower part of island inundated.	124 – 125 m	Kriwoken (1983)
1957	Ice jam in front of settlement; Bankfull stage, partially flooding flats	124 – 125 m	Kriwoken (1983)
1963	Ice jam at channel bend 19 km downstream of island; Many parts of island inundated; full evacuation of residents to Yellowknife	126.1 m	Kriwoken (1983)
		125.9 m	Pilling (2023)
1972	Ice jam downstream of townsite.	124.2 – 126.1 m	Kriwoken (1983)

Year	Description	Estimated Flood Level[1]	Reference
1976	No reported descriptions found.	123.7 – 125.3 m	Kriwoken (1983)
1989	Significant ice jam noted observed at town.		Public Safety Canada (2023)
2021	Severe ice jam caused flooding in Fort Simpson. Rising water triggered shutdown of the local power plant and the evacuation of over 700 people; Many parts of island inundated. Ice jamming occurred downstream at Martin River and the downstream bend ~13 km downstream of Fort Simpson.	125.7 – 125.9 m	Ollerhead and Associates Ltd. (2021)

Notes:
1. All elevations are documented as meters with respect to the "Geodetic Survey of Canada datum", which refers to the Canadian Geodetic Vertical Datum of 1928 (CGVD28).

2021 Breakup Chronology

The following provides a summary of the sequence of events experienced by the Town of Fort Simpson over the 2021 breakup period. The series of events are based on the information gathered during this study and include: local accounts by Roger Pilling; time-lapse photos acquired at WSC gauges; various ground and aerial photographs; *Dehcho Breakup Reports* (which include various government hydrometeorological and earth observation data).

7 May 21	Friday
• Water levels begin to drop slightly (about 0.4 m) at the Liard River gauge (presumably as water goes into storage due to ice accumulation upstream) then rises rapidly, later in the day by nearly 8 m. The Liard River gauge malfunctioned due to high ice later that evening. • The Liard River ice runs into the Mackenzie River. The surge of ice and water push water levels at the Mackenzie River gauge at Fort Simpson up rapidly by approximately 4 m to a gauge elevation of 13.1 m later that evening.	
8-9 May 21	Saturday
• Water levels on the Mackenzie at Fort Simpson continued to rise to a gauge elevation of approximately 14 m by end of day as ice jams alongside the Island. • Long term care residents are evacuated (R. Pilling). • Ice run on the Liard comes to rest with the head downstream of the Liard River gauge (R. Pilling).	
9 May 21	Sunday
• First evacuation order issued around 20:00.	

- Power plant shuts down around 22:00 as Mackenzie River water levels surpass 15 m (more than 6 m higher than the pre-breakup level of 8.8 m).
- 18:00 – aerial flight reconnaissance (R. Pilling) reports a *25 km ice jam from just below the Liard ferry to the mouth of Martin River (approximately 13 km downstream of Fort Simpson). Broken up ice/slush to approx. 1 km below Ft Simpson with pieces gradually getting bigger until Martin River where the ice was intact. The Mackenzie River was intact from Martin Island to Green Island but had moved above Green Island and was up into trees from Strong Point and up to at least Rabbitskin River.*

10 May 21 — Monday

- Water level reaches curb by Nahanni Inn and portions of main street are flooded (R. Pilling).
- Water flowing over causeway by Village office in early morning for approximately 12 hours (R. Pilling).
- Mackenzie River levels approach 16 m and remain around this level for the next few days.

11 May 21 — Tuesday

- Water levels recede slightly at the gauge.
- Ice from Liard River remains in channel with open water lead upstream of confluence below intact ice further upstream on the Mackenzie River (see photo to right from Dehcho Breakup Report, ENR, 2021-05-12).
- Refer to **Figure 4** for images depicting ice jam extents.

12 May 21 — Wednesday

- Ice jam remains in place with Mackenzie levels fluctuating between 15 m and 15.5 m (R. Pilling).
- Refer to **Figure 5** for images depicting ice jam extents.

13 May 21 — Thursday

- *By midday the heel* [head] *of ice jam has moved past Ft Simpson to end of island. WL equalizes on both sides of the island. Till this point WL's on the west side of Ft Simpson Island had been 1-2 m lower* (R. Pilling).
- 15:00 – aerial flight reconnaissance (R. Pilling) reports *heel* [head] *of jam 1-2 km below Ft Simpson. Broken ice/slush to Martin River. Ice had shifted and broken into mid-point of s curve below Martin River, but from exit of s curve downstream the ice was still a solid mass. Mackenzie River above Ft Simpson ice jam had not moved a lot. It was jammed at the Green Island rapids and all ice to Martin Island had shifted down but was holding. Water into the trees in Green Island area but had receded from above Strong Point.*
- Highwater (~15.0 m) reaches steps of the Nahanni Inn.
- Refer to **Figure 5** for images depicting ice jam extents.

14 May 21 — Friday

- Mackenzie River water levels reached a peak reported level of 15.994 m at 16:30 Friday May 14th. [**note:** R. Pilling reports a peak of 16 m at about 17:00].
- ENR Hydrologists Reports: *Verbal communication with Fort Simpson EMO suggests that as of evening of May 13th, the river was open downstream of Fort Simpson for about 4 kms, and then*

	there was a jam which was very packed in. They also saw a jam between approximately Martin Island upstream to about Strong Point – an estimated 25 kms of ice. • Refer to **Figure 5** for images depicting ice jam extents.
15 May 21	Saturday
	• Water levels dropped over the Saturday May 15th down to 14.4 m where they remained until later Monday evening when water levels rapidly receded back down to pre-breakup levels. • Refer to **Figure 6** for images depicting ice jam extents.
17 May 21	Monday
	• ENR Hydrologists Reports: *Ice on the Mackenzie River broke downstream of Fort Simpson and water levels in Fort Simpson have dropped to below 10 m. The Evacuation Order has been removed for Fort Simpson*.

Water levels associated with the sequence of events, described above, are in reference to the water level time series at WSC gauges 10ED001 Liard River near the Mouth and 10GC001 Mackenzie River at Fort Simpson. The water level data is expressed in terms of the gauge heights, which are unique to the respective gauges (refer to **Figure 7**). The Liard River gauge was impacted by ice and stopped recording late Friday evening May 7th. The Fort Simpson gauge was demolished and carried away by moving ice; however, water levels were monitored and recorded periodically by the Town officials while the gauge was inoperable.

A brief recession in water levels preceded the rapid rise at the Liard River gauge on the afternoon May 7th. River ice damaged the gauge later that evening and recordings stopped. Water levels on the Mackenzie along Fort Simpson rose rapidly by approximately 4 m to a gauge elevation of 13.1 m that same evening and continued to rise over the weekend (May 8th and May 9th) on into early Monday. The water level approached 16 m and stayed around this level for the rest of the week reaching a peak reported level of 15.994 m at 16:30 HH Friday May 14th. Water levels dropped over the Saturday May 15th down to 14.4 m where they remained until later Monday evening when water levels rapidly receded back down to pre-breakup levels.

4.2 Open Water Flood Frequency

Open water flood frequency estimates were completed for the WSC gauges on the Liard and Mackenzie rivers. Open water hydrology and the determination of open water flood frequencies were not required for this study. However, a brief flood frequency analysis was completed to estimate the 100-year open water flood to give context to the ice jam flood frequencies (determined below). Open water flood frequency estimates were determined for 10ED002 Liard River near the Mouth and 10GC001 Mackenzie River at Fort Simpson.

4.2.1 10ED002 Liard River near the Mouth

A total of 50 years of annual maximum data was extracted from WSC published records for years 1972-2021 (refer to **Table 12**), including maximum daily discharges (average of discharge values over a daily reporting period) and peak instantaneous discharges. Maximum daily values were published for all years and instantaneous values were published for 44-years. Estimates for missing instantaneous values were derived from the relationship between maximum instantaneous and maximum daily. A linear regression was used to determine this relationship, as depicted in **Figure 8**. The Pearson 3 distribution was found to provide a good fit to the observed data and was used to estimate the 100-year open water flood frequency (discussed in the flood hazard mapping section). **Figure 9** provides a plot of the resulting distribution with the observed data.

Table 12 Maximum Annual Discharge for Liard River near the Mouth (10ED002)

Year	Peak Instantaneous Discharge (m^3/s)	Date	Peak Daily Discharge (m^3/s)	Date
1972	13,800	03-Jun	13,600	04-Jun
1973	15,200	21-Jun	15,000	20-Jun
1974	12,900	21-Jul	12,900	21-Jul
1975	14,500	02-Jul	14,500	02-Jul
1976	11,211		11,100	06-Jul
1977	16,200	06-Jun	16,100	06-Jun
1978	6,120	11-Jun	6,120	11-Jun
1979	13,300	07-Jul	13,200	07-Jul
1980	7,130	12-Jun	7,010	20-Jul
1981	11,500	31-May	11,300	01-Jun
1982	13,029		12,900	21-May
1983	8,400	05-Jun	8,280	05-Jun
1984	10,700	12-Jun	10,600	12-Jun
1985	10,400	09-Jun	10,300	09-Jun
1986	12,300	06-Jul	12,300	06-Jul
1987	10,500	05-Jun	10,500	05-Jun
1988	16,200	18-Jul	16,000	18-Jul

1989	9,221		9,130	09-May
1990	14,400	05-Jun	14,400	05-Jun
1991	9,300	18-Jul	9,150	19-Jul
1992	12,700	19-Jun	12,700	20-Jun
1993	8,140	08-Jun	8,080	10-Jun
1994	10,200	12-Jun	10,100	12-Jun
1995	5,180	20-Jun	5,120	20-Jun
1996	9,580	24-Jul	9,520	24-Jul
1997	10,800	10-Jun	10,700	10-Jun
1998	8,510	01-Jun	8,480	01-Jun
1999	13,900	23-Jun	13,800	23-Jun
2000	7,000	16-Jun	6,970	16-Jun
2001	12,700	16-Jun	12,600	16-Jun
2002	10,200	10-Jun	10,200	10-Jun
2003	7,626		7,550	05-Jul
2004	7,690	14-Jun	7,660	14-Jun
2005	12,700	21-May	12,600	21-May
2006	14,700	20-Jun	14,600	20-Jun
2007	12,900	06-Jul	12,700	06-Jul
2008	12,900	28-Jun	12,900	27-Jun
2009	11,600	13-Jun	11,500	13-Jun
2010	8,030	08-Jun	7,910	08-Jun
2011	12,500	25-Jun	12,400	25-Jun
2012	19,600	13-Jun	19,400	13-Jun
2013	13,400	05-Jun	13,300	05-Jun
2014	9,430	07-Jun	9,280	07-Jun
2015	7,300	30-May	7,270	30-May
2016	7,440	06-Sep	7,350	06-Sep
2017	8,760	07-Jun	8,630	07-Jun
2018	11,211		11,100	29-Jun
2019	6,969		6,900	24-Jun

2020	16,300	20-Jun	16,200	20-Jun
2021	12,300	21-Jun	12,300	21-Jun

4.2.2 10GC001 Mackenzie River at Fort Simpson

The published data series for this gauge is 1938-2021 for a total of 84 years of data. From 1938-1962 data was recorded only from parts of June through summer and into to parts of October. For this period, WSC did publish the annual peak daily value. Where WSC did not publish the annual daily peak value, the hydrograph was assessed to see whether it could be extracted from the daily data. There was insufficient data for 1938, 1947-1948, 1954, 1962-1964, and 2016; these years were removed from the data series. Published maximum discharges were available for 46 years of the data series (1968, 1971-1975, 1977-2014, 2017, 2020). WSC has published peak daily values (annual extremes) for each year in the data series except 1993, this year was extracted from the published daily data series.

Years with missing instantaneous values were estimated from the relationship between maximum annual instantaneous and maximum daily values (as depicted in **Figure 10**). The relationship was based on a linear regression between instantaneous and daily values. The relationship excluded values where the published max instantaneous data and peak daily did not correspond to the same flood (as determined by instances where reported dates differed by more than three days). **Table 13** lists the results data series of annual maximum discharges used to estimate open water flood frequencies. The Pearson 3 distribution was found to provide a good fit to the observed data and was used to estimate the 100-year open water flood frequency (discussed in the flood hazard mapping section). **Figure 11** provides a plot of the resulting distribution with the observed data.

Table 13 Maximum Annual Discharge for Mackenzie River at Fort Simpson (10GC001)

Year	Peak Instantaneous Discharge (m^3/s)	Date	Peak Daily Discharge (m^3/s)	Date
1939	13,340		13,200	06-Jul
1940	15,150		15,000	05-Jul
1941	19,090		18,900	28-Jun
1942	22,430		22,200	14-Jun
1943	18,290		18,100	14-Jul
1944	13,130		13,000	16-Jun
1945	13,740		13,600	14-Jun
1946	11,720		11,600	17-Jun
1947				

1948				
1949	16,570		16,400	27-Jun
1950	22,120		21,900	22-Jun
1951	12,630		12,500	06-Jul
1952	15,150		15,000	03-Jul
1953	14,250		14,100	28-Jul
1954				
1955	18,890		18,700	05-Jul
1956	17,680		17,500	17-Jul
1957	17,280		17,100	03-Jul
1958	12,930		12,800	10-Jun
1959	14,250		14,100	09-Jun
1960	18,690		18,500	27-Jun
1961	23,740		23,500	30-May
1962				
1963				
1964				
1965	16,570		16,400	10-Jun
1966	14,950		14,800	15-Jul
1967	17,170		17,000	03-Jun
1968	17,500	17-Jul	17,500	17-Jul
1969	13,440		13,300	12-Jun
1970	14,850		14,700	14-Jun
1971	16,600	21-Jun	16,500	21-Jun
1972	18,000	04-Jun	17,900	04-Jun
1973	20,800	21-Jun	20,800	21-Jun
1974	20,400	21-Jul	20,300	21-Jul
1975	22,000	02-Jul	21,900	02-Jul
1976	18,590		18,400	06-Jul
1977	23,000	06-Jun	22,900	07-Jun
1978	13,400	12-Jun	13,400	11-Jun
1979	20,800	07-Jul	20,800	07-Jul
1980	12,500	13-Jun	12,500	13-Jun

1981	16,700	01-Jun	16,600	01-Jun
1982	20,900	21-May	20,700	21-May
1983	15,400	05-Jun	15,300	06-Jun
1984	16,800	12-Jun	16,700	12-Jun
1985	18,600	09-Jun	18,500	09-Jun
1986	20,300	06-Jul	20,200	06-Jul
1987	17,200	05-Jun	17,200	05-Jun
1988	22,300	19-Jul	22,200	19-Jul
1989	15,300	17-Jun	15,300	17-Jun
1990	20,000	06-Jun	19,900	06-Jun
1991	17,900	18-Jul	17,800	19-Jul
1992	21,700	20-Jun	21,700	20-Jun
1993	14,800	10-Jun	14,700	01-Jun
1994	18,300	12-Jun	18,200	13-Jun
1995	11,200	21-May	11,100	21-May
1996	17,300	24-Jul	17,200	24-Jul
1997	19,300	23-Jun	19,300	10-Jun
1998	17,400	01-Jun	17,300	01-Jun
1999	20,300	24-Jun	20,000	23-Jun
2000	12,800	15-Jun	12,700	15-Jun
2001	19,800	16-Jun	19,800	16-Jun
2002	17,800	10-Jun	17,800	10-Jun
2003	16,200	14-Jun	16,000	06-Jul
2004	14,000	31-May	14,000	31-May
2005	18,900	21-May	18,800	21-May
2006	22,700	20-Jun	22,600	20-Jun
2007	20,100	06-Jul	20,000	06-Jul
2008	20,300	27-Jun	20,300	27-Jun
2009	18,400	15-Jun	18,400	15-Jun
2010	15,700	07-May	14,200	08-Jun
2011	18,400	25-Jun	18,200	25-Jun
2012	26,000	13-Jun	25,800	13-Jun
2013	20,100	05-Jun	20,100	05-Jun

2014	15,400	07-Jun	15,300	07-Jun
2015	12,830		12,700	30-May
2016				
2017	16,300	07-Jun	16,200	07-Jun
2018	18,790		18,600	29-Jun
2019	13,030		12,900	24-Jun
2020	24,400	20-Jun	24,300	20-Jun
2021	22,730		22,500	21-Jun

4.3 Ice Regime

Freeze-up typically occurs in November when water temperatures reach 0°C and frazil ice begins to form. This initial ice production then leads to a solid ice cover forming over the Liard River, typically before the Mackenzie River. Breakup along the Liard and Mackenzie rivers typically occurs in early May. It usually originates along the Liard River with warm temperatures initiating snowmelt in the headwaters, causing increased discharge (Prowse, 1984). As small tributaries deliver snowmelt water to the Liard River, the increase in water level causes cracking in the ice cover and facilitates the development of an ice run. Intermittent ice jamming may occur as the ice run proceeds downstream. As the Mackenzie River may still have an intact ice cover at this time, the ice run has a potential to form an ice jam which may be present for several days at, or just downstream of the confluence of the two rivers. Eventual ice clearance takes place through melt and an additional increase in discharge (Anderson, 1982). Depositional features located downstream of Fort Simpson island, and a sharp bend in the Mackenzie River located 19 km downstream, can both cause conditions for the ice passage constriction and lead to ice jams downstream of Fort Simpson which may result in backwater flooding at the village (Kriwoken, 1983).

Flooding due to ice jams in this area is influenced by several factors, including: (1) discharge magnitude and timing of sudden release of ice and water along the Liard River, (2) the resistance of the intact Mackenzie River ice cover, and (3) local channel morphology (Prowse, 1984). In addition to the ice passage constrictions downstream of Fort Simpson as described above, the slope of the Liard River decreases from 0.00039 m/m to 0.00005 m/m within 20 km of the mouth and the width of the river increases from 650 m to 2800 m over the last 10 km (Prowse, 1984). These changes to the profile of the riverbed lead to a dramatic decrease in water velocity and increase the possibility for ice to become grounded through the area, both of which lead to reduced movement of ice downstream (Prowse, 1984).

4.4 Ice Jam Data Preparation

Breakup discharge and water level data were inspected on a year-by-year basis to determine the maximum breakup level and breakup discharge at the three gauges, 10ED002 Liard River near the Mouth, 10FB006 Mackenzie River at Strong Point, and 10GC001 Mackenzie River at Fort Simpson. The data for station 10FB006 Mackenzie River at Strong Point was not required for the analysis but is provided for information. The results of the analysis for the aforementioned gauges are listed in **Table 14, Table 15, and Table 16,** respectively. Instances where no data was found are denoted as ND.

Table 14 Peak Spring Breakup Summary – WSC Gauge 10ED002 Liard River near the Mouth

Season	Peak Breakup Date and Time	Peak Breakup Level (m)	Breakup Discharge (m^3/s)	Data Source	Breakup Mechanism
1974	1974-05-09 0:00	4.517	4,810	CRID	Thermal
1975	1975-05-07 0:00	6.559	2,070	CRID	Ice Jam
1976	1976-04-28 0:00	8.321	1,640	CRID	Ice Run
1977	1977-05-10 0:00	3.761	2,830	WSC	Thermal
1978	1978-05-03 8:30	9.318	2,270	CRID	Ice Jam
1979	1979-05-14 14:20	9.251	1,850	CRID	Ice Jam
1980	1980-05-01 0:00	5.483	1,550	CRID	Ice Jam
1981	1981-05-06 0:00	8.102	1,800	CRID	Ice Run
1982	1982-05-10 15:29	11.006	1,500	CRID	Ice Jam
1983	1983-04-30 14:32	11.758	1,750	CRID	Ice Jam
1984	1984-05-01 21:00	6.28	1,640	CRID	Ice Jam
1985	1985-05-10 6:51	12.187	6,900	CRID	Ice Jam
1986	1986-05-10 22:44	12.781	3,200	CRID	Ice Jam
1987	1987-05-05 5:15	8.06	2,300	CRID	Ice Jam
1988	1988-05-04 11:46	10.2	3,700	CRID	Ice Run
1989	1989-05-02 16:41	15.247	3,000	CRID	Ice Jam
1990	1990-05-03 15:10	7.143	3,400	CRID	Ice Run
1991	1991-04-29 5:00	9.575	3,230	CRID	Ice Jam
1992	1992-05-04 10:30	12.162	4,550	CRID	Ice Run
1993	1993-05-03 15:45	9.537	2,480	CRID	Ice Jam

Season	Peak Breakup Date and Time	Peak Breakup Level (m)	Breakup Discharge (m^3/s)	Data Source	Breakup Mechanism
1994	1994-04-30 0:00	10.601	3,750	CRID	Ice Jam
1995	1995-05-02 0:00	10.607	2,800	CRID	Ice Run
1996	1996-05-03 18:00	8.444	2,120	WSC	Ice Jam
1997	1997-05-06 0:00	14.378	4,600	WSC	Ice Jam
1998	1998-04-30 3:30	11.719	4,020	WSC	Ice Jam
1999	1999-04-29 0:00	9.222	3,350	WSC	Ice Jam
2000	2000-05-06 4:15	6.746	2,900	WSC	Ice Jam
2001	2001-05-10 15:15	6.686	2,300	WSC	Ice Jam
2002	2002-05-16 0:00	13.995	3,780	WSC	Ice Run
2003	2003-05-02 0:00	10.519	3,400	WSC	Ice Jam
2004	2004-05-03 0:00	11.037	2,000	WSC	Ice Jam
2005	2005-04-30 0:00	10.536	4,500	WSC	Ice Run
2006	2006-05-05 12:00	12.434	4,060	WSC	Ice Jam
2007	2007-04-28 12:00	11.854	3,000	WSC	Ice Run
2008	2008-05-06 12:00	10.889	5,360	WSC	Ice Run
2009	2009-05-08 3:00	7.721	6,680	WSC	Thermal
2010	2010-04-30 0:00	12.301	6,400	WSC	Ice Jam
2011	2011-05-08 12:10	6.561	5,830	WSC	Thermal
2012	2012-05-05 22:15	9.039	3,020	WSC	Ice Run
2013	2013-05-11 23:10	9.44	2,730	WSC	Ice Run
2014	2014-05-07 15:45	10.081	4,770	WSC	Ice Run
2015	2015-05-01 0:05	10.67	4,480	WSC	Ice Jam
2016	2016-05-02 22:10	6.433	3,770	WSC	Thermal
2017	2017-05-06 9:20	7.424	4,540	WSC	Ice Run
2018	2018-05-07 19:30	9.034	4,380	WSC	Ice Jam
2019	2019-04-22 3:10	7.506	1,920	WSC	Ice Jam
2020	2020-05-04 0:00	11.761	3,450	WSC	Ice Jam
2021	2021-05-07 18:50	11.869	ND	WSC	Ice jam
2022	2022-06-14 9:45	8.240	ND	WSC	ND

Season	Peak Breakup Date and Time	Peak Breakup Level (m)	Breakup Discharge (m^3/s)	Data Source	Breakup Mechanism
2023	2023-05-05 19:30	6.909	ND	WSC	ND

Table 15 Peak Spring Breakup Summary – WSC Gauge 10FB006 Mackenzie River at Strong point

Season	Peak Breakup Date and Time	Peak Breakup Level (m)	Breakup Discharge (m^3/s)	Data Source	Breakup Mechanism
1991	ND	ND	ND	ND	ND
1992	1992-05-07 0:00	9.844	7,000	WSC	Ice Jam
1993	1993-05-03 0:00	10.242	4,380	WSC	Ice Run
1994	1994-05-06 0:00	8.869	5,200	WSC	Thermal
1995	ND	ND	ND	ND	ND
1996	1996-05-10 0:00	8.473	5,800	WSC	Thermal
1997	ND	ND	ND	ND	ND
1998	ND	ND	ND	ND	ND
1999	ND	ND	ND	ND	ND
2000	2000-04-30 19:15	9.386	4,200	WSC	Thermal
2001	2001-05-06 19:30	12.942	7,000	WSC	Ice Jam
2002	2002-04-24 10:30	9.04	2,770	WSC	Thermal
2003	2003-05-09 15:15	9.877	4,800	WSC	Ice Run
2004	ND	ND	ND	ND	ND
2005	2005-05-01 13:45	10.39	5,800	WSC	Ice Run
2006	2006-05-05 10:45	13.001	6,220	WSC	Ice Jam
2007	2007-05-02 5:30	11.341	5,300	WSC	Ice Run
2008	ND	ND	ND	ND	ND
2009	2009-05-08 17:30	10.224	5,800	WSC	Ice Jam
2010	2010-05-02 7:50	10.315	5,800	WSC	Ice Run
2011	2011-05-09 12:15	8.549	4,790	WSC	Thermal
2012	2012-05-08 17:20	10.316	7,120	WSC	Ice Run

Season	Peak Breakup Date and Time	Peak Breakup Level (m)	Breakup Discharge (m^3/s)	Data Source	Breakup Mechanism
2013	2013-05-14 2:25	12.706	5,030	WSC	Ice Run
2014	2014-05-09 1:45	10.568	5,470	WSC	Ice Run
2015	2015-05-02 2:50	9.82	5,860	WSC	Ice Jam
2016	2016-05-03 11:05	9.048	5,880	WSC	Thermal
2017	2017-05-07 7:55	9.603	6,380	WSC	Thermal
2018	2018-05-09 21:45	11.54	7,230	WSC	Ice Jam
2019	2019-04-20 15:05	10.267	4,430	WSC	Ice Run
2020	2020-05-10 6:25	11.84	7,690	WSC	Ice Jam
2021	2021-05-13 20:35	15.956	8,460	WSC	Ice Jam
2022	2022-03-15 7:45	9.705	ND	WSC	ND
2023	2023-05-05 6:10	12.541	ND	WSC	Ice Jam

Table 16 Peak Spring Breakup Summary – WSC Gauge 10GC001 Mackenzie River at Fort Simpson

Season	Peak Breakup Date and Time	Peak Breakup Level (m)	Breakup Discharge (m^3/s)	Data Source	Breakup Mechanism
1963	ND	ND	ND	ND	ND
1964	ND	ND	ND	ND	ND
1965	ND	ND	ND	ND	ND
1966	ND	ND	ND	ND	ND
1967	ND	ND	ND	ND	ND
1968	ND	ND	ND	ND	ND
1969	ND	ND	ND	ND	ND
1970	ND	ND	ND	ND	ND
1971	ND	ND	ND	ND	ND
1972	1972-05-13 14:00	14.521	4,470	CRID	Ice Jam
1973	1973-05-03 23:00	11.122	8,210	CRID	Ice Run

Season	Peak Breakup Date and Time	Peak Breakup Level (m)	Breakup Discharge (m^3/s)	Data Source	Breakup Mechanism
1974	1974-05-12 21:00	9.613	11,900	CRID	Thermal
1975	1975-05-09 4:40	9.226	8,210	CRID	Ice Jam
1976	1976-04-30 5:00	13.993	8,500	CRID	Ice Jam
1977	1977-05-04 15:50	10.775	6,090	CRID	Ice Run
1978	1978-05-05 16:00	11.15	5,660	CRID	Ice Jam
1979	1979-05-15 1:30	10.147	6,000	CRID	Ice Run
1980	1980-04-30 0:10	7.686	5,400	CRID	Ice Run
1981	1981-05-07 10:15	12.056	7,400	CRID	Ice Jam
1982	1982-05-11 6:19	11.056	10,000	CRID	Ice Run
1983	1983-05-10 13:19	8.599	10,000	CRID	Thermal
1984	1984-05-04 11:10	8.091	6,300	CRID	Ice Jam
1985	1985-05-12 4:16	13.761	10,400	CRID	Ice Jam
1986	1986-05-12 8:39	12.74	6,700	CRID	Ice Jam
1987	1987-05-05 18:30	11.813	6,850	CRID	Ice Run
1988	1988-05-04 15:45	12.841	7,200	CRID	Ice Run
1989	1989-05-03 23:24	14.949	9,000	CRID	Ice Run
1990	1990-05-04 15:05	10.872	9,600	CRID	Ice Jam
1991	1991-05-04 14:13	12.717	6,900	CRID	Ice Jam
1992	1992-05-05 13:05	14.281	13,700	CRID	Ice Run
1993	1993-05-03 18:15	10.675	6,880	CRID	Ice Run
1994	1994-05-03 9:46	9.667	9,500	CRID	Ice Run
1995	1995-05-02 23:00	10.697	6,130	CRID	Ice Run
1996	1996-05-07 2:48	11.299	10,700	WSC	Ice Jam
1997	1997-05-18 17:00	11.066	14,800	WSC	Ice Jam
1998	1998-05-01 9:15	13.517	10,600	WSC	Ice Jam
1999	1999-05-08 14:00	8.336	8,960	WSC	Thermal
2000	2000-05-03 16:30	7.358	6,000	WSC	Thermal
2001	2001-05-07 16:55	7.847	9,230	WSC	Thermal
2002	2002-05-16 16:25	11.504	8,300	WSC	Ice Run

Season	Peak Breakup Date and Time	Peak Breakup Level (m)	Breakup Discharge (m^3/s)	Data Source	Breakup Mechanism
2003	2003-05-02 0:00	13.86	6,300	WSC	Ice Jam
2004	2004-05-12 17:30	8.622	6,750	WSC	Ice Jam
2005	2005-04-30 0:00	11.899	9,950	WSC	Ice Run
2006	2006-05-05 17:20	13.296	10,300	WSC	Ice Jam
2007	2007-05-02 7:05	13.386	10,800	WSC	Ice Jam
2008	2008-05-06 10:00	11.768	12,300	WSC	Ice Run
2009	2009-05-08 4:15	9.304	15,300	WSC	Thermal
2010	2010-04-29 17:10	11.816	11,800	WSC	Ice Run
2011	2011-05-08 11:15	9.855	9,790	WSC	Ice Run
2012	2012-05-07 8:30	11.737	11,800	WSC	Ice Jam
2013	2013-05-13 1:00	12.243	12,200	WSC	Ice Run
2014	2014-05-08 4:00	11.178	10,300	WSC	Ice Run
2015	2015-05-03 0:30	11.543	9,500	WSC	Ice Jam
2016	2016-05-03 9:45	8.659	ND	WSC	Ice Run
2017	2017-05-09 0:15	8.276	9,600	WSC	Ice Run
2018	2018-05-06 0:00	7.691	10,600	WSC	Thermal
2019	2019-04-23 22:15	10.06	5,240	WSC	Ice Jam
2020	2020-05-05 13:35	12.69	8,500	WSC	Ice Run
2021	2021-05-14 16:30	15.994	15,600	WSC	Ice Jam
2022	14-Jun-22	9.978	ND	ND	Ice Run
2023	25-May-23	6.991	ND	ND	Thermal

4.5 Ice Jam Flood Frequency

Whereas flood *flow* (stream discharge) is the parameter of interest for open water analysis, flood *level* is the parameter of interest for ice jam flood analysis. This is because it is not possible to ascribe a unique flood level to each breakup flood flow. For a particular breakup discharge there are a range of flood levels owing to different ice-affected backwater conditions. And so, for ice jam flood level frequency analysis, the more meaningful parameter is *level*. While the parameter used to express flood magnitude (level versus discharge) differs, the resulting flood frequency magnitudes are technically equivalent.

Two different approaches were considered to estimate ice jam flood frequency for this study: a *direct method* based on observed flood levels and an *indirect* method based on flood levels derived from a very large population of synthesized flood levels.

4.5.1 Direct Method

The direct method approach was an intuitive approach that undertook a simple frequency analysis of the peak breakup levels. This approach relied solely on peak water level data at breakup without consideration of the breakup ice conditions associated with the peak. The direct method analysis provides an initial estimate of flood level frequencies at the gauge. For this approach, a simple plotting position formula (**Equation 1**) was applied to the ranked annual maximum flood levels to estimate the probability of non-exceedance, P, for each rank, m, and total number of samples, N, using the Cunnane plotting position parameter, a = 0.4.

$$P = \frac{m-a}{N+1-2a} \qquad \textbf{Equation 1}$$

The results of the analysis are depicted as probability plots in **Figure 12**, and **Figure 13**. For 10ED002 Liard River near the Mouth and 10FB006 Mackenzie River at Strong Point, respectively. The data for the Liard River were all part of the systematic record and the charts were created using a standard plotting position formula. For the Mackenzie River, two curves are provided – one for the systematic record and one for a combined record that includes historic flood events (prior to the systematic record). A modified plotting position formulae was used to plot the combined record for 10GC001 Mackenzie River at Fort Simpson (**Figure 13**). This approach was limited to gauge 10GC001 as there were no historical flood accounts available for the other gauge.

The modified formula was based on the threshold-exceedance plotting positions recommended in USGS Bulletin 17C (USGS, 2018). The modified approach allowed for the inclusion of the sparse historical data spanning years 1828 to 1918, reported by Kriwoken (1983). The historic events included in the analysis are depicted in **Figure 3** (adapted Kriwoken, 1983). The line associated threshold level (~123.75 m) is added to the figure for comparison.

The flood frequencies implied by the probability plots are indicative of the flood level magnitudes over a range of flood recurrence intervals at each gauge site. The indirect methods, described below, were used to fit a flood frequency distribution to these observed data and the gauges and extend the estimation of regulatory flood levels throughout the entire study area.

4.5.2 Joint Probability Analysis

There are many different drivers impacting the magnitude of ice jam flooding including the following.

- Antecedent conditions preceding breakup, such as competency of the ice cover (thickness, type, and state of decay) and/or discharge and corresponding water levels.

- The prevailing meteorological conditions during their development and the potential for a concurrent major rainfall event.
- The resulting breakup mechanism (e.g. mechanical or thermal) and evolution of the ice jam accumulation.

The relative contribution of each factor on flood magnitude (directly or indirectly) is complex. There are no practical equations available to quantify relationships between many of the important drivers and flood level magnitude. It is not practical to explicitly account for all the various driving factors by a typical joint probability analysis.

The current state of practice for estimation of flood frequency magnitude is to rely on historical hydrometric data. For ice jam floods, the combined effect of all the different drivers impacting ice jam flood magnitude is ultimately expressed as flood level at the gauge. Fortunately, there exists historic flood level data with relatively long records at the WSC gauges within the study reaches.

The indirect method used to determine ice jam flood frequency in this study, is a type of joint probability analysis. The procedure followed a Monte Carlo approach that uses statistical methods to quantify the combined effects of the dominant drivers (or causative factors) that contribute to the whole set of flood level data. The adopted methodology, detailed in the following section, follows that described by Healy and Kovachis (2023) and is detailed in the next section.

4.5.3 Indirect Method – Monte Carlo Analysis

The indirect method attempted to quantify the causative factors that contribute to the characteristics of the whole set of data rather than individual events and follows an approach similar to the so-called G-C method described by Beltaos (2021). The approach accounts for the variation in ice conditions at breakup and relies on a range of ice-affected flood level conditions along the study reach according to breakup type.

The analysis begins with preparation of the data used by the Monte Carlo workflow as follows.

1. Conduct a year-by-year inspection of the breakup data to determine the peak breakup level, corresponding discharge, and dominant breakup mechanism (or *type*). In this study, three different breakup types were identified as thermal, mechanical resulting in a fully developed ice jam, and mechanical resulting in an ice-run or partially developed ice jam.
2. Determine the breakup discharge frequency relationship. The breakup discharge flood frequency distributions for the Liard and Mackenzie river study reaches are depicted on **Figure 14** and **Figure 15**, respectively.
3. Estimate the relative ratios of breakup types based on the breakup types determined in the preceding step. These provide the probability of occurrence factors for the various breakup types used by the Monte Carlo analysis. For this study, the probability factors for the Liard

River were estimated as 13.5 % for thermal, 27.5 % for mechanical – ice run, and 59.0 % for mechanical – ice jam. For the Mackenzie River, they were estimated as 15.0 % for thermal, 46.8 % for mechanical – ice run, and 38.3 % for mechanical – ice jam.

4. Develop a family of ice-affected flood level profiles for each breakup type. This was achieved by computing water level profiles over a range of ice conditions and breakup discharges. This provides a set of rating curves at each model cross section according to breakup type.

The Monte Carlo workflow preceded according to the following steps which are illustrated in **Figure 16**. The workflow resulted in a very large population of breakup flood levels that was used to estimate the ice jam flood frequency distribution – it was completed separately for each study reach.

1. Randomly select a value from the breakup discharge frequency distribution (recall **Figure 14** or **Figure 15**).
2. Randomly select a breakup mechanism based on the probability factors for the various breakup types (recall step 3 above).
3. Determine the breakup flood level associated with the randomly selected breakup discharge value and randomly selected breakup type according to the breakup rating curves pre-calculated in step 4 above.
4. Store the breakup flood level to the synthesized population of breakup levels for and repeat the process many, many, times (e.g. 10,000 + iterations). The degree of statistical confidence increases with a very high number of iterations. It limits the variation in the flood level magnitudes associated with the extreme AEP values by ensuring samples are selected within the extreme range.
5. Rank and plot the series with a standard plotting position formula to form a distribution of breakup flood levels and compare to the estimated breakup flood levels based on observational data.

The resulting Monte Carlo distributions as compared to the observational data are provided in **Figure 17** and **Figure 18** for the Liard and Mackenzie rivers, respectively.

5 OPEN WATER HYDRAULICS

The first step towards development of the ice jam model was to create an open water model calibrated to surveyed water levels. The follow describes the steps taken to develop the open water model.

5.1 Data Preparation

The hydraulic modelling relied on bed and overbank elevation data gathered by NHC in the summer of 2024 (detailed in a previous section) for the main channel geometry and the DTM for the overbank geometry. The orthorectified aerial imagery was also used to assist in aligning the model cross sections and channel centreline.

In some cases, an existing hydraulic model can be found from a previous study and these previously developed models can provide useful information for a new or updated model. No evidence was found to suggest a previously developed model existed – the geometry of the current model relied on recently collected data only.

5.1.1 Model DTM

The project DTM (McElhaney 2020) used to inform the channel geometry and complete the subsequent flood mapping sufficiently covered the mapping domain and most of the cross sections. The channel survey was extended approximately 15 km downstream of the project DTM to the narrow bend where ice jam toes are known to occur. To facilitate model development beyond the limits of the project DTM the model DTM was extended with the ArcticDEM DSM.

5.1.2 Highwater Marks

Ollerhead and Associates surveyed eight HWMs from the 2021 ice jam flood identified by silt marking left on structures and witness testimony. The data is documented in a report with accompanying raw data (Ollerhead and Associates 2021). In addition to these high water marks, six high water marks were measured by Roger Pilling, a previous WSC employee and resident of Fort Simpson.

An ice envelope curve based on high water marks collected by NHC in 1975 from the 1963 flood event on the Liard River was collected and digitized for use in the calibration of the Liard River model.

5.1.3 Flood Photography

Photos taken from within an aircraft during the 2021 flooding event by local filmmaker Jonathan Antoine. Photos taken from within an aircraft at approximately the peak of the flood event on May 14, 2021 (15:12 - 15:19 MST) and provided by Kevin Corrigan, Senior Administrative Officer of Fort Simpson. Also included are photos collected at the WSC hydrometric gauge station 10GC001 (Mackenzie River at Fort Simpson) on the same date and around the same time (15:16 and 16:15 MST).

5.2 Open Water Model Construction

The U.S. Army Corps of Engineer's Hydrologic Engineering Center River Analysis System (HEC-RAS) computer program (Version 6.5, 2024) was used to perform hydraulic modelling for this study. The basic inputs required by HEC-RAS are cross sections spaced throughout the study reach that represent the geometry of the river channel and floodplain, roughness coefficients for the channel and overbank areas at each cross section, a specified water level, rating curve, slope at the downstream boundary, and an inflow discharge, at the upstream boundary.

5.2.1 Geometric Layout

The approach followed to develop key components of the model geometric layout was:

- The channel centreline was defined along the middle of the main channel and was digitized using ArcGIS tools and visual referencing of the DTM, hillshade, and aerial imagery. A single continuous centreline was created to represent each modeled reach. Three reaches were modelled for this study. The modelled reaches are as follows.
    - *Liard River* reach extending from the upstream study limit to the confluence of the Liard and Mackenzie River. The total reach length is approximately 17 km.
    - *Mackenzie River* reach extending from the upstream study limit to confluence of the Liard and Mackenzie River (approximately 9.7 km) down, continuing below the confluence of the Liard and Mackenzie River to the downstream study limit. The total length is approximately 24.4 km.
- Flow paths were created coincident with the river centerline and along the left and right floodplains, representing the length of the main channel, left overbank, and right overbank flow paths. Distances between cross sections were measured along flow path lines. The model requires these distances for estimating energy losses between cross sections within the main channel and the left and right overbank areas.
- Model cross section transects were digitized at each surveyed cross section as follows. First, a main channel portion was digitized across the main channel overtop of the surveyed channel and bank point data. Then, the main channel portion was extended left and right across the floodplain (overbank areas). The overbank portions were aligned perpendicular to the anticipated path of the floodplain flows. Cross section elevation values from the survey point data were projected onto the cross section lines using the RAS Mapper GIS toolset through a conflation process. Elevations in the overbank areas were determined by extracting elevation values from the underlying DTM along the cross section polylines. The available bare-earth DTM and ArcticDEM DSM were used for the model construction.

The determination of the left and right banks, referred to as model bank stations, involved examining the geometry of cross sections and analyzing the Digital Terrain Model (DTM) of the channel. These model bank stations were strategically positioned to delineate the boundaries of

the modeled left overbank, main channel, and modeled right overbank sections of the cross sections. Additionally, they were placed to reflect variations in roughness within both the channel and floodplains. It's important to note that while these model bank stations serve to represent hydraulic conditions within the channel and floodplain, they may not precisely align with the actual banks of the main channel. Their primary function is to simulate the hydraulic behavior of the channel and its surrounding floodplains within the model framework.

The resulting model cross sections and model channel centreline for the Mackenzie River and (**Figure 19** through **Figure 22**) and Liard River (**Figure 23** and **Figure 24**).

5.2.2 Channel and Overbank Roughness

Manning's roughness values were used to simulate roughness in the modelled reaches. Manning's roughness is an empirical coefficient used to account for energy losses due to a combination of factors including surface roughness and channel sinuosity. Manning's roughness also varies somewhat with discharge. The Manning's roughness values adopted for the present study are discussed further in a subsequent section on model parameters.

5.2.3 Expansion and Contraction Coefficients

To account for the effect of flow contraction or expansion losses on the energy balance between successive cross sections, HEC-RAS multiplies the absolute difference in velocity head by a coefficient. These coefficients range from 0.10 for gradual transitions to 0.80 for abrupt transitions (Brunner, 2016).

5.2.4 Boundary Conditions

Boundary conditions are required at the inflow (upstream) and outflow (downstream) boundaries of the model. The inflow boundary condition is the discharge. The outflow boundary condition could be a water level (through fixed stage or rating curve) or a friction slope with which the water level will be calculated by HEC-RAS assuming a normal depth approximation.

5.2.5 Ineffective Flow Areas

Ineffective flow areas can be specified within portions of cross sections where water will pond but there is no appreciable flow. One common example of using ineffective flow area is in cross sections upstream and downstream of a bridge or culvert where flow is obstructed by elevated road embankments. In HEC-RAS, ineffective flow areas can be defined as either a permanent or non-permanent type. Permanent ineffective flow areas stay ineffective regardless of the water surface elevation, whereas temporary ineffective flow areas become effective when water surface elevation exceeds a defined elevation. The configuration of ineffective flow areas depends on site-specific circumstances and engineering judgement.

5.2.6 Geometric Database

The geometric database provides all the components of the HEC-RAS model geometry, including cross sections, internal hydraulic structures, and boundary conditions. Each component is described below. Additional information and data are provided as part of the electronic deliverables of the study.

A total of 51 cross sections were created and used to construct the model for this study: 34 cross sections in the Mackenzie River, and 17 cross sections of the Liard River. The steps taken to generate the cross section data were as follows:

- Cross section alignments within the channel were established generally following the alignments of the cross section survey. The overbank portions were aligned perpendicular to the anticipated flow direction.
- Two separate station-elevation data sets were created for each cross section.
- The first data set was created by projecting surveyed data points perpendicularly onto the channel portion of the cross section line.
- The second data set was created by extracting elevation values from the DTM along the cross section lines excluding the channel portion covered by the survey data.
- The two station-elevation data sets were combined. For each cross section, the number of elevation points for the overbanks were reduced using the minimize-area-change point filter option in HEC-RAS, so that the total number of the points is within the HEC-RAS limit of 500 points. To reduce noise within the data collected by the sounder the sections were further reduced to only include 150 points for the Liard River, and 200 points for the Mackenzie River
- Distances between consecutive cross sections were established within the HEC-RAS model following the established channel centerline and central flow paths for the left and right overbank areas.

5.2.7 Model Calibration

Before any ice jam simulations could be run on the Mackenzie and Liard River Models, each model was calibrated to open water conditions for a low flow and high flow conditions. To ensure accurate water levels the following parameters were modified:

- Manning's roughness coefficient for the channel and floodplain.
- Ineffective flow areas at each model cross section.
- Expansion and contraction loss coefficients.

Of these parameters, Manning's roughness for the river channel is typically the primary calibration parameter. Challenges and limitations inherent in the calibration process included:

- Availability and accuracy of the calibration data.
- Proper identification of highwater mark locations.
- Uncertainties in estimates of the flood peak discharge.
- Insufficient channel geometry data.

The general calibration approach involved adjusting Manning's roughness values to ensure computed water levels closely matched observed levels for selected events. Adjustments were made on a reach-averaged basis. High flow events were preferred for calibration, although WSC gauge rating curve data and/or low flow events could also be utilized.

In this study, the primary challenge affecting calibration efforts was the absence of highwater mark data for open water flood events within the study reaches. However, it is possible to extract a water surface profile from the non-flattened LiDAR DTM from July 14, 2020. The mean daily discharge on this date is for the Liard and Mackenzie is shown in **Table 16**. A comparison of the computed water levels to the extracted LiDAR surface for the same discharge in HEC-RAS is shown in **Figure 25** and **Figure 26**. It is expected that some elevation errors are present within the non-hydro-flattened LiDAR water surface profile as wet surfaces typically reflect a LiDAR pulse differently than dry ground. While the extracted profile likely provides a reasonable representation of the water surface during the time of the LiDAR flight, it is not comparable to the data quality that is achieved by topographic GPS surveys and should therefore be interpreted with caution. In addition, it should be noted that since the LiDAR did not cover any of the Mackenzie River downstream of RS 15077, the LiDAR could not be used to calibrate this section of the model.

Table 17 Recorded Discharges associated with LiDAR profile

River	Gauge	Discharge (m^3/s)
Mackenzie River	10GC001	19,300
Liard River	10ED002	10,200

A low flow calibration was completed utilizing the water level measurements collected as part of the June 5 to June 10, 2024 survey by NHC. Water levels were surveyed at each cross section, typically along both the left and right banks. As the survey was completed over several days, with the Mackenzie River being surveyed on June 7 through 8, and the Liard being surveyed on June 8 and June 9. Discharges for all dates of the survey are shown in **Table 17**. As the discharges changed between the different surveyed dates, the highest discharge and lowest discharge was simulated to get a reasonable range of water surface profiles to compare to the surveyed water surface values. A comparison of the surveyed water surface profile to the simulated water surface profile using the discharges below can be found in in **Figure 25** and **Figure 26**.

Table 18 Recorded Discharges associated with surveyed water surface profile

Date	Discharge (m^3/s)	
	Mackenzie River	Liard River
June 7, 2024	7,650	3,600
June 8, 2024	7,920	3,800
June 9, 2024	8,110	4,000

Additionally, the provided rating curve table for both the 10ED002 and 10GC001 WSC gauges was used to calibrate both the Liard and Mackenzie Rivers locally. Included in the WSC rating curve tables were the direct measurements used to synthesize the WSC curve. These values were found to be more relevant for calibration than just the curve. Comparisons between the modelled rating curve and the WSC rating curve (termed "WSC ERT 9 Rating Curve" and "WSC ERT 10.0 Rating Curve") and corresponding direct measurements can be found in in **Figure 27** and **Figure 28**.

5.3 Model Parameters and Options

The following sections describe the key model parameters and options adopted in the HEC-RAS model. These include Manning's roughness values for channel and overbank areas; contraction and expansion loss coefficients; ineffective areas; and roadway weir coefficient.

5.3.1 Manning's Roughness Coefficient

Manning's roughness is used to account for an array of energy losses that may vary with respect to discharge. A minimum of three (one channel and two overbank) roughness values were used within each cross section. Where appropriate, roughness was varied horizontally across the section to capture changes in river and floodplain characteristics. **Table 19** summarizes the selected channel and floodplain roughness values at each model cross section.

Table 19 Description of bed material and land cover types within the study reach

Reach Description	Channel Roughness	Channel Remarks	Overbank Roughness	Overbank Remarks
Mackenzie River	0.028	Natural gravely channel	0.070-0.10	Mostly treed area with some development through the town of Fort Simpson
Liard River	0.027	Natural gravely channel	0.10	Mostly treed area

The channel and overbank roughness values mentioned in the table above are directly utilized for all flood frequency flows.

5.3.2 Expansion and Contraction Coefficients

To account for the effect of flow contraction and expansion losses on the energy balance between successive cross sections, HEC-RAS multiplies the absolute difference in velocity head by a coefficient. The default values of 0.1 and 0.3 (for expansion and contraction coefficients) were utilized throughout the entire model domain.

5.3.3 Boundary Conditions

The two scenarios were run with different downstream boundary conditions depending on the discharge. **Table 20** lists the different discharges for the different discharge scenarios. Since the LiDAR did not extend to RS 0 on the Mackenzie River, the normal depth based on the surveyed water surface elevation slope of 0.0001 m/m was used instead of a known water surface elevation (W.S.E.).

Table 20 Description of downstream boundary conditions for the open water calibration scenarios

Flow Scenario	River	Downstream Boundary Condition
Low Flow	Liard River	Known W.S.E = 114.866 (Right Channel) Known W.S.E = 115.342 (Left Channel)
	Mackenzie River	Known W.S.E = 111.67 m
High Flow	Liard River	Known W.S.E = 118.78 m
	Mackenzie River	Normal Depth S = 0.0001 m/m

5.3.4 Ineffective Flow Areas

Ineffective flow areas were specified at cross sections in the HEC-RAS model based on a review of the local terrain and floodplain features both at and between cross sections. Ineffective flow areas can be specified within portions of cross sections where water is expected to pond, and where the velocity of that water, in the downstream direction, is expected to be close to or equal to zero (Brunner, 2016). The downstream direction is taken relative to the cross section lines defined in the model, so the orientation of cross sections was considered when specifying ineffective flow areas.

Ineffective flow areas in the model may be specified as either permanent or non-permanent. Permanent ineffective flow areas apply regardless of the water surface elevation, whereas non-permanent ineffective flow areas become effective above a defined elevation. The configuration

of permanent and non-permanent ineffective flow areas were specified depending on site-specific circumstances and engineering judgement.

The general principles for determining ineffective flow areas were as follows:

- Non-permanent ineffective flow areas were used to "fill" local depressions on the floodplain that are obstructed by higher ground upstream or downstream. These areas were assumed to become engaged in the active flow area (or effective) once the water level exceeded the elevation of the adjacent ground.
- Permanent ineffective flow areas were used to permanently "fill" relic channels, tributary channels or excavated holes that would otherwise have incorrectly added flow area to the cross section.
- Permanent ineffective flow areas were defined where flow patterns were likely to be influenced by nearby bridge abutments and roadway embankments crossing the floodplain. These types of obstructions tend to direct flows towards the bridge opening. Several site-specific factors were taken into account when configuring ineffective flow areas at bridges and culverts in the study area, including: distance from the cross section to the bridge, terrain features, bridge geometry, and skew of the bridge opening relative to the river.
- Ineffective flow areas behind railroad and highway embankments were assessed on a case by case basis. Aerial imagery, LiDAR, and historic information were used to determine if there were indications of flow behind and/or above embankments. Areas behind and below the height of the embankment were modelled as effective flow only if there was no downstream obstruction or if there was an indication of flow moving in the downstream direction. Otherwise, permanent ineffective flow areas were set to the top of embankment elevation, allowing areas behind embankments (assumed permeable) to be shown as wet and isolated but not conveying flow. Areas above embankments generally conveyed flow once the embankment was overtopped, unless an upstream or downstream obstruction was present causing local ponding or dead zones with limited flow.

For this hydraulic model, there were only a few ineffective flow areas which were required. The most notable of these being a permanent ineffective flow area within the snye along the west side of the Fort Simpson Island. This channel is permanently blocked by the highway embankment and would likely only become active once the road embankment becomes overtopped. This ineffective flow area spans from RS 24300 to RS 20237.

A non-permanent ineffective flow area was added to the model along the shoals downstream of the Fort Simpson Island for the low flow scenario. It was observed during the survey that there was no flow within any of the side channels through this area. It is assumed that these channels would become activated again once the discharge and corresponding water levels increase.

One other permanent ineffective flow area was added to the Liard River model, downstream of the Liard River Ferry along the right bank, where a small tributary feeds into the channel, the channel was included in the overall cross section, but was set as ineffective as it would not contribute to the flows within the Liard, but is expected to back up if an ice jam were to occur.

6 ICE JAM MODEL DEVELOPMENT

The basic inputs required by the ice model are much the same as those required by an open water model (i.e., river cross sections along known lengths of channel, roughness coefficients for the channel and overbank areas at each cross section, a specified or computed water level at the downstream model boundary, and a discharge at all upstream model boundaries). In addition to these basic inputs, the ice model requires at each model cross section: a prescribed ice cover condition, under ice roughness, and a set of ice jam parameters characterizing the properties of the ice jam. These ice model inputs are used to solve for the under-ice hydraulics and ice jam stability relationship. As this is the case, it was considered acceptable to use the calibrated open water model previously discussed, with some adjustments to better facilitate the modelling of ice conditions.

6.1 Model Refinements

While the open water model was generally considered acceptable for use in the ice jam model, certain modifications were necessary to better facilitate ice jam modelling. These model refinements may include adjustment to the bank stations to better represent the ice jam “width” and the addition of extra cross sections, typically created by interpolating existing surveyed cross sections.

6.1.1 Additional Cross Sections

Additional cross sections may be necessary to perform a stable ice thickness assessment. Due to the surveyed cross sections having a relatively uniform spacing and being positioned at major changes within the river morphology, it was found unnecessary to interpolate additional cross sections.

6.2 Ice-Specific Model Parameters

Aside from the model refinements, ice jam specific parameters are necessary to produce a stable ice jam model. These include composite roughness, which was determined through calibration to known ice jam events. In addition to other parameters which include initial ice thickness, internal friction angle, ice jam porosity, coefficient of lateral to longitudinal stress, and maximum under ice velocity.

Composite Roughness

The composite ice roughness (n_0) is a product of the bed roughness (n_b) and the under ice roughness (n_i). For this study, the bed roughness calibrated for the open water model was held constant and the adjustments were made to the under ice roughness. Hydraulic calculations by the model rely on the composite roughness, n_o, which is calculated internally by the model according to the relationship expressed in **Equation 2**:

$$n_o = \left(\frac{n_i^{3/2} + n_b^{3/2}}{2}\right)^{2/3} \qquad \textbf{Equation 2}$$

where n_i and n_b are the bed and bottom of ice roughness values, respectively.

Initial Ice Thickness

Initial ice thickness was initially set as the average of the average ice thicknesses measured by WSC as part of their field notes. For the Mackenzie River the average ice thickness ranged from 0.8 m to 1.8 m, with an average ice thickness of 1.1 m. For the Liard River the average ice thickness ranged from 0.8 m to 1.8 m, with an average thickness of 1.1 m. Therefore, an initial ice thickness of 1.1 m was used for the analysis. For the downstream boundary condition for both the Liard and Mackenzie River's the normal slope was used for the downstream boundary condition.

Jam Stability Parameters

The jam stability parameters are required as input to the HEC RAS model to solve for the ice jam thickness profile. These include: the internal friction angle of the jam; the ice jam porosity; and the coefficient of lateral to longitudinal stress in the jam. Ice jam strength properties can not be measured directly in the field and consequently they are not reported for observed events. Default values were selected for the jam stability parameters in this model.

Ice Jam Porosity: Ice jam porosity represents the volume fraction of the interstitial spaces in the ice accumulation. It is assumed to be the same above and below the water surface. The default value of p = 0.4 was adopted for this study.

Internal Friction and Coefficient of Lateral to Longitudinal Stress: The default parameters in HEC-RAS for the internal friction angle and stress coefficient are ϕ = 45° and k_1 = 0.33.

7 ICE JAM MODEL CALIBRATION

The ice jam profiles using the above parameters were generated and calibrated to known ice jam high water marks.

7.1 Summary of High Water Marks

Historical highwater data for ice affected flood in the Village of Fort Simpson were found from different sources. Ice jam high water marks for the 2021 events were collected courtesy of Roger Pilling, and re-surveyed by NHC, where found, to confirm the elevations. In addition to the high water marks collected by Roger Pilling, Ollerhead and Associates collected additional highwater marks that were concentrated in three different areas. Summaries of the available high water mark data for the 2021 calibration event is provided in **Table 21**.

Highwater mark data was not available for the for Liard River. Calibration for the Liard was based on comparisons to breakup discharge data determined for the WSC gauge (10ED002), listed in **Table 13**. During the 2024 survey a few debris piles were found along the lower reach of the Liard River. The debris was most likely left behind from a previous highwater event and while it is difficult to confirm, we suspect that these piles may have been formed during the recent 2021 ice jam flood. The elevation of these piles were surveyed and the surveyed levels were included for comparison to the Liard River computed ice jam flood profiles.

Table 21 2021 Mackenzie River Ice Jam High Water Marks

Point Description	Distance from d/s Boundary (m)	u/s Model XSEC	Distance from u/s Model XSEC	Estimated 1963 Ice Profile elevation	Source
Fort Simpson Lodging Shop Floor	4,054	22,338	509	125.841	Roger Pilling
WSC Shop	6,054	22,915	204	125.579	Roger Pilling
Airfield Hangar	7,054	22,915	402	125.708	Ollerhead and Associates
Liquor Store	8,054	22,915	365	125.787	Roger Pilling
Golf Course Hole 1	9,054	23,542	506	125.663	Roger Pilling
Residential garage floor	10,054	23,542	341	125.75	Roger Pilling
Arbour	11,053	24,300	680	125.807	Ollerhead and Associates
Baseball Field	12,052	24,300	300	125.826	Ollerhead and Associates

7.2 Calibration Approach

Using parameters listed above, the ice jam profiles were adjusted to match the high water marks listed in **Table 20** and breakup water elevations at 10ED002 in **Table 13**. The locations of the surveyed highwater marks are depicted in **Figure 29**. Calibration was achieved by modifying the under ice roughness to match the surveyed high water marks.

7.3 Calibration Results

Based on the calibration approaches and highwater marks in Table 20, the ice jam profile was able to be determined. The below provides a summary of the calibration results for the Mackenzie and Liard Rivers.

7.3.1 2021 Mackenzie River Breakup

Mackenzie River was calibrated using the data collected by Ollerhead and Associates (2021) and Roger Pilling (resurveyed by NHC). The discharge associated with the maximum water level was found to be 15,900 m^3/s. To start, the model was calibrated with an ice roughness matching the bed roughness of 0.030. It was found that a roughness of 0.047 matched the high water marks recorded for this event reasonably well. The resulting composite roughness coefficient was 0.037. The resulting water surface profile for jamming of the Mackenzie River during this event is depicted on **Figure 30**. The resulting ice jam rating curves for this calibrated roughness is depicted on **Figure 31**.

7.3.2 Liard River Rating Curve Calibration

An ice jam affected rating curve was developed using the estimated maximum water levels and corresponding discharges determined for breakup at the 10ED002 WSC gauge (RS 15057). Discharges associated with the rating curve ranged from 1000 m^3/s to 16000 m^3/s. Starting with an under ice roughness matching the bed roughness of 0.027, the roughness was gradually increased until it enveloped most of the available breakup water level data. It was found that an ice roughness of 0.075 enveloped most of the available data, resulting in a composite roughness of 0.060. The resulting ice jam rating curve, compared to the available ice affected breakup data and direct measurements collected by WSC are depicted on **Figure 32**. The computed ice jam water surface profile associated with this composite roughness for the discharge estimated for the 2021 breakup (6240 m^3/s) is depicted on **Figure 33**. Clearly identifiable highwater marks were not found along the Liard River during the NHC survey, however there were several piles of debris that were found and surveyed for comparison. The driftwood may be considered inadequate for calibration, but it was found to be useful for comparison to the estimated Liard River 2021 ice jam flood profiles.

7.3.3 Calibration Results Summary

Under ice coefficients for the Mackenzie River for the 2021 flood were calibrated to a value of 0.045. This was determined with a discharge of 15,900 m^3/s.

Under ice roughness for the Liard River using available breakup water elevation data were calibrated to a 0.075. This was determined using a rating curve with discharges ranging from 1000 m^3/s to 16000 m^3/s.

7.4 Sensitivity Analysis

A sensitivity analysis was completed on the calibrated ice jam model to determine the effects of changing the dominant model calibration parameter, Manning's roughness, on computed flood levels. Mannings roughness values were varied for open water, thermal ice, and ice jam conditions over the ranges listed in **Table 22**. The resulting sensitivity of the computed water levels to changes in Manning's roughness are illustrated by the calculated rating curves at the WSC gauges on the Mackenzie and Liard rivers depicted in **Figure 34** and **Figure 35**, respectively. For flood events associated with a 100-year to 200-year regulatory flood magnitude, the computed water levels vary by approximately ± 0.65 m and ± 0.50, for the Mackenzie and Liard rivers, respectively.

Table 22 Range of Manning's roughness values for sensitivity tests

Test	Manning's Roughness		
	Calibrated	Low Value	High Value
Open Water	0.028	0.023 (-0.05)	0.033 (+0.05)
Thermal Ice	0.028	0.023 (-0.05)	0.033 (+0.05)
Ice Jam	0.047	0.042 (-0.05)	0.052 (+0.05)

8 FLOOD MAPPING

The flood mapping provides a visual display of inundation for a given flood scenario. This study provides flood hazard mapping scenarios for the 100-year and 200-year regulatory floods. A notable difference in the current regulatory maps from the previous FDRP map is the current extent of inundation is determined from a sloping water surface profile whereas the previous FDRP map extent was based on a flat, constant water surface profile.

The methods used to determine the extent of inundation and hazard areas within are described as follows.

8.1 Inundation Mapping

The methodology used to create the flood inundation maps followed these steps, details of which are provided in the subsequent sections.

1. Create a 3D water surface elevation (WSE) triangular irregular network (TIN) that is representative of a contiguous flood level profile along modelled reaches, floodplain, and overland flow areas.
2. Create a 2D WSE grid with elevation values assigned to grid cells based on the values found in the WSE TIN.
3. Create a depth grid based on the WSE grid and underlying DTM.
4. Create inundation polygons based on the depth grid such that the polygon extents delineate positive depth areas, with polygon edges following zero depth contours.
5. Adjust the inundation polygons manually for areas where depths and hydraulic connectivity cannot be adequately resolved by the preceding steps.
6. Finalize the inundation extents, including smoothing and removal of isolated areas.

8.1.1 Water Surface Elevation TIN

The TIN inputs were based on the model geometry and water levels calculated for each cross section. Additional geometry was included to define the limits of the model and mapping domain. The inputs used to create the TIN are listed below. Feature information used to inform the TIN is included in parenthesis.

- Cross section lines (isoline with constant water surface elevation along cross section line). Cross section lines were extended from each end to ensure the TIN surface covered areas of ineffective flow between cross sections (e.g. backwater areas and small tributaries).
- Perimeter feature for clipping mapping results to the mapping domain.

Additional manual editing features used to modify the TIN were as follows.

- Polygons around areas of constant water surface elevation to inform manual edits for backwater and level pools – used to model backwater into the Snye.
- Breakline features to inform TIN interpolation. For example, a bounding polygon was used for the backwater area in the Snye to ensure features used to inform the backwater elevation in the Snye did not influence elevations elsewhere that were based on the flood elevation profile along the main channel.

The above inputs were then combined to create a WSE TIN with standard GIS TIN creation tools.

8.1.2 WSE and Depth Grids

The WSE grid was created directly from the WSE TIN using ArcGIS Pro tools. The WSE grid provides a raster data set with water surface elevation values at the same cell resolution and is congruent with the underlying Digital Terrain Model (DTM). The depth grid was created by subtracting the underlying DTM elevation values from the WSE grid values. WSE and depth values are based on the Canadian Geodetic Vertical Datum of 2013 (CGVD2013a; Epoch 2010.0).

8.1.3 Inundation Polygons

Inundation polygons were created through a series of steps, described as follows.

Filtered Depth Mask: The first step was to create an inundation mask of wetted areas found within the depth grids. This step is based solely on positive depth values with no filtering. Negative depth values indicate dry cells and are assigned a *NoData* value. Positive depth values denote wet cells and were assigned a value of 1. This mask was denoted as the positive depth mask. The positive depth mask was further processed and filtered to aggregate contiguous areas of wet cells and remove patchy dry areas. This also minimizes the creation of small self-intersecting loops and knots in the resulting inundation polygon. This final mask was denoted as the filtered depth mask.

Inundation Polygons: Inundation polygons are created through a series of steps, beginning with conversion of the filtered depth mask into polygons. These initial inundation polygons were further processed by: ensuring there are no multipart polygons and dissolving contiguous polygon features; removing small, isolated polygon areas; and, filling small holes inside polygons.

Inundation Areas Classification: The inundation polygons were then examined and visually classified as direct inundation areas isolated areas of inundation (which were subsequently removed from the final inundation polygon). The final polygon area (isolated areas removed) was then used to mask the WSE and depth gridded datasets.

Final Inundation Extents: The final polygon areas (areas of direct inundation) were then smoothed to create the final inundation extents. Further visual checks were conducted to ensure proper nesting of flood extent limits across the range of flood frequency estimates.

8.2 Flood Hazard Mapping

8.2.1 Floodway and Flood Fringe Terminology

The following provides terminology adopted for this study pertaining to the flood hazard mapping. The descriptions below provide an additional detail to the general definitions provided in the guidelines.

Flood Hazard Map

A flood hazard map defines the areas at risk of flooding (flood hazard area) for the specified regulatory flood and subdivides that flood hazard area into the floodway and flood fringe. Flood hazard maps may include additional flood hazard information to support community planning.

Floodway

The floodway carries most of the discharge during the regulatory flood event. Under open water conditions, it is the area where the flow is deepest, fastest, and most destructive. For ice conditions it also includes areas exposed to moving ice – it is difficult to envision a condition under which moving ice would not be considered dangerous and destructive. Criterion based on flow velocities would rarely apply or be impractical since high velocities would most always be associated with depths greater than 1 m or a moving ice condition.

Flood Fringe

The flood fringe depicts areas of flood hazard area outside of the floodway. The flood fringe typically represents areas with shallower, slower, and less destructive flooding but it may contain areas considered to be of significant hazard. Under ice-affected conditions, the flood fringe may or may not be occupied by ice. This will depend on whether the ice thickness exceeds the water depth into specific areas of the flood fringe.

8.2.2 Regulatory Floods

The regulatory flood typically represents a severe flood with a low annual exceedance probability, such as AEP = 1%. The 1% and 0.5% AEP events, equivalent to 100-yr and 200-yr recurrence intervals, were selected in consultation with the technical committee, as flood magnitudes to be mapped.

Regulatory flood profiles were created for the following scenarios.

- 100-year ice jam flood (AEP = 1%).
- 200-year ice jam flood (AEP = 0.5%).

The resulting flood profiles for these scenarios are plotted in **Figure 36** and **Figure 37** for the Liard and Mackenzie rivers, respectively. These flood level profiles were those corresponding to the 1% and 0.5% exceedance elevation values determined, section-by-section, from the Monte Carlo analysis. The calculated flood elevations for these scenarios are tabulated in **Appendix C** River stations are denoted in kilometres on the plots and metres in the appendix, following the model river cross section stationing. Regulatory flood levels estimate at the gauge locations are listed in **Table 22**. The corresponding model cross section is denoted by the river station (RS).

Table 23 Estimated Flood Frequency Levels: Mackenzie River at Fort Simpson (10GC001) and Liard River near the Mouth (10ED002)

Scenario	Mackenzie River at Fort Simpson (10GC001): RS 22338 m		Liard River near the Mouth (10ED002): RS: 15057 m	
	Gauge Height (m)	Elevation (m)[1]	Gauge Height (m)	Elevation (m)[1]
100-year Open Water	10.25	119.87	9.59	124.39
20-year Ice Jam	14.12	123.74	14.15	128.95
100-year Ice Jam	16.03	125.65	15.85	130.65
200-year Ice Jam	16.50	126.12	16.48	131.28

1. Canadian Geodetic Vertical Datum of 2013 (CGVD2013a)

For this study, the 100-year ice jam and 200-year ice jam flood scenarios were adopted as the regulatory floods used for development of the ice jam flood hazard maps. The other floods are provided for comparison.

8.2.3 Floodway Determination

The following criteria were considered in determination of the floodway.

- **Depth and Velocity:** Areas where depths exceed 1 m or where flow velocities are greater than 1 m/s were considered to be part of the floodway. For this study, the regulatory flood is an ice jam flood and so depths were the dominant criteria.
- **Hydraulic Smoothing:** In some instances, exceptions to the depth and velocity criterion can be made to support creation of a hydraulically smooth floodway. Consideration for these adjustments are typically limited to small backwater areas or ineffective flow areas.
- **Active Channel:** The floodway must always include the main channel.
- **Previously Defined Floodway:** When a floodway is being updated (from a previously defined floodway) consideration must be given for potential need for additional criteria pertaining to the previously defined floodway. The need for, and definition of, any additional criteria should be determined with the project manager in consultation with the community.

- **Areas in the Floodway:** The floodway extends fully across the channel. Areas within the floodway extents that do not exceed the floodway determination criteria (e.g. small islands or areas not exceeding the 1 m depth or 1 m/s velocity) are included in the floodway. Exceptions may be made for larger islands with extensive dry areas or areas protected by engineered flood control structures. Determination of these areas was done with approval by the project manager and in consultation with the community.

For this study, the 1 m depth criterion governed the floodway extents for both the 100-year and 200-year ice jam flood scenarios.

8.2.4 Flood Hazard Maps

The resulting flood hazard maps are included in **Appendix D** and **Appendix E**, for the 1% AEP (100-year) and 0.5% AEP (200-year) ice jam floods, respectively. The floodway is depicted on the flood hazard mapping as a darker shade of red than the surrounding flood fringe areas which are depicted in a lighter red to pink tone.

9 CLIMATE CHANGE CONSIDERATIONS

9.1 Objective

The objective of this assessment is to present a qualitative review of foreseeable or plausible climate change impacts pertaining to ice jam flooding experienced by the communities at Fort Simpson and reaches near the confluence of the Mackenzie and Liard rivers. To meet this objective, we review the technical literature on ice jam flooding most pertinent to this region, as well as the quantitative climatic projections for seasonal air temperature and streamflow made available by the Canadian government. The resulting review presents a qualitative assessment of the future evolution of ice jam flood risk under climate change and a first picture of the factors to consider towards a more quantitative assessment.

The goals of the Government of the Northwest Territories Climate Change Strategic Framework[1] are as follows:

1. Transition to a strong, healthy economy that uses less fossil fuel, thereby reducing greenhouse gas emissions by 30% below 2005 levels by 2030.
2. Improve knowledge of the climate change impacts occurring in the NWT.
3. Build resilience and adapt to a changing climate.

[1] https://www.gov.nt.ca/ecc/en/services/climate-change/2030-nwt-climate-change-strategic-framework

The context and motivation for this assessment follows, primarily, under the second goal. Further details pertaining to goal 2 are provided in **Appendix F**.

9.2 Climate Setting

The Mackenzie River primarily flows from the south to the northwest and then north. Typically, the breakup sequence begins in April (in the south) and progresses northward over a period of about 10 weeks. This creates conditions favourable for the development of ice jams and associated flooding. Significant ice jam floods have occurred during spring breakup on the Mackenzie River and its tributaries, including the Liard River. The community of Fort Simpson is often at risk of ice jam flooding over spring breakup.

With climate change, Arctic regions are warming well above global average rates, and northern subbasins of the Mackenzie River (below Fort Simpson) may continue warming faster than the more southern subbasins, upstream of Fort Simpson. If this trend continues it would influence the breakup progression. The outcome of a shift in the breakup progression with respect to ice jam frequency and severity is uncertain.

The Mackenzie Basin, upstream of Fort Simpson, experiences most of its rainfall between May and September. While snowfall can occur in any month, most of the snowfall occurs from October to April. Maximum flood levels on the Liard and Mackenzie rivers occur during freshet peaks with the delivery of snowmelt water during spring break up. Minimum flows are experienced during the winter season.

9.3 Climate Change Information

This section provides an overview of the available data and key findings of relevant studies pertaining to climate change in a northern setting, characteristic of this study. The review emphasized information relating to river ice processes influencing breakup ice jam flooding.

9.3.1 Climate Projection Data

The most scientifically defensible method for obtaining projections of climatic variables for any specific global region utilizes computerized models of the earth's climate, known as global climate models (GCMs). GCMs are increasingly being referred to as earth system models (ESMs) – a name that reflects that they now include more detailed representations of interactions between the land surface and the atmosphere including geochemical cycles and climate feedback. Different ESMs have been developed in research institutions around the world and are continuously being improved upon with the incorporation of new findings and datasets. The results of several dozen ESMs from multiple institutions are compiled every few years and available to the public.

A new report is released every few years by the Intergovernmental Panel on Climate Change (IPCC) summarizing the ESMs' projections, as well as peer-reviewed research based on those projections and environmental monitoring. The most recent is the IPCC's Sixth Assessment report released in 2021-2023, and its various volumes are available from the government of Canada data portal online[2]. Downscaled seasonal air temperature and precipitation data were downloaded for the Liard watershed from the Canadian government's IPPC data portal. The projection data informing this study arose from the Coupled Model Intercomparison Project no. 6 dataset (CMIP6). Further explanation of the CMIP6 datasets and associated emission scenarios, rationale for the choice in downscaled data sets, and associated emission scenarios are detailed in **Appendix F**. The emission scenarios, referred to herein, are explanatory storylines referred to as *shared socio-economic pathways* (SSPs) that relate to different future greenhouse gas concentrations scenarios, denoted as *representative concentration pathways* (RCPs). The scenarios adopted for this study are listed **Table 23**.

Table 24 Adopted Global Emission Scenarios (adopted from Riahi et al., 2017)

Scenario	Description
Low Emissions SSP1-2.6	The world shifts gradually, but pervasively, toward a more sustainable path, emphasizing more inclusive development that respects perceived environmental boundaries. Management of the global commons slowly improves, educational and health investments accelerate the demographic transition, and the emphasis on economic growth shifts toward a broader emphasis on human well-being. Driven by an increasing commitment to achieving development goals, inequality is reduced both across and within countries. Consumption is oriented toward low material growth and lower resource and energy intensity.
Moderate Emissions SSP2-4.5	The world follows a path in which social, economic, and technological trends do not shift markedly from historical patterns. Development and income growth proceeds unevenly, with some countries making relatively good progress while others fall short of expectations. Global and national institutions work toward but make slow progress in achieving sustainable development goals. Environmental systems experience degradation, although there are some improvements and overall the intensity of resource and energy use declines. Global population growth is moderate and levels off in the second half of the century. Income inequality persists or improves only slowly and challenges to reducing vulnerability to societal and environmental changes remain.

Projections of seasonal mean temperature and precipitation corresponding to the Liard River watershed above Fort Simpson are depicted on **Figure 38** and **Figure 39**, respectively. Projections for other portions of the watershed were checked (though not shown) and projected

[2] https://www.ipcc.ch/

trends were found to be very similar for other subbasins; in spite of the substantial differences in topography, vegetation, permafrost, and local climate. And so, the trends corresponding to the Lower Liard River subbasin were considered to be indicative of the entire watershed – examination of all subbasins offered no additional interpretive value (and thus, are not shown herein). Data depicted in the figures was extracted from the Canadian government ClimateData portal[3].

Mean ensemble values for each season are represented by the solid lines. Ensemble simulations for the historical period are represented in black (ensemble mean) and the grey shaded area (which ranges from the lowest to highest value of the individual ESMs). This historical period, for which the projections have been bias-corrected to approximately match observations, ranges from 1950 to 2013. Starting in 2014, the blue and green lines indicate projections for SSP1-2.6 and SSP2-4.5, respectively. The shaded blue and green areas range from the lowest to highest value of the individual ESMs. Warming in the contemporary period (2011-2040) is similar for the two SSPs, but in future periods becomes more pronounced for SSP2-4.5 compared to the lower-emissions SSP1-2.6. Rates of warming are considerable for all seasons, and especially large for the winter season. The sharpest rate of temperature rise is seen in the contemporary period, 2011-2040.

Projected air temperatures of ensemble mean projections (indicated by the solid blue and green lines of **Figure 38**) for the fall season were found to be crossing the 0°C line into non-freezing temperatures in the late contemporary (2011-2040) to early future (2040-2070) periods. For the spring season, temperatures cross over the 0°C line in the contemporary period (2011-2040). For precipitation, moderate increases are projected for all seasons, for both SSPs, with SSP2-4.5 tending toward larger increases (as depicted in **Figure 39**). The combination of projected higher air temperature and higher precipitation will produce higher mean streamflow in the fall and spring. Further, a progressive thawing of the permafrost could further affect seasonal flows with a change in hydrologic response over the spring melt period. Shorter winter seasons could result in thinner, weaker ice covers. The potential for winter rainfall events could lead to the occasional mid-winter breakup of the ice cover events by dynamic processes.

9.3.2 Study-specific Climate Research

The foreseeable outcomes of the climate projections, implied by the data in previous section, on ice jam flood frequency and severity were explored on the basis of review of the scientific literature found to be most relevant to this topic and study area. Some of the publications reviewed in this study were themselves literature reviews including Turcotte et al. (2019), while others focused on particular aspects of river ice processes (as documented in **Appendix F**). The

[3] https://climatedata.ca

review was documented in the context of the following processes considered important (for this study) towards understanding the impacts of climate change on ice jam frequency and severity.

- Snow accumulation and snowmelt
- Streamflow
- Ice formation and growth
- Breakup characteristics
- Channel morphology

Snow accumulation and snowmelt

The climate projections indicate a shorter winter period with increased temperature and increased precipitation which suggest the following trends.

- A reduced snowpack with less snow water equivalent available for the spring melt can contribute to a decrease in spring runoff peaks.
- For a projected increase in temperature and precipitation, the rate of snowmelt, attributed to thermal processes and rain-on-snow conditions, would also increase – suggesting an increase in spring runoff peaks.
- A reduced snow thickness on established ice covers which would increase the rate of heat transfer between the solid ice cover and air. This would tend to increase the rate of thermal ice growth over periods of freezing temperatures and increase the rate of thermal decay during episodes of above zero temperatures.

These projections present competing trends in both peak spring runoff rates and ice cover growth. For this desktop review, it is not apparent as to whether there is a dominant process (in either mechanism) to suggest a clear trend in either ice thickness and or spring runoff peaks.

Streamflow

As a result of warming in the fall and spring, seasonal flows throughout the southern Mackenzie River will experience changes in their seasonal means and seasonal peak flow frequencies. An increase in precipitation and a delay in the timing towards freezing air temperatures falling below 0°C, may implicate a progressive transition from snowfall to rainfall and higher mean seasonal flows and peak flows in this season. However, the anticipated increase in evapotranspiration (attributed to warming temperatures) affords more basin storage with dryer soils which would tend to offset any increase seasonal flows. Von de Wall et al. (2010) noted a trend toward earlier arrival of the spring freshet throughout the Mackenzie River basin.

Potential implications of permafrost warming and thaw are potentially significant to changes in streamflow. St. Jacques and Sauchyn (2009) surmised that thawing of permafrost will increase

infiltration capacity and amplify baseflow, which may augment minimum flows in winter. Permafrost thaw can also amplify surface runoff response and therefore peak flows, due to increased surface connectivity. This phenomenon was studied specifically for the lower Liard River basin by Connon et al. (2014). Changes in the landscape following permafrost thaw may also change the way in which water is stored and cycled on the landscape.

Climate projections on temperature and precipitation indicate an increase in both seasonal average and peak runoff rates though the ice-affected period and breakup. These changes in the hydrograph have implications on river ice which are described within the relevant processes that follow.

Ice formation and growth

Ice formation begins in the fall as freezing temperatures cool the water to just below 0°C (denoted as a *supercooled* condition) at which time the ice begins to form in the river and collect on the surface to form a cover. This cover of ice continues to grow in thickness over the winter period until it eventually decays and breaks up in the spring. A list of potential effects of climate projections relating to ice formation and growth are as follows.

- Increase in flows in late autumn and early winter can delay and prolong freeze-up resulting in thicker yet potentially less stable ice covers (Prowse et al., 2007; Burrell et al., 2023). Thicker covers advance upstream at a slower rate and a less stable cover is more prone to breakup.
- The growth of the cover over the winter season relies on persistently freezing temperatures. It is intuitive that as mean temperatures increase, initial ice formation (the fall freeze-up) is delayed, and winter ice growth diminishes.

Breakup characteristics

Climate projections indicate changes in the breakup characteristics in response to an increase in freeze-up level, an earlier onset of breakup, and an increase in peak runoff rates. The changes are described as follows. An expanded description of these deductions are provided by (Beltaos et al., 2006; Turcotte et al., 2019; and Zhao, 2012).

- A higher freeze-up level would require a higher streamflow threshold capable of initiating ice breakup which can potentially reduce the frequency of ice jams. However, when ice jams do occur, they will tend to be more severe due to the incrementally higher flows.
- An earlier onset of breakup could present comparatively weaker covers due to limited thermal thickening over a shortened winter period. This suggests an increase in the frequency of mechanical breakups and possibly an increase in the rate of the advancing breakup front. However, it is not apparent to the authors as to how this may impact ice jam severity.

Channel morphology

Climate projections indicate an increase in the rate of permafrost melt, which can result in a weakening of the banks and change in sediment supply (Ettema and Day, 2004). While these changes are expected to lead to some degree of morphological change, those changes are site specific, and can vary along the reach. It is uncertain how these changes may affect ice jam frequency and severity (Turcotte et al., 2019).

9.4 Trends in Historical Breakup Data

Historical data developed for this study (peak breakup discharge, and peak breakup water levels) were examined for trends. Annual time series of peak breakup level, peak breakup discharge, and associated breakup dates are depicted on **Figure 40**, **Figure 41**, and **Figure 42**, respectively. The trends found in the historical data are as follows.

- Linear fits to the historical **level** data suggests a downward trend in Mackenzie breakup levels and upward trend in Liard breakup levels. However, the P-Values for these trends (0.4334 and 0.1913, respectively) indicate high probabilities (43% and 19%) there is no trend in the data. Therefore, it is not possible to reliably discern a trend in breakup levels from the historical data.
- For historical breakup **discharge**, there is an upward trend in the historical data for both the Mackenzie River (P-Value = 0.0203) and Liard River (P-Value = 0.0034). These relatively low P-Values (less than 0.05) indicate a low probability the datasets had no trend.
- Linear trends fit to historical **breakup dates** (expressed in Julian days) suggested a downward trend (denoting an earlier occurrence of breakup). However, the P-Values for these trends indicated high probabilities (47% and 38%) there is no trend in the data. Therefore, it is not possible to reliably discern a trend in breakup dates from the historical data.

9.5 Qualitative Assessment

The qualitative assessment considers the climate projections on temperature and precipitation (recall **Figure 38**, **Figure 39**) and trends in the historical breakup data (recall **Figure 40**, **Figure 41**, and **Figure 42**). From these trends, inferences were made concerning their impacts on ice jam flood frequency and severity. The following is based on the authors' understanding of river ice processes and is supported by the relevant research reviewed during this study. The following lists key findings from this qualitative assessment.

- **Temperature** projections indicate a warming in the fall season with mean air temperatures reaching 0° C by the mid-century period (2041-2070).

- **Precipitation** projections indicate a "slight" to "moderate" increases in mean precipitation in the fall and winter seasons, respectively for the mid-century period (2041-2070).
- The **combined** affects of these temperature and precipitation projections lead to the following.
    - An increase in mean streamflow over freeze-up, and a prolonged freeze-up period. This can contribute to thicker, more competent ice covers on average or at usual lodging points.
    - An increase in peak flows over breakup causing an increase in the frequency of mechanical breakups and more severe ice jams.
    - A reduction in thermal ice growth leading to the development of less competent ice covers over the winter period. This is attributed to warmer temperatures, insulating effects of increased snow cover, and a shorter ice growth period.
    - An increase in freeze-thaw cycles over winter which could lead to the creation of mid-winter breakup jams or secondary consolidation of existing freeze-up ice jams.
    - A progressive thawing of the permafrost.

9.6 Uncertainty

This qualitative assessment provides an overview of the potential trends in ice jam severity and frequency for the Liard and Mackenzie rivers near the confluence and around the Village of Fort Simpson. The findings of this assessment indicate a changing climate that will influence the frequency and severity of ice jam flooding, the degree to which is uncertain. As detailed in **Appendix F**, climate projections for temperature and precipitation are uncertain, especially for precipitation. Further, the projected impacts of these projections on ice jam severity and frequency should not be considered to persist indefinitely. Somewhat implicit in the assumptions by the authors under this assessment is that the current physiography, hydrography, and to some extent, ice regime, also represent a future condition associated with the climate projections. This may be reasonable for the nearer contemporary period (2011-2040) however, it may become less likely as we progress towards the end of the future period (2041-2070). The potential effects of Great Slave Lake on the regional climate may not be well represented by the CMIP6 earth system models – lake effects could moderate climatic changes (Huziy an Sushama, 2017).

9.7 Summary

The results of this assessment suggest either an increase or decrease in both severity and frequency of ice jam flooding arising from trends in the historical observations and projected climate scenarios. It is difficult to discern which responses to climate change are dominant; however, most tend to point towards an increase in ice jam frequency. Additional analysis

supported with a more comprehensive review of the findings of other researchers would be required to determine the dominant responses and attempt to quantify the incremental change in ice jam flood frequency and severity.

Nevertheless, the trends found in this qualitative study indicate that an increase in both magnitude and severity of ice jam floods are plausible, if not likely. As such, it is prudent to anticipate more frequent ice jam flooding in the future. The trends identified herein (as represented by CMIP6 dataset) are indicative of the contemporary and future terms (2011-2070) and are not considered applicable beyond the future period (approaching 2070 and later), that is, the frequency and severity of ice jam flooding are not forever increasing.

10 REFERENCES

Anderson, J.C. (1982). Liard and Mackenzie River Ice Break-up, Fort Simpson region, NWT, 1982. Environment Canada. Ottawa, ON.

Beltaos, S. (1995a). Breakup forecasting. Proceedings of the 8th Workshop on River Ice Winter Environments of Regulated River, Kamloops, British Columbia, 463-482

Beltaos, S. (1995b). *River ice jams*. Highlands Ranch, Colorado, USA.

Beltaos, S. (2002). Effects of climate on mid winter ice jams. Hydrological Processes. 16(4), 789–804.

Beltaos S. (2003).Threshold between mechanical and thermal breakup of river ice cover. Cold Regions Science and Technology. 37(1):1–13.

Beltaos, S. (2007). Hydro-climatic impacts on the ice cover of the lower Peace River. Hydrological Processes, 22(17), 3252–3263.

Beltaos, S. (2021). Assessing the Frequency of Floods in Ice-Covered Rivers under a Changing Climate: Review of Methodology. Geosciences. 2021(11)514-33, https://doi.org/10.3390/geosciences11120514

Beltaos, S., and Bonsal, B. (2021). Climate change impacts on Peace River ice thickness and implications to ice-jam flooding of Peace-Athabasca Delta, Canada. Cold Regions Science and Technology, 186, 103279. doi:10.1016/j.coldregions.2021.103279.

Beltaos, S., and Burrel, B. (2002). Climatic change and river ice breakup. Canadian Journal of Civil Engineering, 30(1).

Beltaos, S., and Prowse, T. (2009). River-ice hydrology in a shrinking cryosphere. Hydrological Processes, 23(1), 122–144. doi:10.1002/hyp.7165.

Beltaos, S., Prowse, T., Bonsal, B., MacKay, R., Romolo, L., Pietroniro, A., and Toth, B. (2006). Climatic effects on ice-jam flooding of the Peace-Athabasca Delta. Hydrological Processes, 20(19), 4031–4050. doi:10.1002/hyp.6418.

Brown, G. (2019). Application of a Hydrologic Model for Predicting River Ice Breakup. University of Waterloo. Waterloo ON. [online] Available from: https://uwspace.uwaterloo.ca/items/8972f8f3-d79f-4f12-8cf5-8fd6d7305002

Brown, L. C., and Duguay, C. R. (2010). The response and role of ice cover in lake-climate interactions. Progress in Physical Geography: Earth and Environment, 34(5), 671–704. doi:10.1177/0309133310375653.

Brunner, G.W. (2016). HEC-RAS, River Analysis System Hydraulic Reference Manual, US Army Corps of Engineers, Hydrologic Engineering Center Report CPD-69, February 2016, 547 pp.

Burn, D. H., Abdul Aziz, O. I., and Pietroniro, A. (2004). A Comparison of Trends in Hydrological

Variables for Two Watersheds in the Mackenzie River Basin. Canadian Water Resources Journal.

Burrell, B. C., Beltaos, S., and Turcotte, B. (2023). Effects of climate change on river-ice processes and ice jams. International Journal of River Basin Management, 21(3), 421–441. doi:10.1080/15715124.2021.2007936.

Burrell, B. C., Hokuna, M., Beltaos, S., Kovachis, N., Turcotte, B., and Jasek, M. (2015). Flood Hazard and Risk Delineation of Ice-Related Floods: Present Status and Outlook. CGU HS Committee on River Ice Processes and the Environment 18th Workshop on the Hydraulics of Ice Covered Rivers, Quebec City, QC, Canada.

Bush, E., and Lemmen, D. S. (2019). Canada's Changing Climate Report, Government of Canada, ON, 444p.

Chen, D. et al. (2021). Framing, context, and methods. Chapter 1. In Climate Change 2021: The Physical Science Basis, 147–286 (Cambridge University Press, 2021). [online] Available from: https://www.ipcc.ch/report/ar6/wg1/downloads/report/IPCC_AR6_WGI_Chapter01.pdf.

Coles, A. 2020a. NWT Flood Events

Coles, A. 2020b. Flood Maps of the Northwest Territories.

Connon, R. F., Quinton, W. L., Craig, J. R., and Hayashi, M. (2014). Connon, R.F., Quinton, W.L., Craig, J.R., and Hayashi, M. 2014. Changing hydrologic connectivity due to permafrost thaw in the lower Liard River valley, NWT, Canada. Hydrol. Processes, 28: 4163–4178. doi: 10.1002/hyp.10206. Hydrological Processes, 28, 4163–4178. doi:10.1002/hyp.10206.

Das, A., Rokaya, P., and Lindenschmidt, K.-E. (2020). Ice-jam flood risk assessment and hazard mapping under future climate. *Water Resources Planning and Management*, 146.

De Rham, L. Dibikie, Y., Belataos, S., Peters, D., Bonsal, B., and Prowse, T. (2020). A Canadian River Ice Database from the National Hydrometric Program Archives, Earth Syst. Sci. Data, 12, 183501860, https://doi.org/10.5194/essd-12-1835-2020, 2020.

Dessai, S., and Hulme, M. (2004). Does climate adaptation policy need probabilities? Climate Policy, 4(2), 107–128.

Dibike, Y., Prowse, T., Saloranta, T., and Ahmed, R. (2011). Response of Northern Hemisphere lake-ice cover and lake-water thermal structure patterns to a changing climate. Hydrological Processes, 25(19), 2942–2953. doi:10.1002/hyp.8068.

Ettema, R., and Daly, S. F. (2004). Sediment Transport Under Ice. Hanover, N.H. 63 pp.

Gidden, M. J. et al. (2019). Global emissions pathways under different socioeconomic scenarios for use in CMIP6: a dataset of harmonized emissions trajectories through the end of the century. Geosci. Model Dev., 12, 1443–1475.

Gillett, N. P. (2024). Halving of the uncertainty in projected warming over the past decade. npj Climate and Atmospheric Science, 7(1), 1–3. doi:10.1038/s41612-024-00693-3.

GNWT (2023). 2021 Spring Flooding - After Action Review. Government of Northwest Territories.

Healy, D. and Kovachis, N. (2023). Case Studies on Ice Jam Flood Frequency Estimation. Conference: 22nd Workshop on the Hydraulics of Ice Covered Rivers, Canmore, Alberta.

Huard, D., Fyke, J., Capellán-Pérez, I., Matthews, H. D., and Partanen, A.-I. (2022). Estimating the likelihood of GHG concentration scenarios from probabilistic integrated assessment model simulations. Earth's Future, 10. doi:10.1029/2022EF002715. [online] Available from: https://doi.org/10.1029/2022EF002715.

Huziy, O., and Sushama, L. (2017). Lake–river and lake–atmosphere interactions in a changing climate over Northeast Canada. Climate Dynamics, 48(9–10), 3227–3246. doi:10.1007/s00382-016-3260-y.

Jasper, J.N., and Kerr K.A. (1992). An Historic Flood: 1988 Flooding in the Liard and Mackenzie River Basins. Environment Canada, Yellowknife NWT.

Jumikis, A. R. (1977). Thermal Geotechnics.

Kriwoken, L. (1983). Historical Flood Review: Fort Simpson, Fort Norman, Fort Good Hope, Fort McPherson, Aklavik, Fort Liard, Nahanni Butte. Environment Canada. Ottawa ON.

Kwong, J., and Gan, Y. T. (1994). Northward Migration of Permafrost Along the Mackenzie Highway and Climatic Warming. Climatic Change, 26(4), 399–419.

Mackenzie River Basin Committee. (1981). Mackenzie River Basin Study Report. Mackenzie River Basin Committee, Canada.

McElhanney. (2020). NWT LiDAR Survey for Various Sites: Fort Simpson. Report prepared for Government of the Northwest Territories by McElhanney Ltd. Vancouver BC.

Michel, B. (1971). Winter Regime of Rivers and Lakes. Hanover, NH, USA.

Nakićenović, N. et al. (2000). Special Report on Emissions Scenarios. Cambridge University Press. [online] Available from: https://www.ipcc.ch/site/assets/uploads/2018/03/sres-en.pdf.

Northwest Hydraulic Consultants (NHC). (1974). Fort Simpson Water Intake Mackenzie River. Prepared for Strong, Lamb & Associates by Northwest Hydraulic Consultants. Edmonton AB.

Northwest Hydraulic Consultants (NHC). (1976). River Bed Investigation Fort Simpson Water Intake and Sewerage Outfall. Completed for Strong, Lamb, & Nelson Ltd by Northwest Hydraulic Consultants. Edmonton AB.

Northwest Hydraulic Consultants (NHC). (2021). Case Studies. Northwest Hydraulic Consultants. Edmonton AB.

Ollerhead and Associates. (2021). Spring 2021 Flood Level Mapping in the communities of Fort Simpson and Jean Marie River, Northwest Territories. Ollerhead and Associates. Yellowknife NWT.

O'Neil, H. C. L., Prowse, T. D., Bonsal, B. R., and Dibike, Y. B. (2017). Spatial and temporal

characteristics in streamflow-related hydroclimatic variables over western Canada. Part 2: future projections. Hydrology Research, 48(4), 932–944. doi:10.2166/nh.2016.045.

O'Neill, B. C., Kriegler, E., Riahi, K., Ebi, K. L., Hallegatte, S., Carter, T. R., Mathur, R., and van Vuuren, D. P. (2014). A new scenario framework for climate change research: the concept of shared socioeconomic pathways. Climatic Change, 122(3), 387–400. doi:10.1007/s10584-013-0905-2.

Park, H., Yoshikawa, Y., Oshima, K., Kim, Y., Ngo-Duc, T., Kimball, J. S., and Yang, D. (2016). Quantification of warming climate-induced changes in terrestrial Arctic River ice thickness and phenology. Journal of Climate, 29(5), 1733–1754.

Pilling, R. (2023). Email correspondence.

Prowse, T. D. (1984). Liard and Mackenzie River ice break-up Fort Simpson Region, N.W.T., 1983. Environment Canada. Ottawa, ON.

Prowse, T. D. (1985). Hydrometeorologic Conditions Prevailing During the 1984 River Ice Breakup, Fort Simpson Region, N.W.T. Environment Canada. Ottawa ON.

Prowse, T. D. (1986). Ice Jam Characteristics, Liard-Mackenzie rivers confluence. Canadian Journal of Civil Engineering. 1986;8(6):653-65. [online] Available from: https://cdnsciencepub.com/doi/10.1139/l86-100

Prowse, T. D., Bonsal, B. R., Duguay, C. R., and Lacroix, M. P. (2007). River-ice break-up/freeze-up: a review of climatic drivers, historical trends and future predictions. Annals of Glaciology, 46, 443–451. doi:10.3189/172756407782871431.

Riahi, K., van Vuuren, D. P., Kriegler, E., Edmonds, J., O'Neill, B. C., Fujimori, S., Bauer, N., Calvin, K., Dellink, R., Fricko, O., Lutz, W., Popp, A., Cuaresma, J. C., Kc, S., Leimbach, M., Jiang, L., Kram, T., Rao, S., Emmerling, J., Ebi, K., Hasegawa, T., Havlik, P., Humpenöder, F., Da Silva, L. A., Smith, S., Stehfest, E., Bosetti, V., Eom, J., Gernaat, D., Masui, T., Rogelj, J., Strefler, J., Drouet, L., Krey, V., Luderer, G., Harmsen, M., Takahashi, K., Baumstark, L., Doelman, J. C., Kainuma, M., Klimont, Z., Marangoni, G., Lotze-Campen, H., Obersteiner, M., Tabeau, A., and Tavoni, M. (2017). The Shared Socioeconomic Pathways and their energy, land use, and greenhouse gas emissions implications: An overview. Global Environmental Change, 42, 153–168. doi:10.1016/j.gloenvcha.2016.05.009.

Rokaya, P., Lindenschmidt, K.-E., Pietroniro, A., and Clark, M. (2022). Modelling of ice jam floods under past and future climates: A review. Journal of Hydrology X, 15(1). doi:https://doi.org/10.1016/j.hydroa.2022.100120.

Rühland, K. M., Evans, M., and Smol, J. P. (2023). Arctic warming drives striking twenty-first century ecosystem shifts in Great Slave Lake (Subarctic Canada), North America's deepest lake. Proceedings of the Royal Society B: Biological Sciences, 290(2007), 20231252. doi:10.1098/rspb.2023.1252.

Shiogama, H., Fujimori, S., Hasegawa, T., Hayashi, M., Hirabayashi, Y., Ogura, T., Iizumi, T., Takahashi, K., and Takemura, T. (2023). Important distinctiveness of SSP3–7.0 for use in

impact assessments. Nature Climate Change, 13. doi:10.1038/s41558-023-01883-2.

St. Jacques, J., and Sauchyn, D. J. (2009). Increasing winter baseflow and mean annual streamflow from possible permafrost thawing in the Northwest Territories, Canada. Geophysical Research Letters, 36(1), 2008GL035822. doi:10.1029/2008GL035822.

Stefan, J. (1891). Über die Theorie der Eisbildung, insbesondere über die Eisbildung im Polarmeere. Annalen der Physik und Chemie, 42, 269–286.

Turcotte, B. (2021). Flooding processes and recent trends in ice-induced high-water levels along rivers of Northwestern Canada. CGU HS Committee on River Ice Processes and the Environment, Saskatoon.

Turcotte, B., Burrell, B., and Beltaos, S. (2019). The Impact of Climate Change on Breakup Ice Jams in Canada: State of knowledge and research approaches. Conference: 20th Workshop on the Hydraulics of Ice Covered Rivers.

Turcotte, B., Morse, B., and Anctil, F. (2012). Impacts of precipitation on the cryologic regime of stream channels. Hydrological Processes, 26(17), 2653–2662. doi:10.1002/hyp.9438.

Turcotte, B., Morse, B., Bergeron, N. E., and Roy, A. G. (2011). Sediment transport in ice-affected rivers. Journal of Hydrology, 409(1–2), 561–577. doi:10.1016/j.jhydrol.2011.08.009.

Venmans, F., and Carr, B. (2024). Literature-informed likelihoods of future emissions and temperatures. Climate Risk Management, 44, 100605. doi:10.1016/j.crm.2024.100605.

Von de Wall, S. J., de Rham, L. P., and Prowse, T. D. (2010). The river ice break-up season in Canada: Variations in water levels and timing. Hancock, MA, pp. 11.

van Vuuren, D. P., Edmonds, J., Kainuma, M., Riahi, K., Thomson, A., Hibbard, K., Hurtt, G. C., Kram, T., Krey, V., Lamarque, J.-F., Masui, T., Meinshausen, M., Nakicenovic, N., Smith, S. J., and Rose, S. K. (2011). The representative concentration pathways: an overview. Climatic Change, 109(1–2), 5–31. doi:10.1007/s10584-011-0148-z.

University of Minnesota. (2024). ArcticDEM. University of Minnesota – PGC. Saint Paul, MN, USA. [Online]. Available from: https://www.pgc.umn.edu/data/arcticdem/. Accessed on August 22, 2024.

USGS. (2018). Guidelines for Determining Flood Flow Frequency – Bulletin 17C. U.S. Geological Survey, Reston, Virginia. 2018.

Warden, J. W., Rezvani, R., Najafi, M. R., and Shrestha, R. R. (2024). Projections of rain-on-snow events in a sub-arctic river basin under 1.5°C–4°C global warming. Hydrological Processes, 38(8), e15250. doi:10.1002/hyp.15250.

Zhao, L. (2012). River ice breakup forecasting using artificial neural networks and fuzzy logic systems (Doctor of Philosophy Thesis thesis). University of Alberta.

FIGURES

Government of Northwest Territories / Gouvernement des Territoires du Nord-Ouest; Canada; nhc	SCALE – AS SHOWN	FORT SIMPSON FLOOD HAZARD MAPPING STUDY
		STUDY LOCATION
	Job: 1008469 / *Date: APR-2025*	*FIGURE 1*

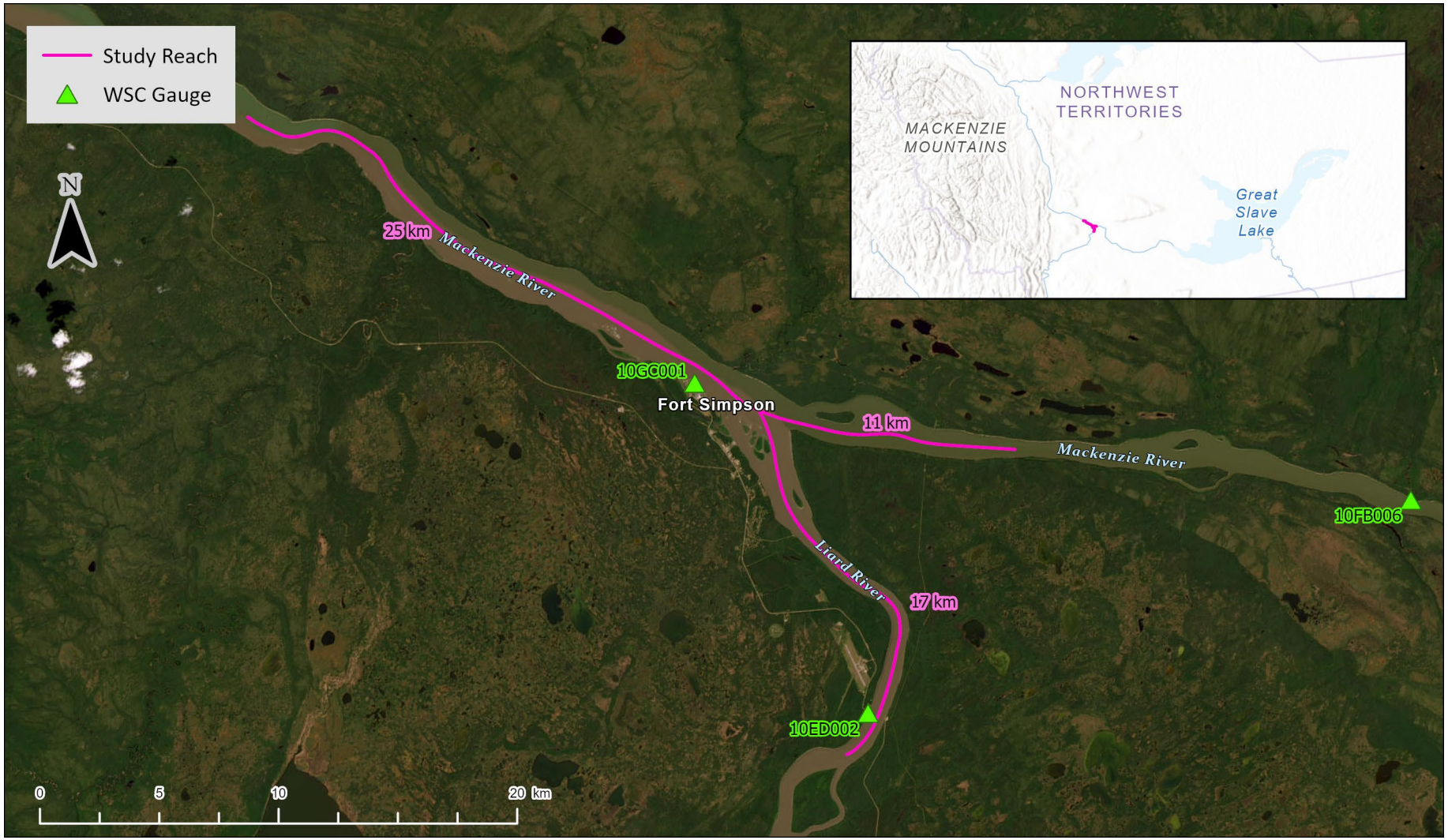

Government of Northwest Territories / Gouvernement des Territoires du Nord-Ouest; Canada; nhc	SCALE – AS SHOWN	FORT SIMPSON FLOOD HAZARD MAPPING STUDY ***STUDY REACH***
	Job: 1008469 / *Date: APR-2025*	*FIGURE 2*

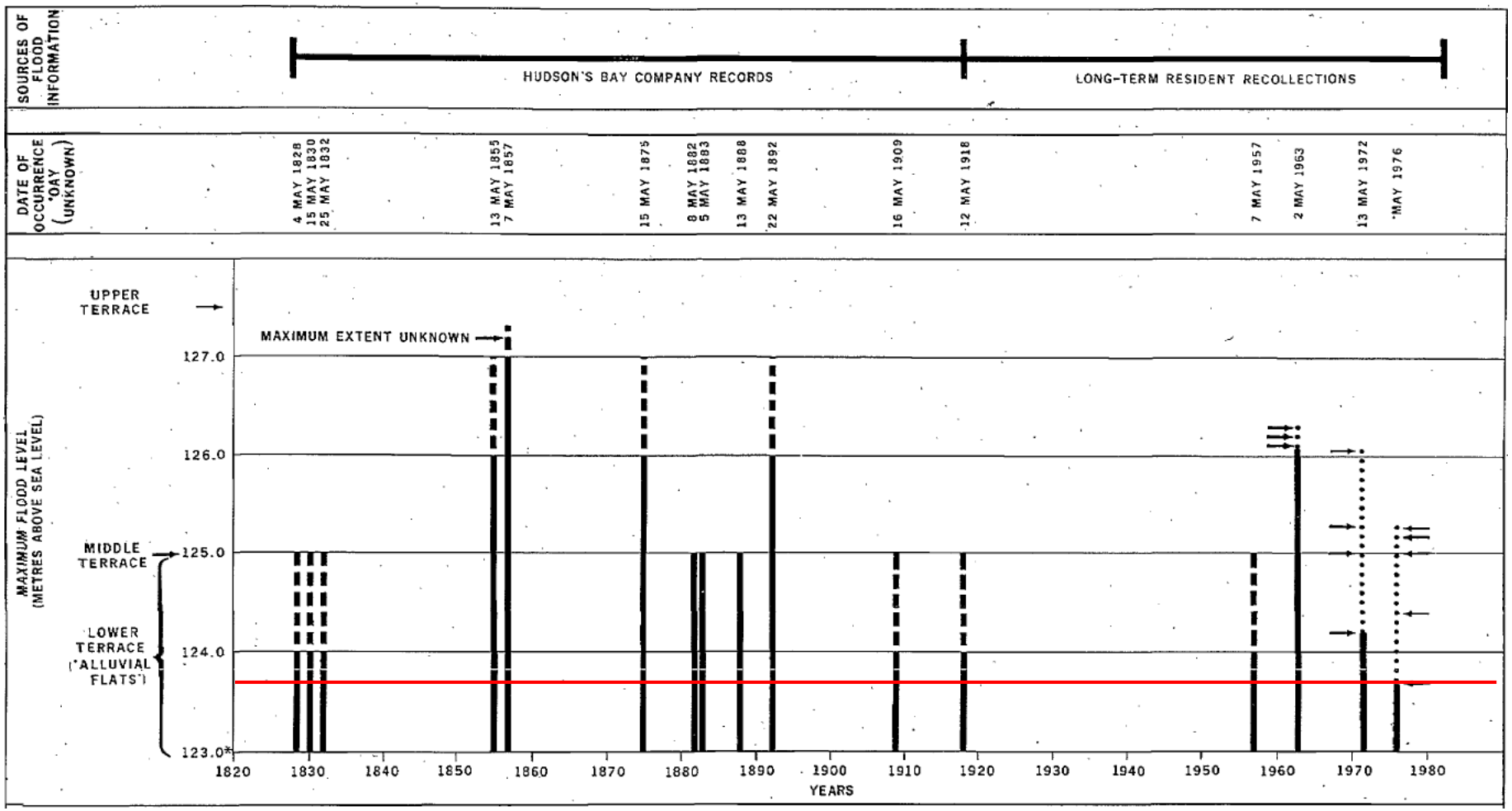

Notes: 1. Figures is adapted from Kriwoken, L. (1983).
2. Elevation reference GSC 1984 datum.

Threshold level, approximately 123.75 m.

Government of Northwest Territories / Gouvernement des Territoires du Nord-Ouest

Canada

nhc

UNITS – AS SHOWN

Job: 1008469

Date: APR-2025

FORT SIMPSON FLOOD HAZARD MAPPING STUDY

REPORTED HISTORICAL FLOOD LEVELS AT FORT SIMPSON

FIGURE 3

*Fork in the Rivers looking upstream on the Mackenzie River, **11 May 2021** (Photo Credit : Goose Flying Service).*

*Mouth of Martin River looking upstream on the Mackenzie River, **11 May 2021** (Photo Credit: Goose Flying Service).*

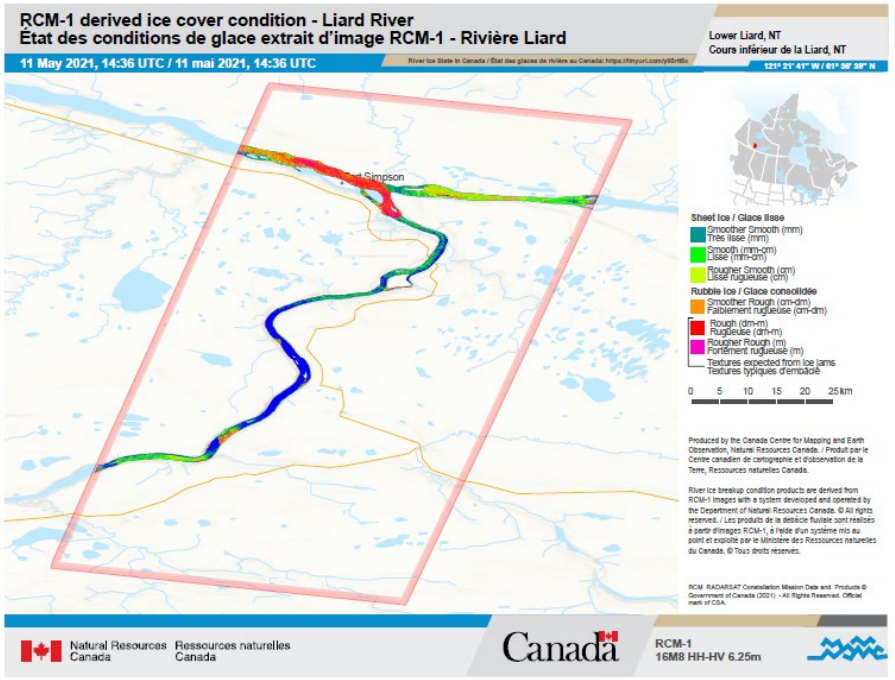

*RADARSAT Constellation imagery of the Liard and Mackenzie rivers near Fort Simpson. Image was acquired at **1200 on 11 May 2021**. Image processing provided by Natural Resources Canada. Blue denotes open water.*

Government of Northwest Territories / Gouvernement des Territoires du Nord-Ouest; Canada; nhc		FORT SIMPSON FLOOD HAZARD MAPPING STUDY ***2021 BREAKUP ICE CONDITIONS ON MAY 11TH***
	Job: 1008469	Date: APR-2025
		FIGURE 4

*Sentinel-1 Imagery of Fort Simpson acquired at on **12 May 2021 at 22:00**. Black sections denote open water. 'Pebbly' sections denote ice jams. It appears that the ice jam around Martin River (downstream of Fort Simpson) is starting to clear.*

*Fort Simpson, **14 May 2021** (Photo Credit: Leonard, Fort Simpson Facebook Bulletin).*

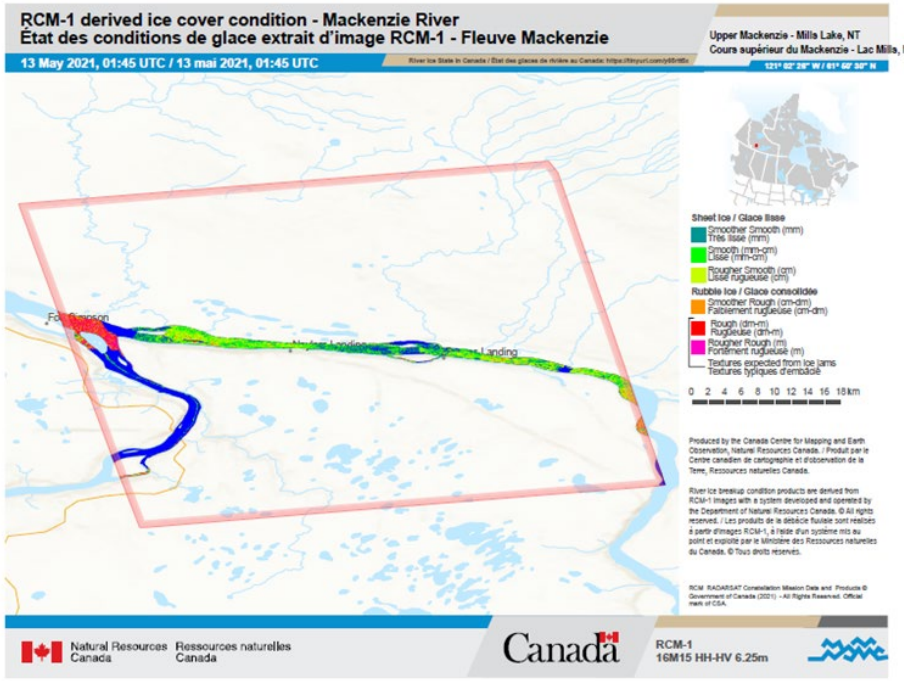

*RADARSAT Constellation imagery of the Liard and Mackenzie rivers near Fort Simpson. Image was acquired at **08:30 on 13 May 2021**. Image processing provided by Natural Resources Canada. Blue denotes open water.*

Government of Northwest Territories
Gouvernement des Territoires du Nord-Ouest

Canada

nhc

FORT SIMPSON FLOOD HAZARD MAPPING STUDY

2021 BREAKUP
ICE CONDITIONS ON MAY 12TH, 13TH & 14TH

Job: 1008469

Date: APR-2025

FIGURE 5

*Photos of the ice jams on the Mackenzie as of **15 May 2021**, downstream from Fort Simpson. (Photo credit: Troy Bradbury).*

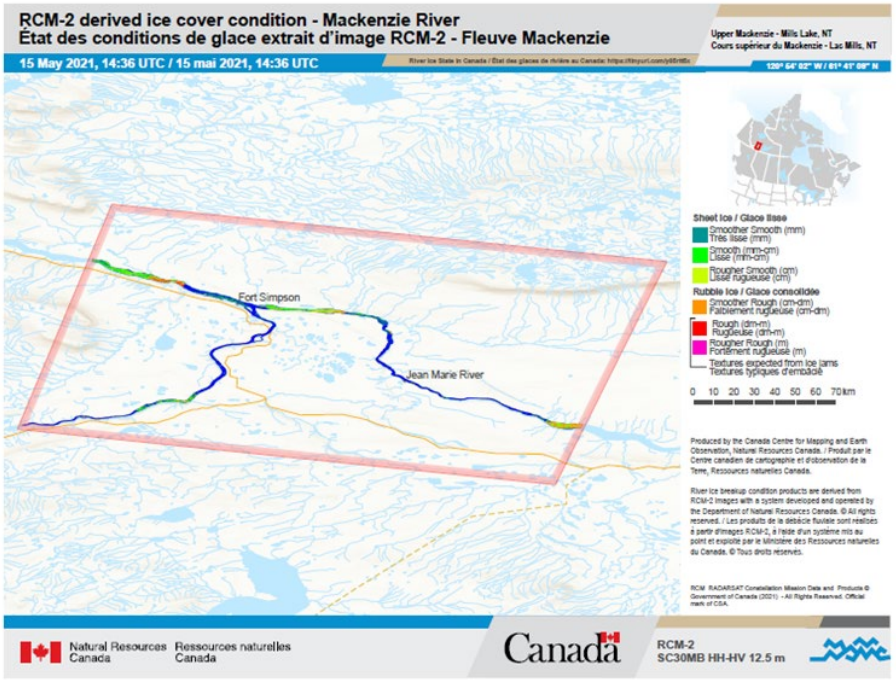

*RADARSAT Constellation imagery of the Upper Mackenzie River near Fort Simpson and Jean Marie River. Image was acquired at **10:00 on 15 May 2021**. Image processing provided by Natural Resources Canada. Ice jams that are pictured above are circled in red on this radar image.*

Government of Northwest Territories
Gouvernement des Territoires du Nord-Ouest

Canada

nhc

FORT SIMPSON FLOOD HAZARD MAPPING STUDY

2021 BREAKUP
ICE CONDITIONS ON MAY 15TH

Job: 1008469

Date: APR-2025

FIGURE 6

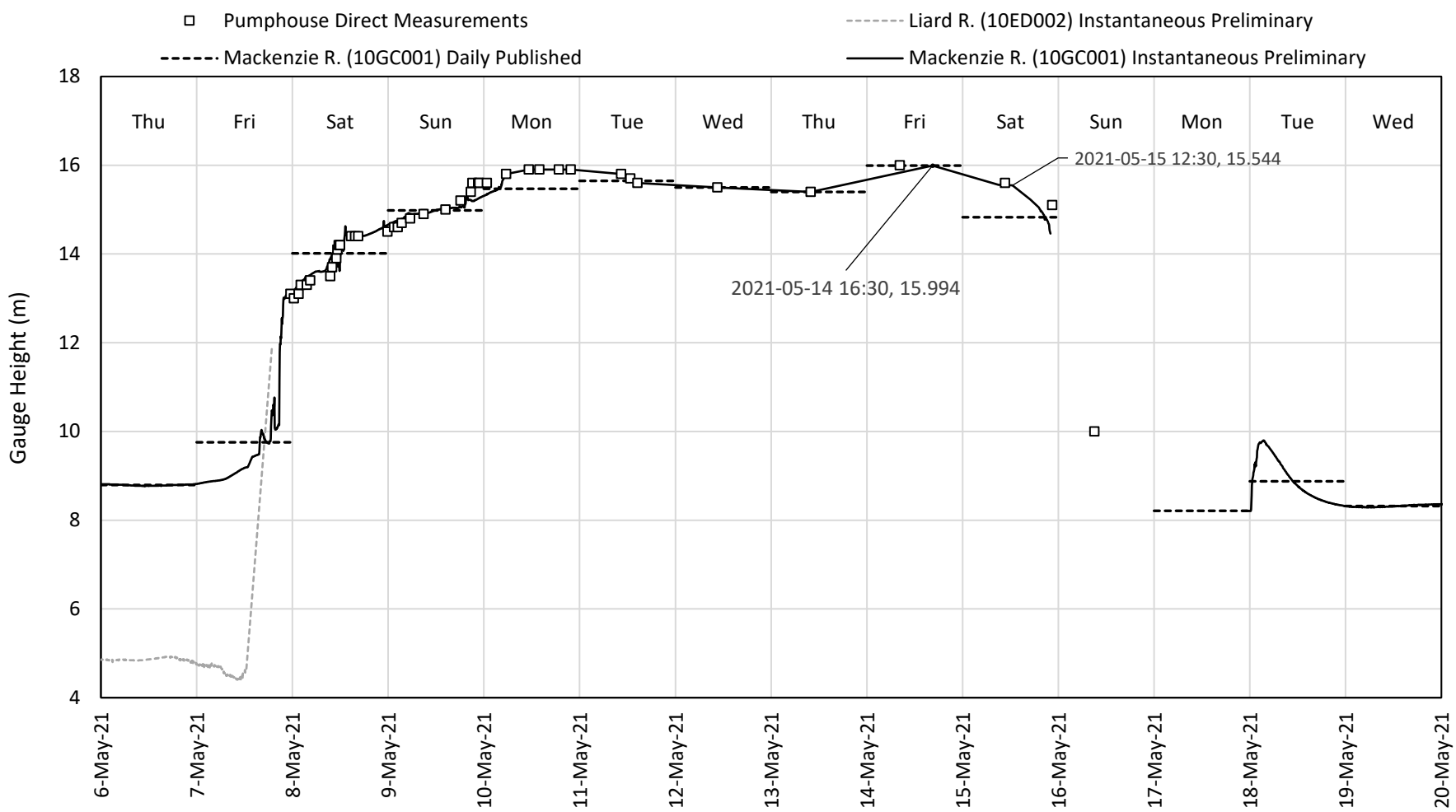

Government of Northwest Territories
Gouvernement des Territoires du Nord-Ouest

Canada

nhc

UNITS – AS SHOWN

FORT SIMPSON FLOOD HAZARD MAPPING STUDY

2021 BREAKUP LEVELS: MACKENZIE RIVER AT FORT SIMPSON AND LIARD RIVER NEAR THE MOUTH

Job: 1008469

Date: APR-2025

FIGURE 7

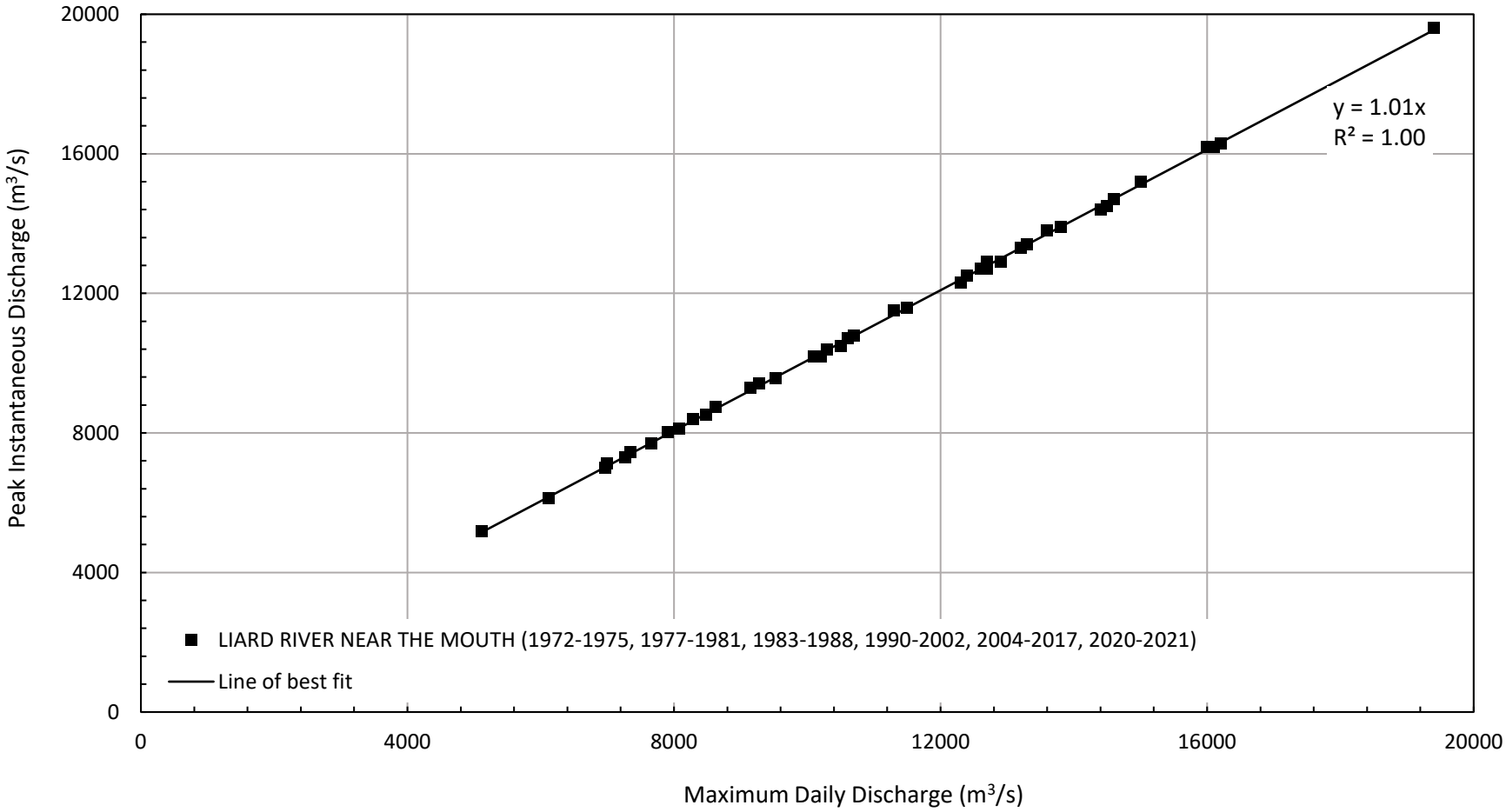

Government of Northwest Territories
Gouvernement des Territoires du Nord-Ouest

Canada

nhc

UNITS – AS SHOWN

Job: 1008469

Date: APR-2025

FORT SIMPSON FLOOD HAZARD MAPPING STUDY

PEAK INSTANTANEOUS VS MAXIMUM DAILY DISCHARGE LIARD RIVER NEAR THE MOUTH (10ED002)

FIGURE 8

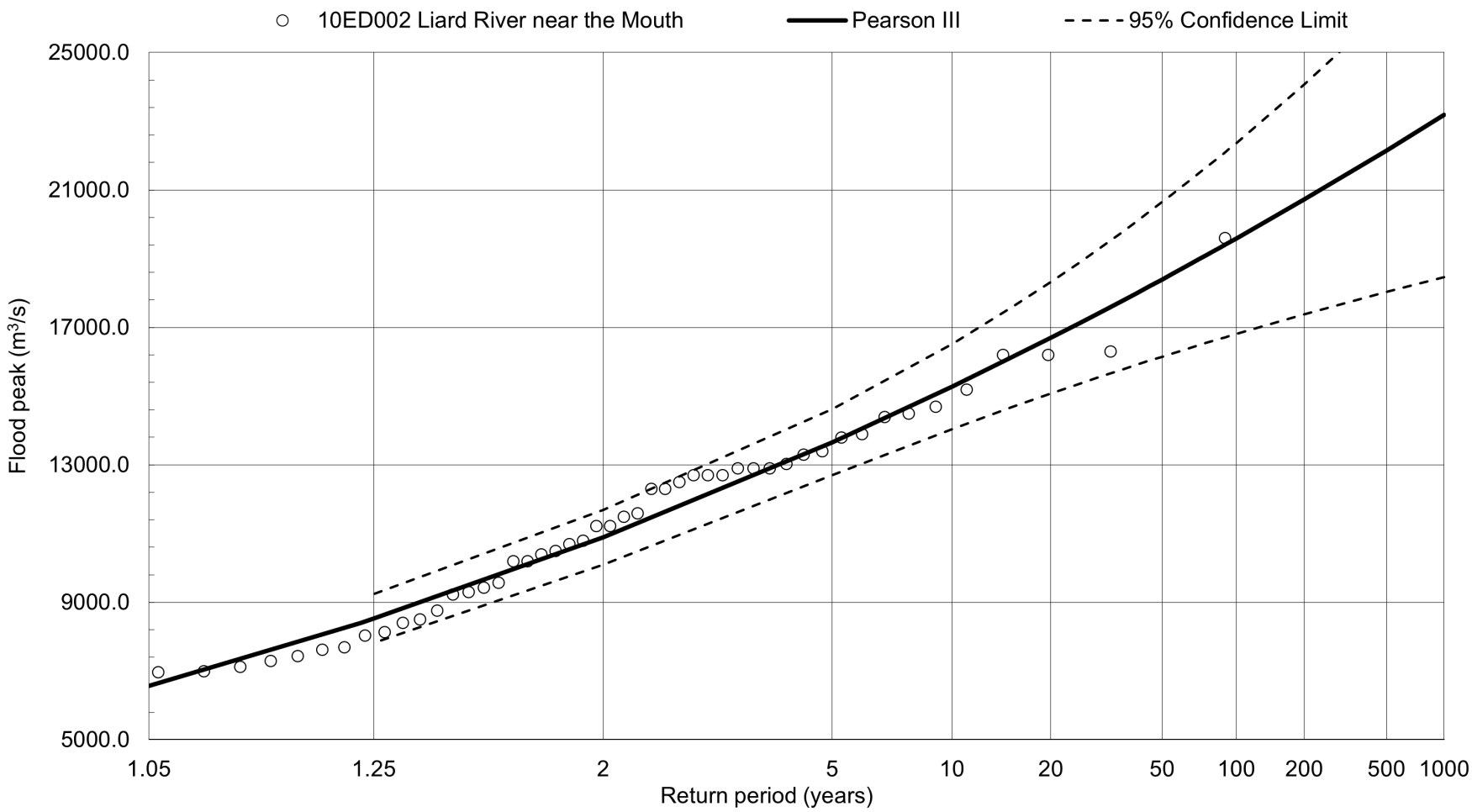

Government of Northwest Territories
Gouvernement des Territoires du Nord-Ouest

Canada

nhc

UNITS – AS SHOWN

Job: 1008469

Date: APR-2025

FORT SIMPSON FLOOD HAZARD MAPPING STUDY

OPEN WATER FLOOD FREQUENCY DISTRIBUTION LIARD RIVER NEAR THE MOUTH (10ED002)

FIGURE 9

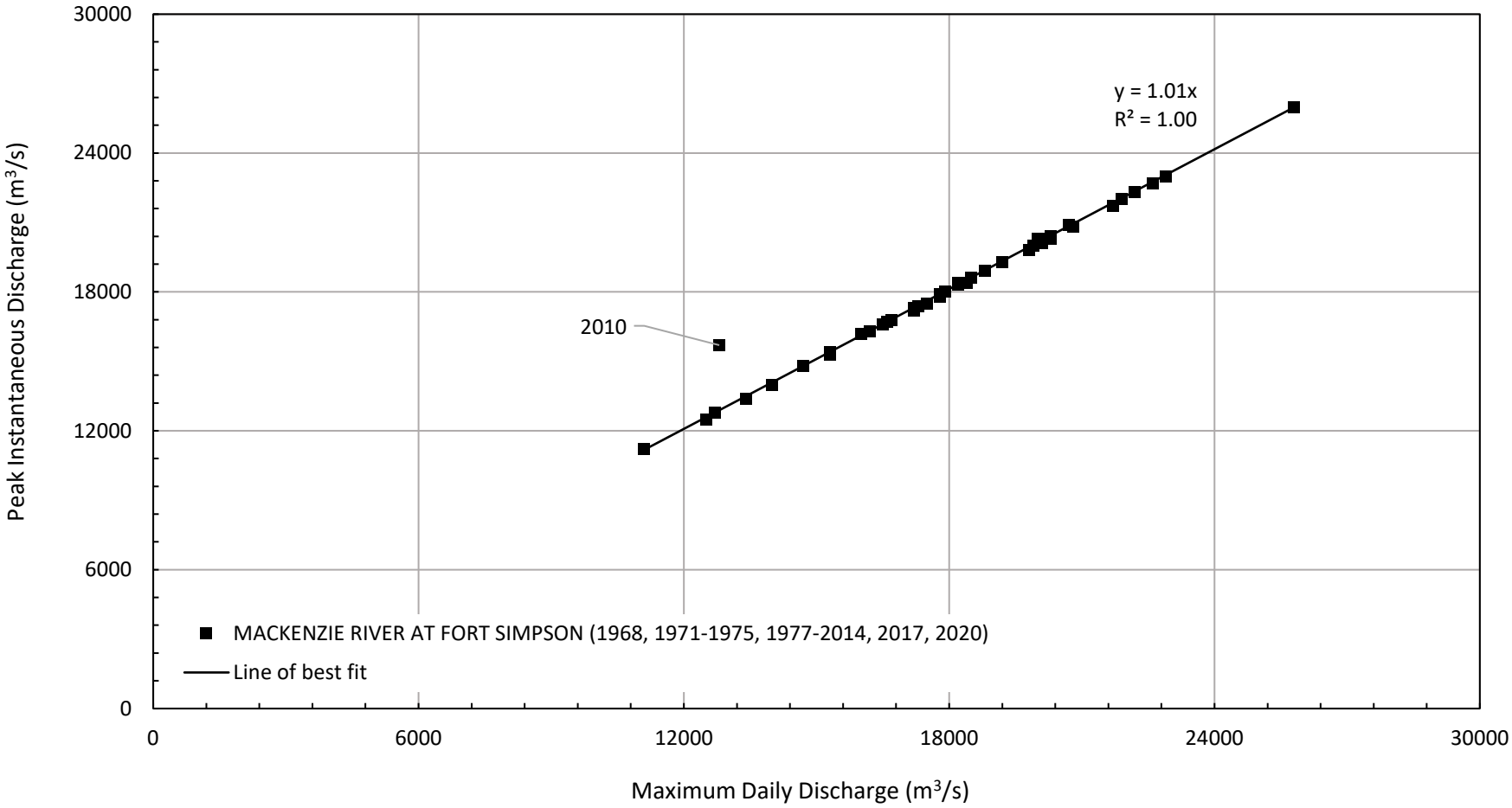

Government of Northwest Territories
Gouvernement des Territoires du Nord-Ouest

Canada

nhc

UNITS – AS SHOWN

Job: 1008469

Date: APR-2025

FORT SIMPSON FLOOD HAZARD MAPPING STUDY

PEAK INSTANTANEOUS VS MAXIMUM DAILY DISCHARGE MACKENZIE RIVER AT FORT SIMPSON (10GC001)

FIGURE 10

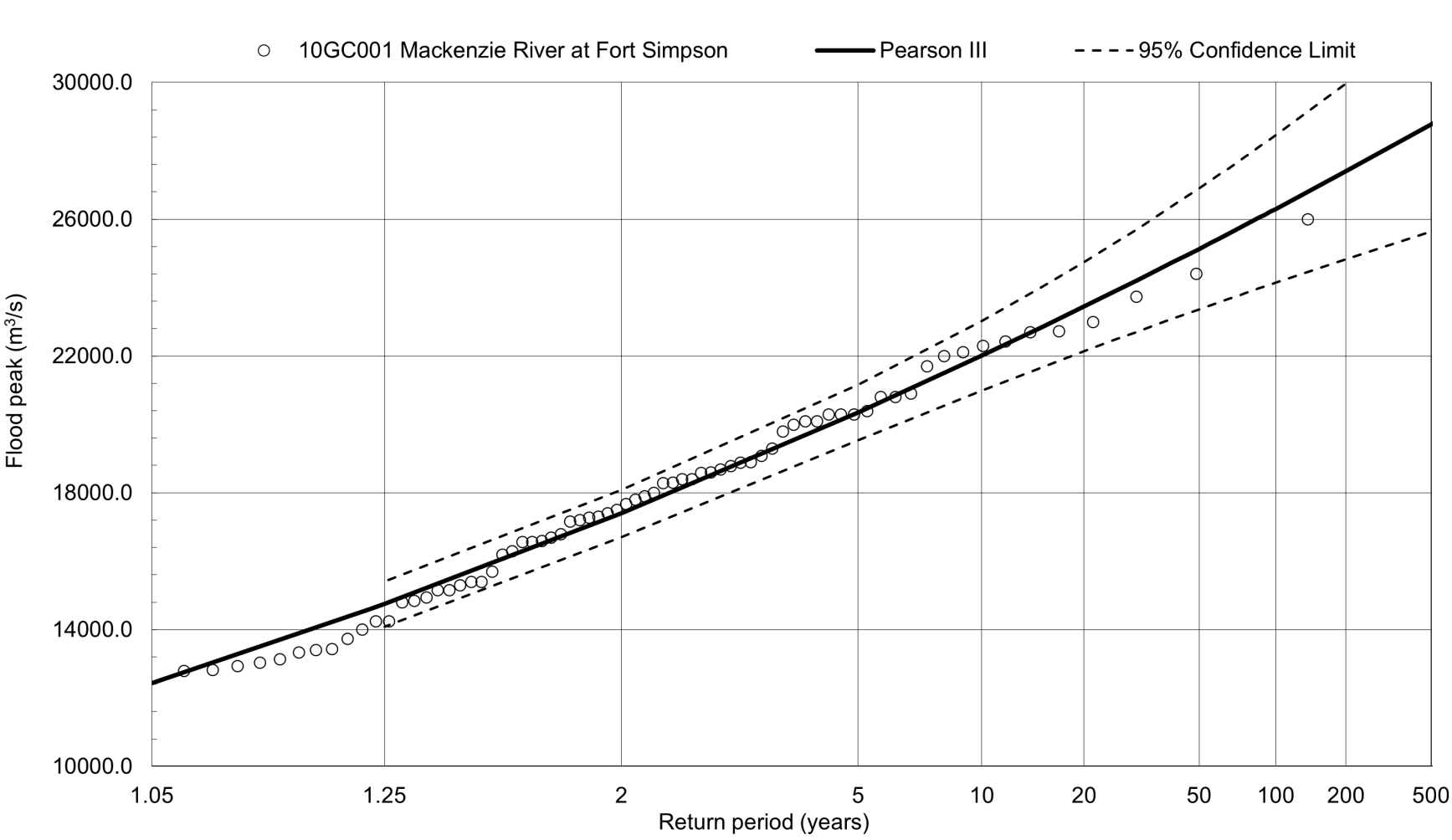

Government of Northwest Territories
Gouvernement des Territoires du Nord-Ouest

Canada

nhc

UNITS – AS SHOWN

Job: 1008469

Date: APR-2025

FORT SIMPSON FLOOD HAZARD MAPPING STUDY

OPEN WATER FLOOD FREQUENCY DISTRIBUTION MACKENZIE RIVER AT FORT SIMPSON (10GC001)

FIGURE 11

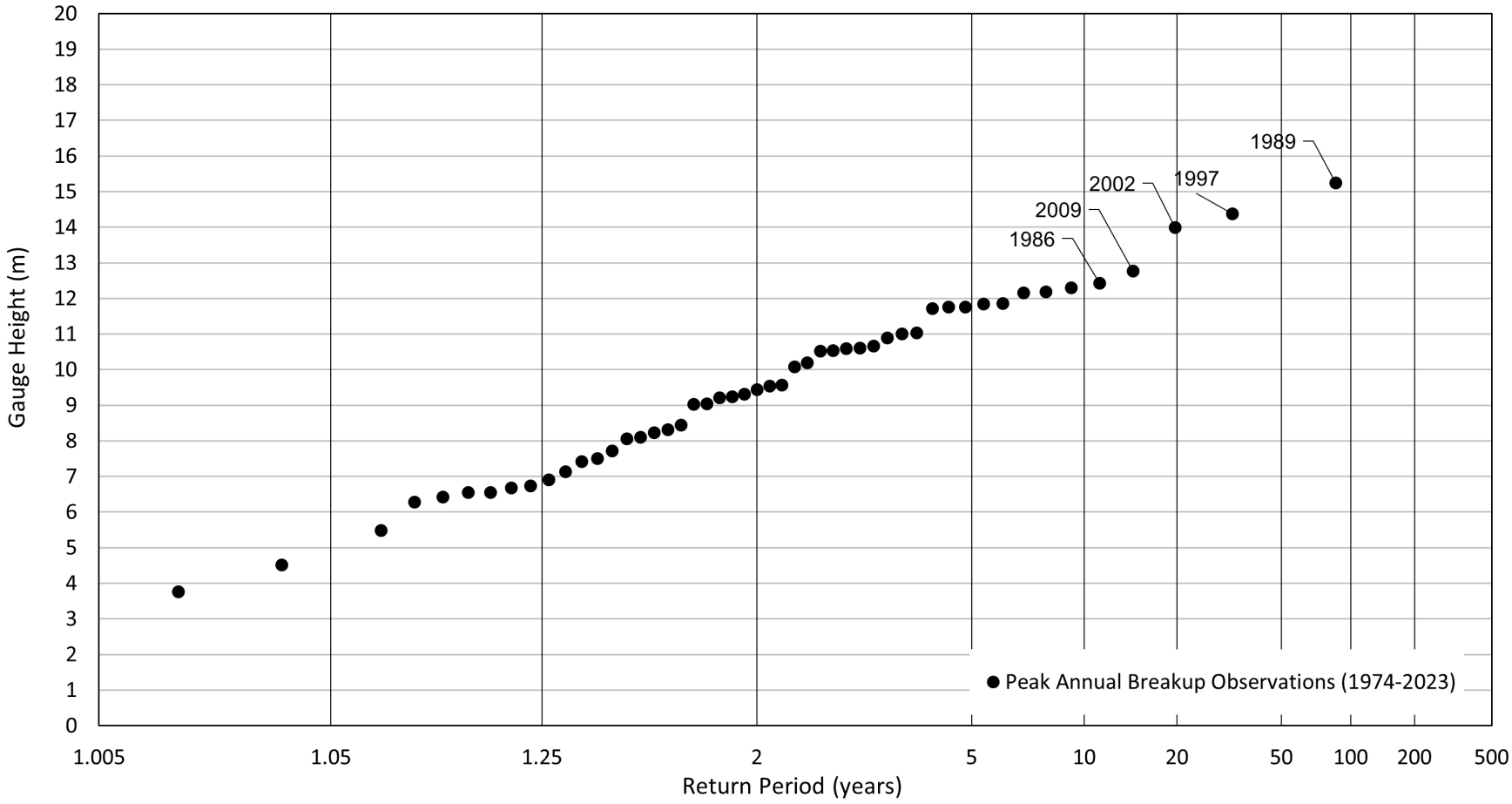

Government of Northwest Territories
Gouvernement des Territoires du Nord-Ouest

Canada

nhc

UNITS – AS SHOWN

Job: 1008469

Date: APR-2025

FORT SIMPSON FLOOD HAZARD MAPPING STUDY

FLOOD LEVEL FREQUENCY LEVELS
LIARD RIVER NEAR THE MOUTH (10ED002)

FIGURE 12

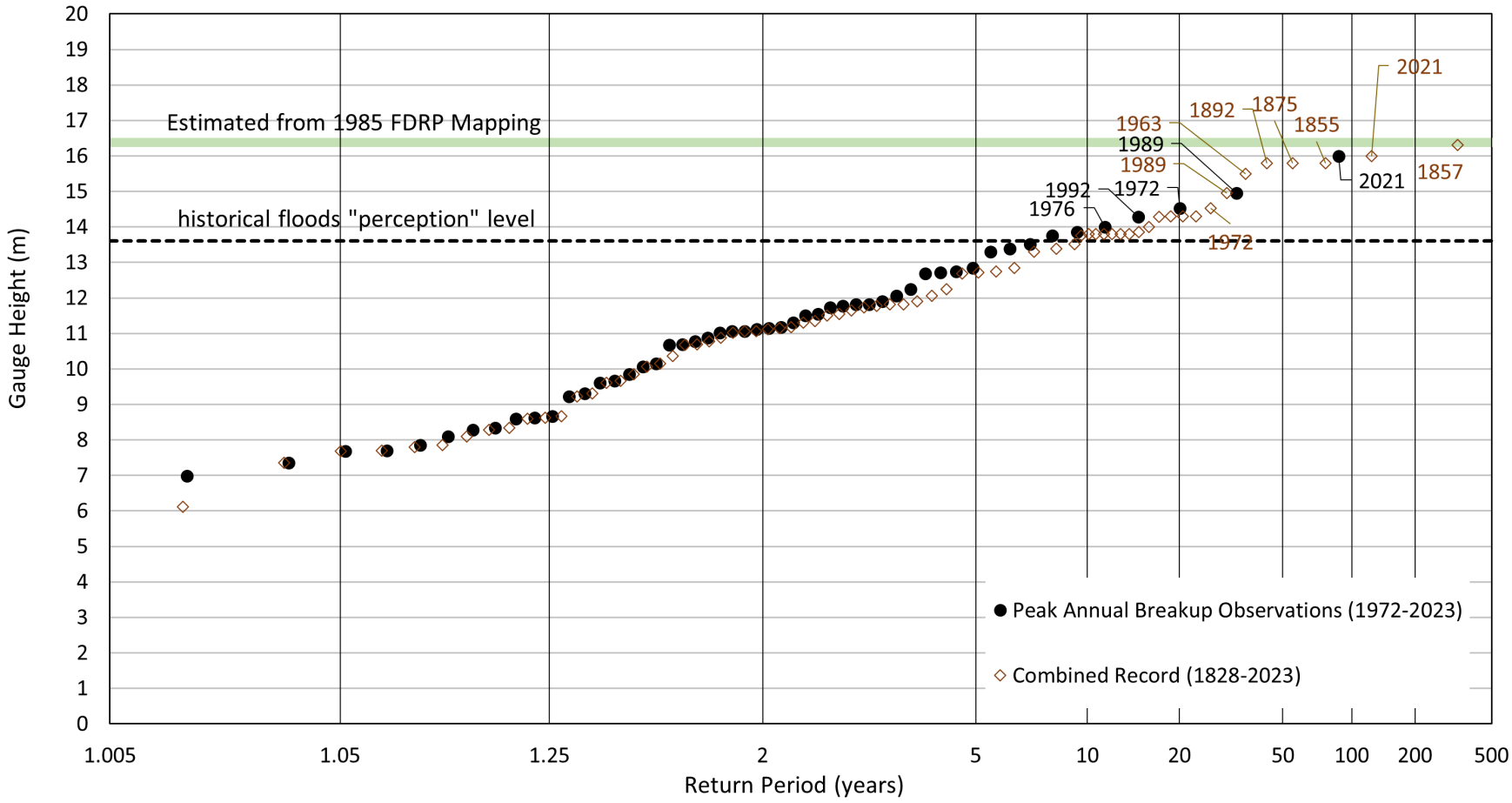

Government of Northwest Territories
Gouvernement des Territoires du Nord-Ouest

Canada

nhc

UNITS – AS SHOWN

Job: 1008469

Date: APR-2025

FORT SIMPSON FLOOD HAZARD MAPPING STUDY

FLOOD LEVEL FREQUENCY LEVELS
MACKENZIE RIVER AT FORT SIMPSON (10GC001)

FIGURE 13

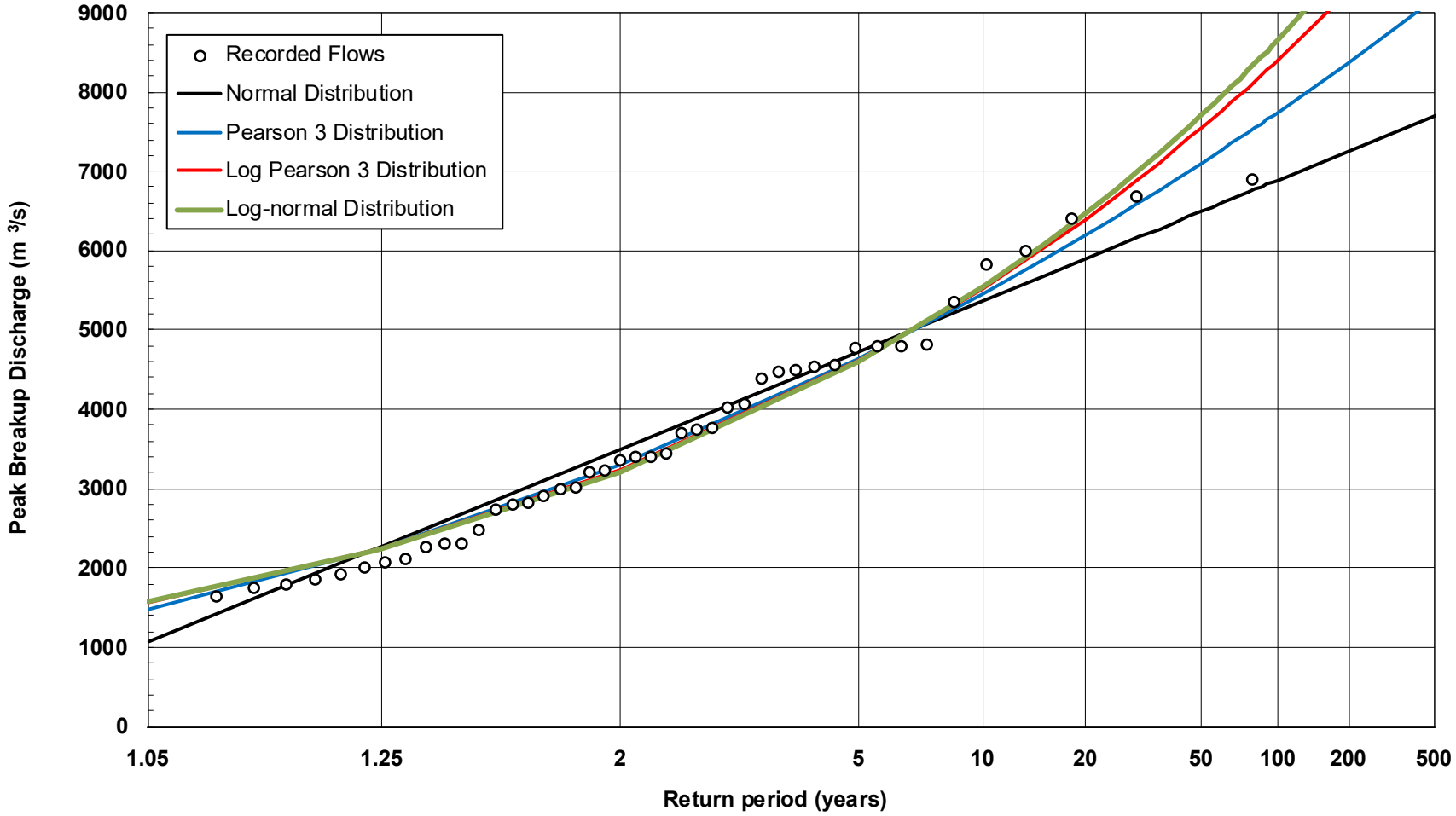

Government of Northwest Territories
Gouvernement des Territoires du Nord-Ouest

Canada

nhc

UNITS – AS SHOWN

Job: 1008469

Date: APR-2025

FORT SIMPSON FLOOD HAZARD MAPPING STUDY

BREAKUP DISCHARGE FLOOD FREQUENCY
LIARD RIVER NEAR THE MOUTH (10ED002)

FIGURE 14

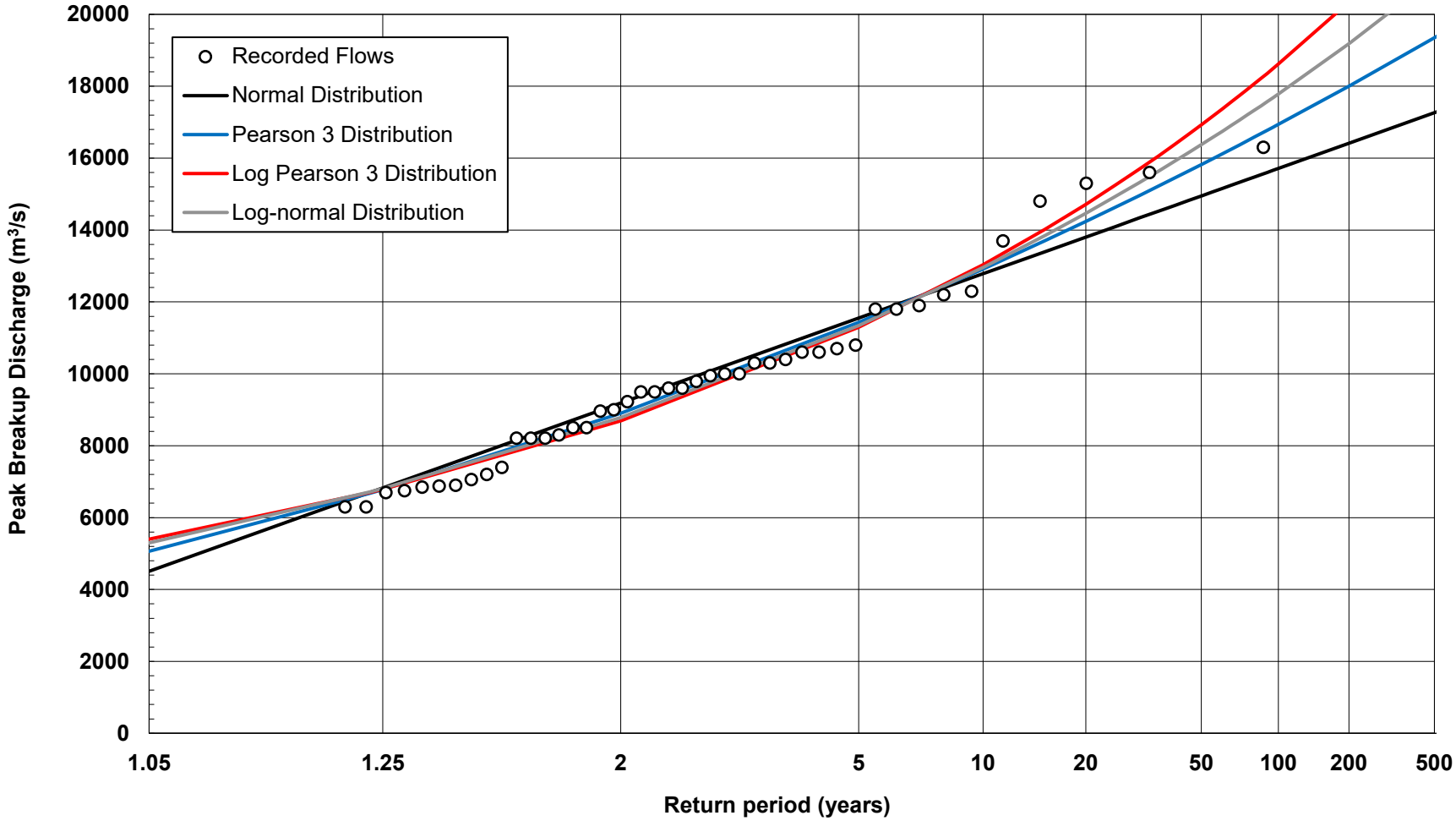

Government of Northwest Territories
Gouvernement des Territoires du Nord-Ouest

Canada

nhc

UNITS – AS SHOWN

Job: 1008469

Date: APR-2025

FORT SIMPSON FLOOD HAZARD MAPPING STUDY

BREAKUP DISCHARGE FLOOD FREQUENCY
MACKENZIE RIVER AT FORT SIMPSON (10GC001)

FIGURE 15

Determine peak breakup level and discharge by year and characterize by breakup mechanism.

Year	Breakup Discharge (m^3/s)	Peak Breakup Gauge Height (m)	Breakup Mechanism
...	...	...	...
2014	4770	10.08	Ice Run
2015	4480	10.67	Ice Jam
2016	3770	6.43	Thermal
2017	4540	7.42	Ice Run
2018	4380	9.03	Ice Jam
...	...	...	...

Develop a family of breakup flood level profiles for each breakup type (resulting in rating curves at each river station).

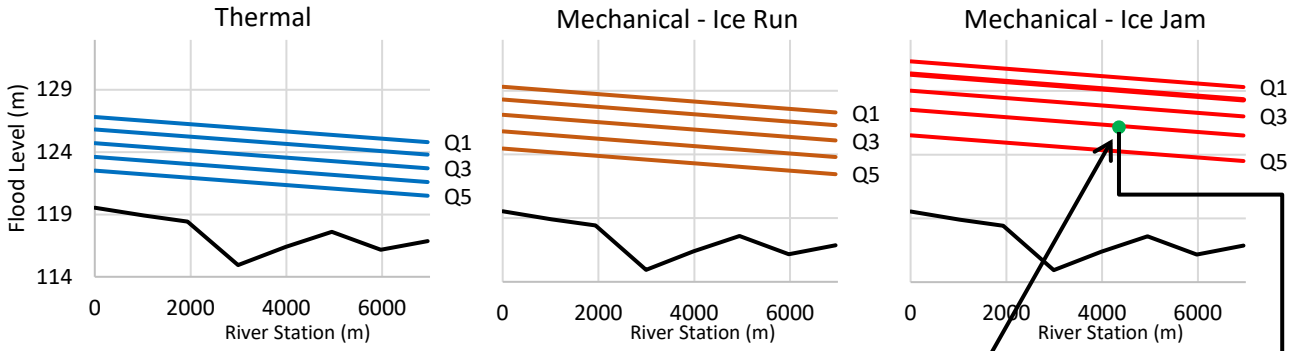

Estimate probability factors by breakup mechanism.

$P_{mechanical} = 0.84$, $P_{thermal} = 0.16$

$P_{jam\ if\ mechanical} = 0.68$, $P_{ice\ run\ if\ mechanical} = 0.32$

Estimate breakup discharge frequency distribution.

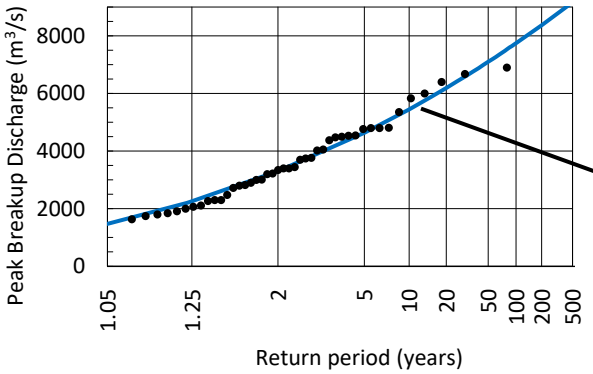

1. Randomly select a value from the breakup discharge frequency distribution

2. Randomly select a breakup mechanism based on probability factors.

3. Determine the breakup flood level based on the breakup type and the respective breakup discharge – water level relationship.

4. Store the breakup flood level to the synthesized population of breakup levels for each section and repeat the process (e.g. 10,000 + iterations).

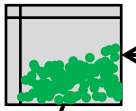

5. Rank and plot the series with a standard plotting position formula to form a distribution of breakup flood levels and compare to the estimated breakup flood levels based on observational data.

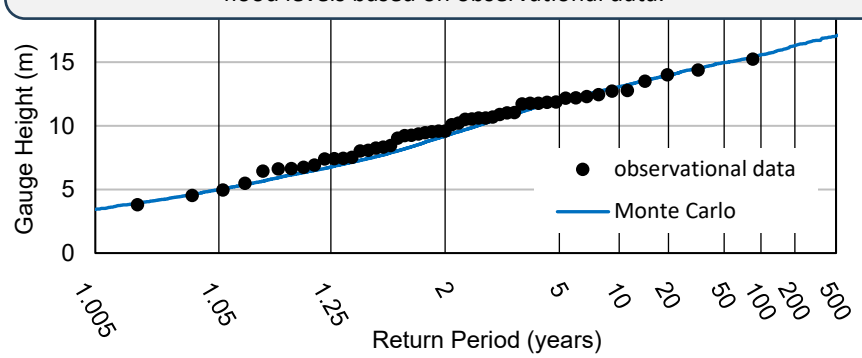

Government of Northwest Territories / Gouvernement des Territoires du Nord-Ouest

Canada

nhc

NOTE: All values in this figure are hypothetical and are for information only.

FORT SIMPSON FLOOD HAZARD MAPPING STUDY

MONTE CARLO ANALYSIS WORKFLOW

Job: 1008469

Date: APR-2025

FIGURE 16

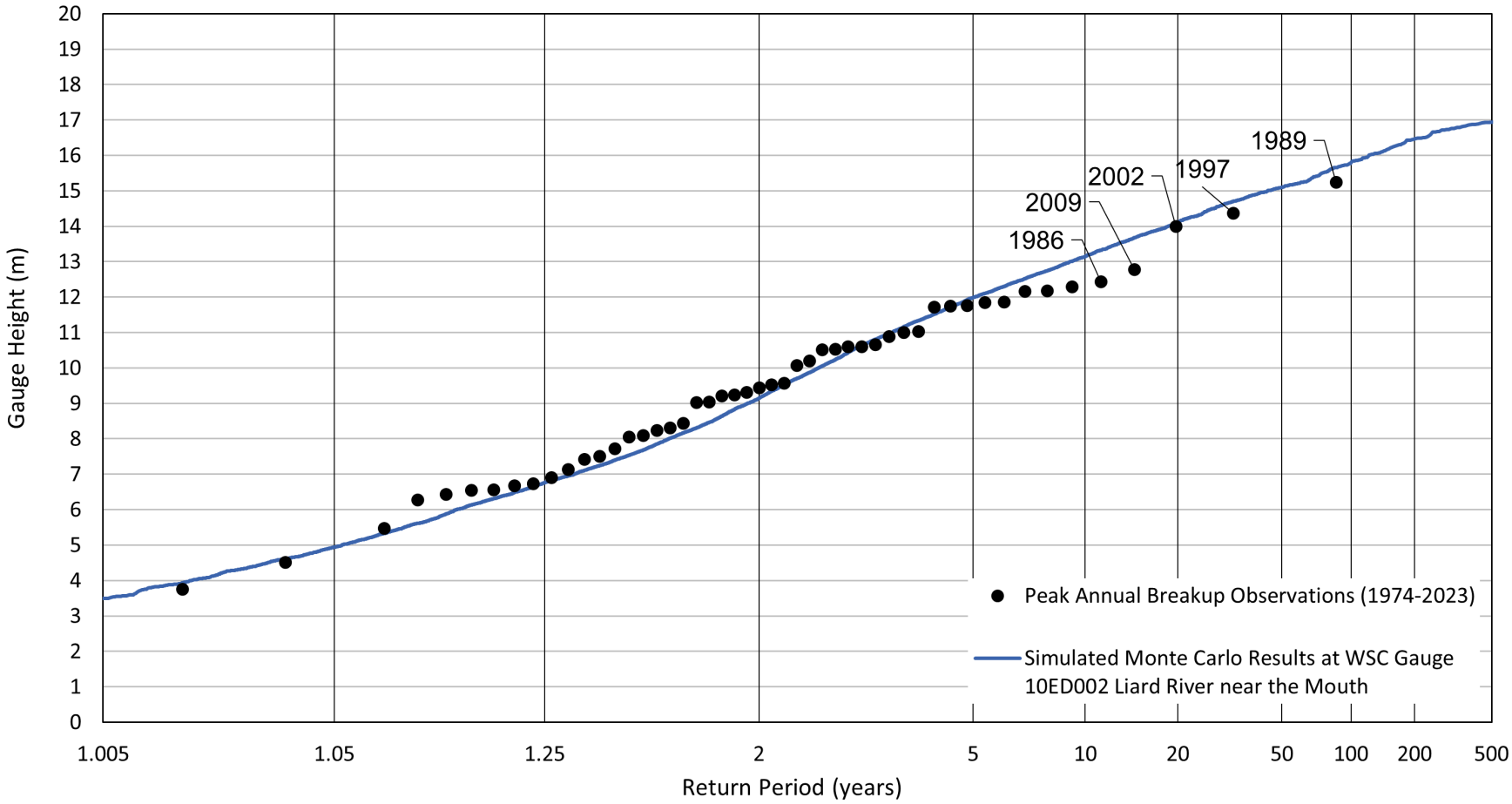

Government of Northwest Territories / Gouvernement des Territoires du Nord-Ouest; Canada; nhc	SCALE – AS SHOWN	FORT SIMPSON FLOOD HAZARD MAPPING STUDY
	UNITS – AS SHOWN	***MONTE-CARLO SIMULATED RESULTS LIARD RIVER NEAR THE MOUTH (10ED002)***
	Job: 1008469 / *Date: APR-2025*	*FIGURE 17*

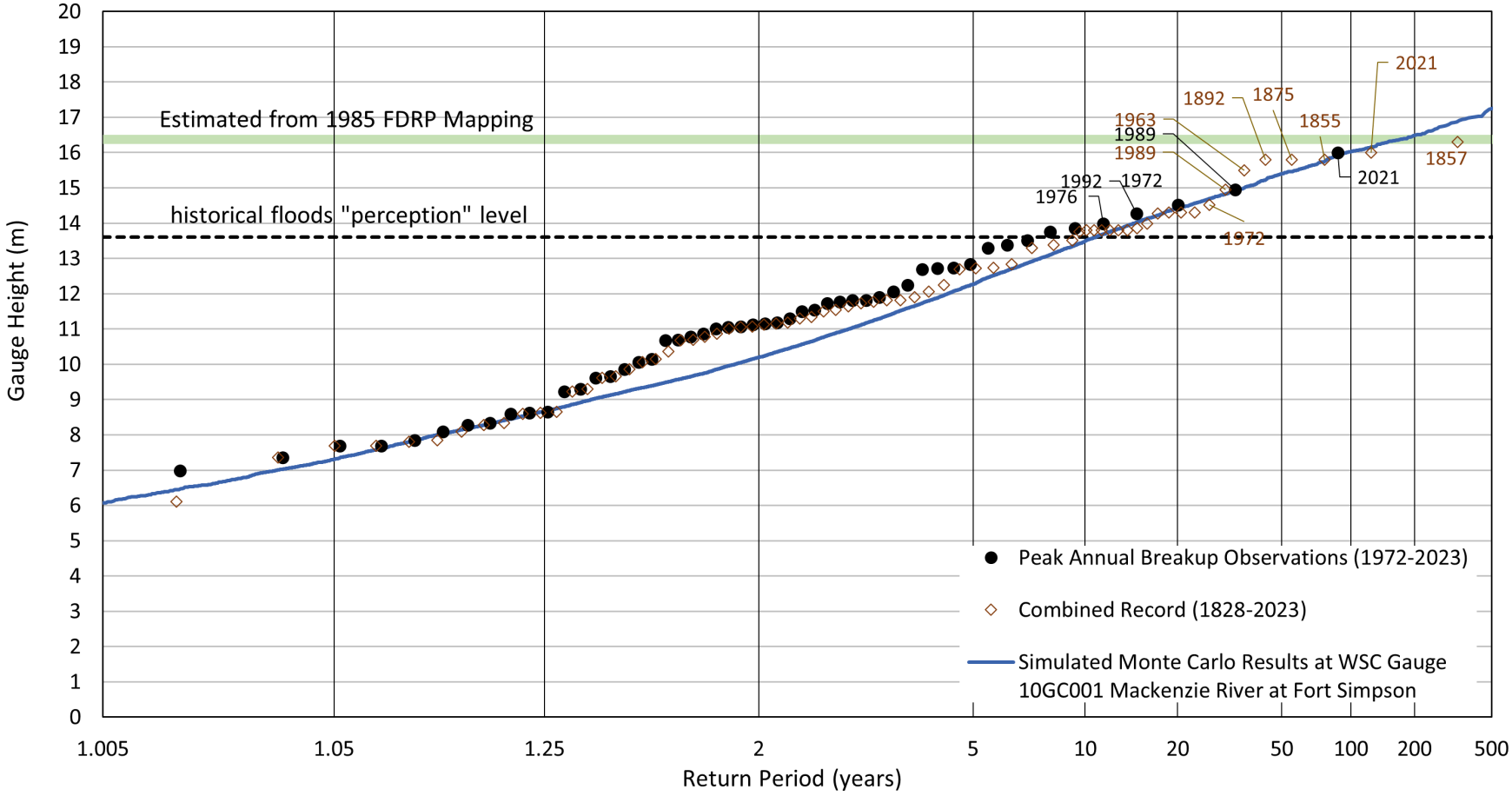

Government of Northwest Territories
Gouvernement des Territoires du Nord-Ouest

Canada

nhc

SCALE – AS SHOWN

UNITS – AS SHOWN

Job: 1008469

Date: APR-2025

FORT SIMPSON FLOOD HAZARD MAPPING STUDY

MONTE-CARLO SIMULATED RESULTS
MACKENZIE RIVER AT FORT SIMPSON (10GC001)

FIGURE 18

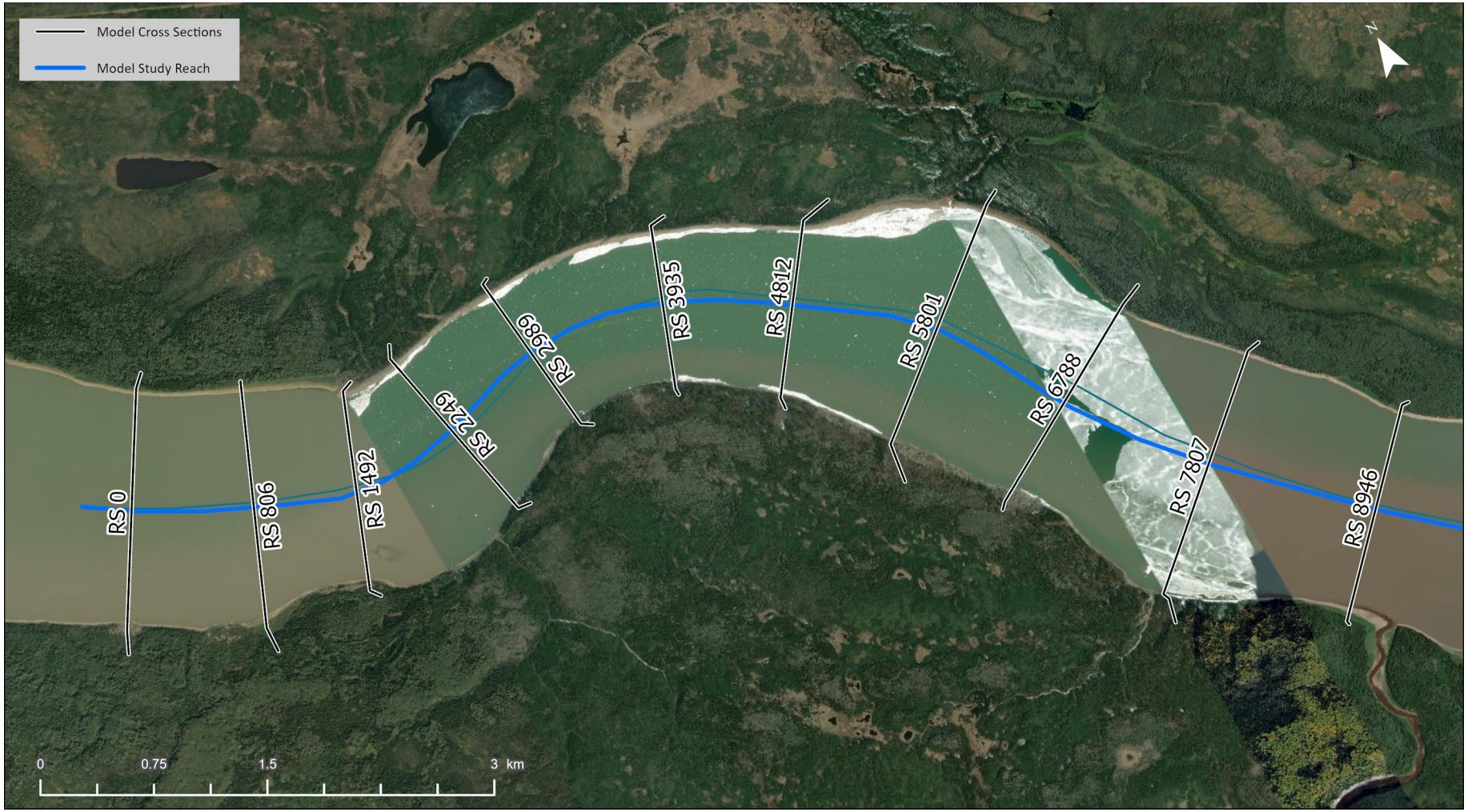

Government of Northwest Territories
Gouvernement des Territoires du Nord-Ouest

Canada

nhc

SCALE – AS SHOWN

FORT SIMPSON FLOOD HAZARD MAPPING STUDY

RIVER CENTRELINES AND MODEL CROSS SECTIONS MACKENZIE RIVER (REACH 1 OF 4)

Job: 1008469

Date: APR-2025

FIGURE 19

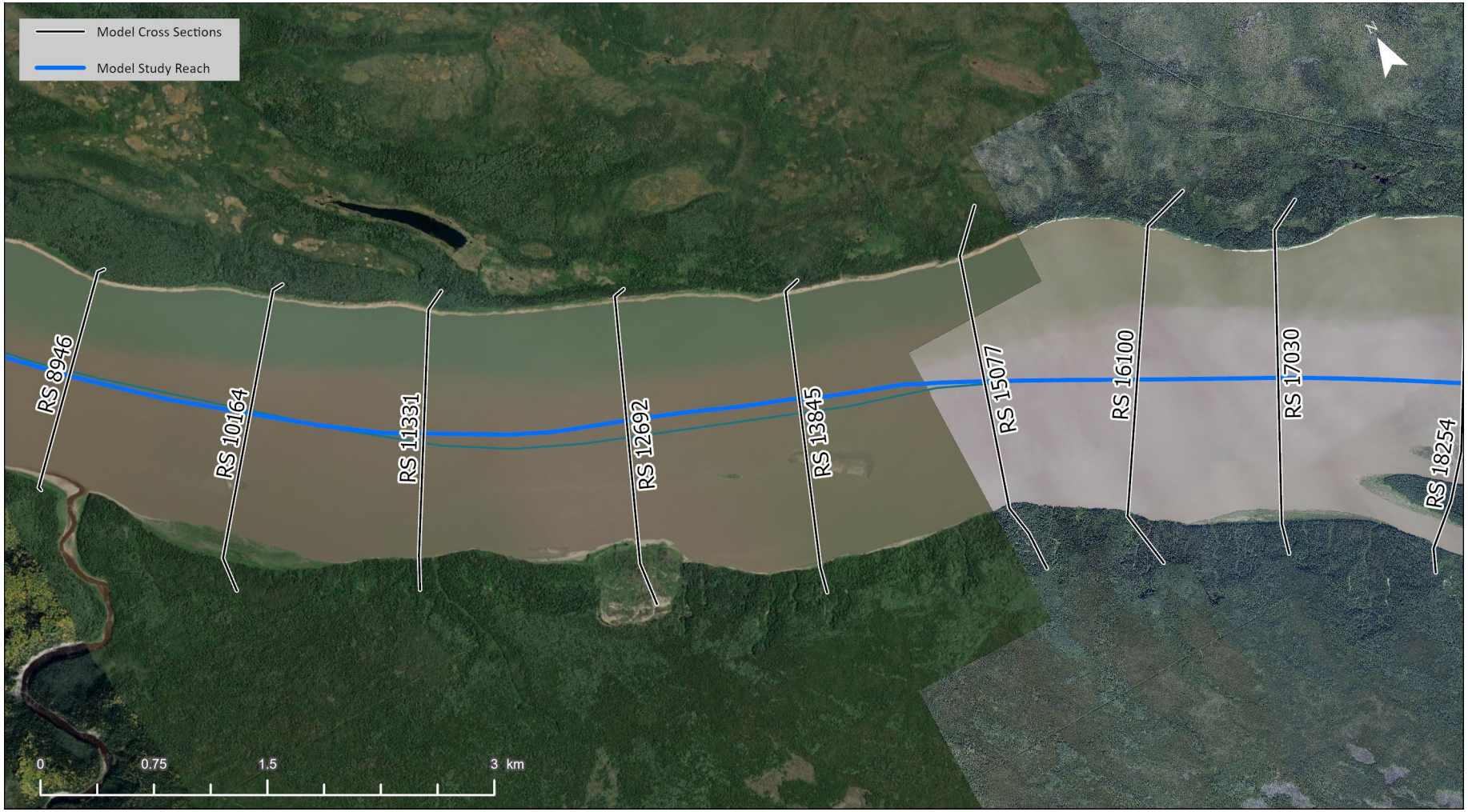

Government of Northwest Territories / Gouvernement des Territoires du Nord-Ouest; Canada; nhc	SCALE – AS SHOWN	FORT SIMPSON FLOOD HAZARD MAPPING STUDY
		RIVER CENTRELINES AND MODEL CROSS SECTIONS MACKENZIE RIVER (REACH 2 OF 4)
	Job: 1008469 / *Date: APR-2025*	*FIGURE 20*

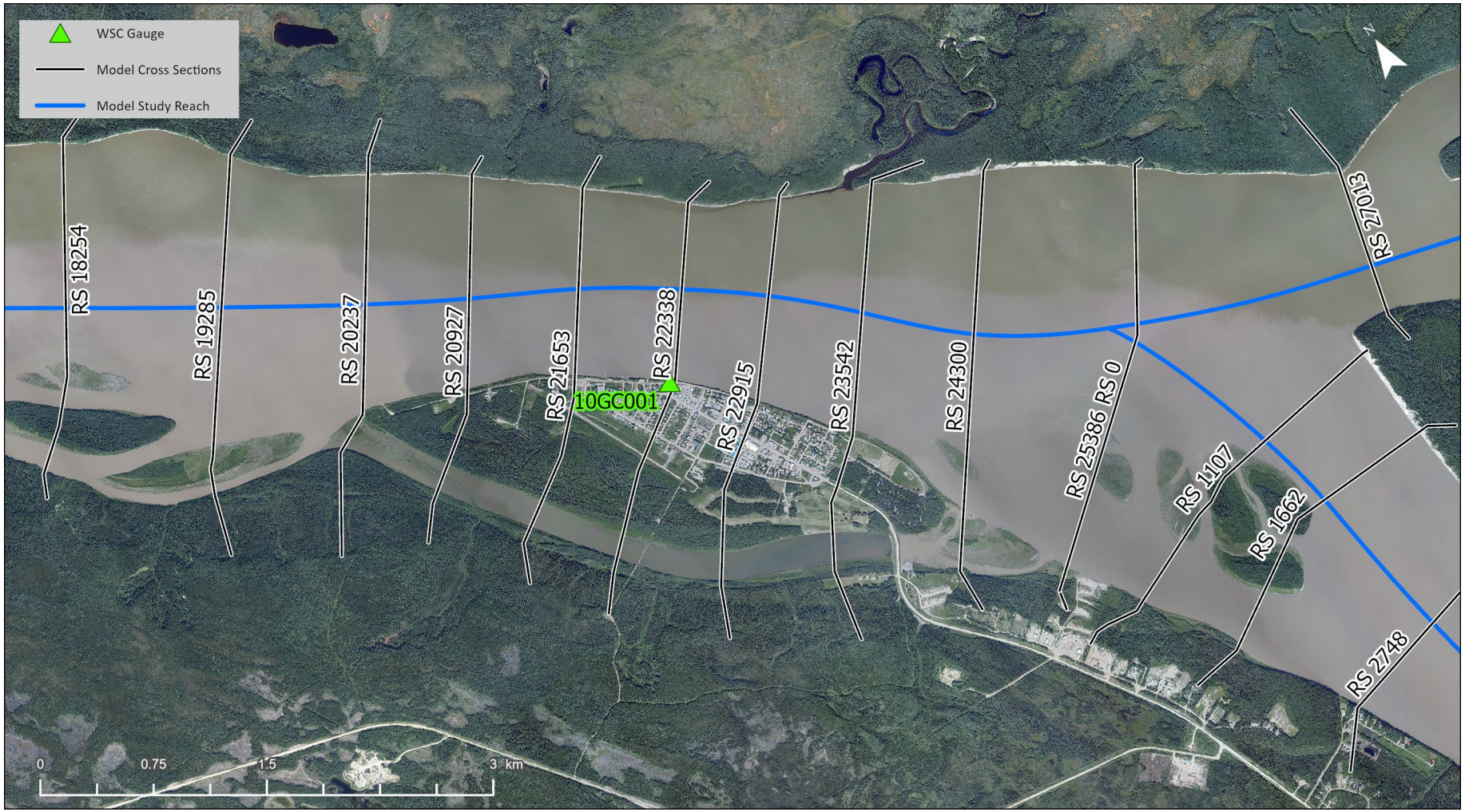

Government of Northwest Territories / Gouvernement des Territoires du Nord-Ouest; Canada; nhc	SCALE – AS SHOWN	FORT SIMPSON FLOOD HAZARD MAPPING STUDY
		RIVER CENTRELINES AND MODEL CROSS SECTIONS MACKENZIE RIVER (REACH 3 OF 4)
	Job: 1008469 / *Date: APR-2025*	*FIGURE 21*

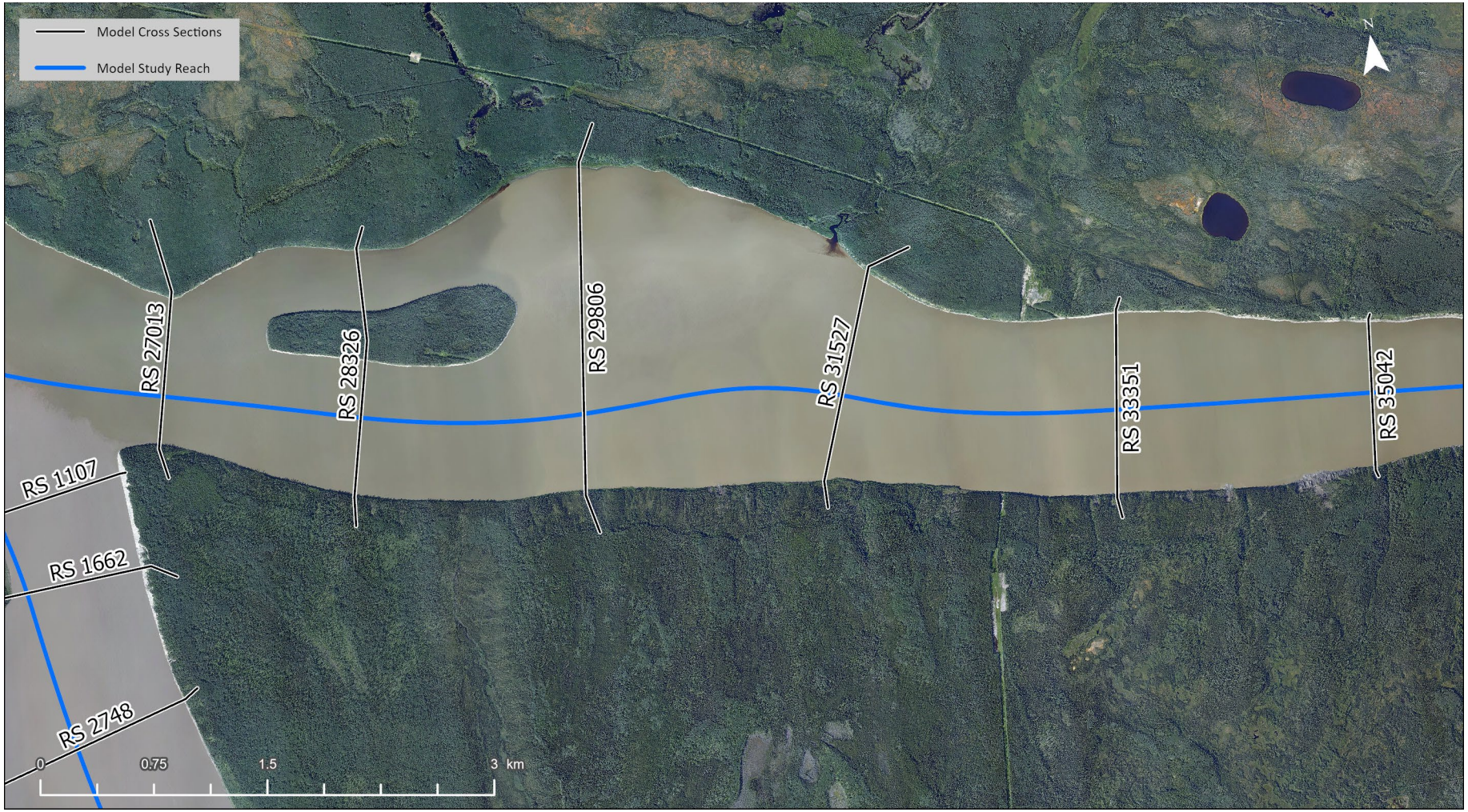

Government of Northwest Territories
Gouvernement des Territoires du Nord-Ouest

Canada

nhc

SCALE – AS SHOWN

FORT SIMPSON FLOOD HAZARD MAPPING STUDY

RIVER CENTRELINES AND MODEL CROSS SECTIONS MACKENZIE RIVER (REACH 4 OF 4)

Job: 1008469

Date: APR-2025

FIGURE 22

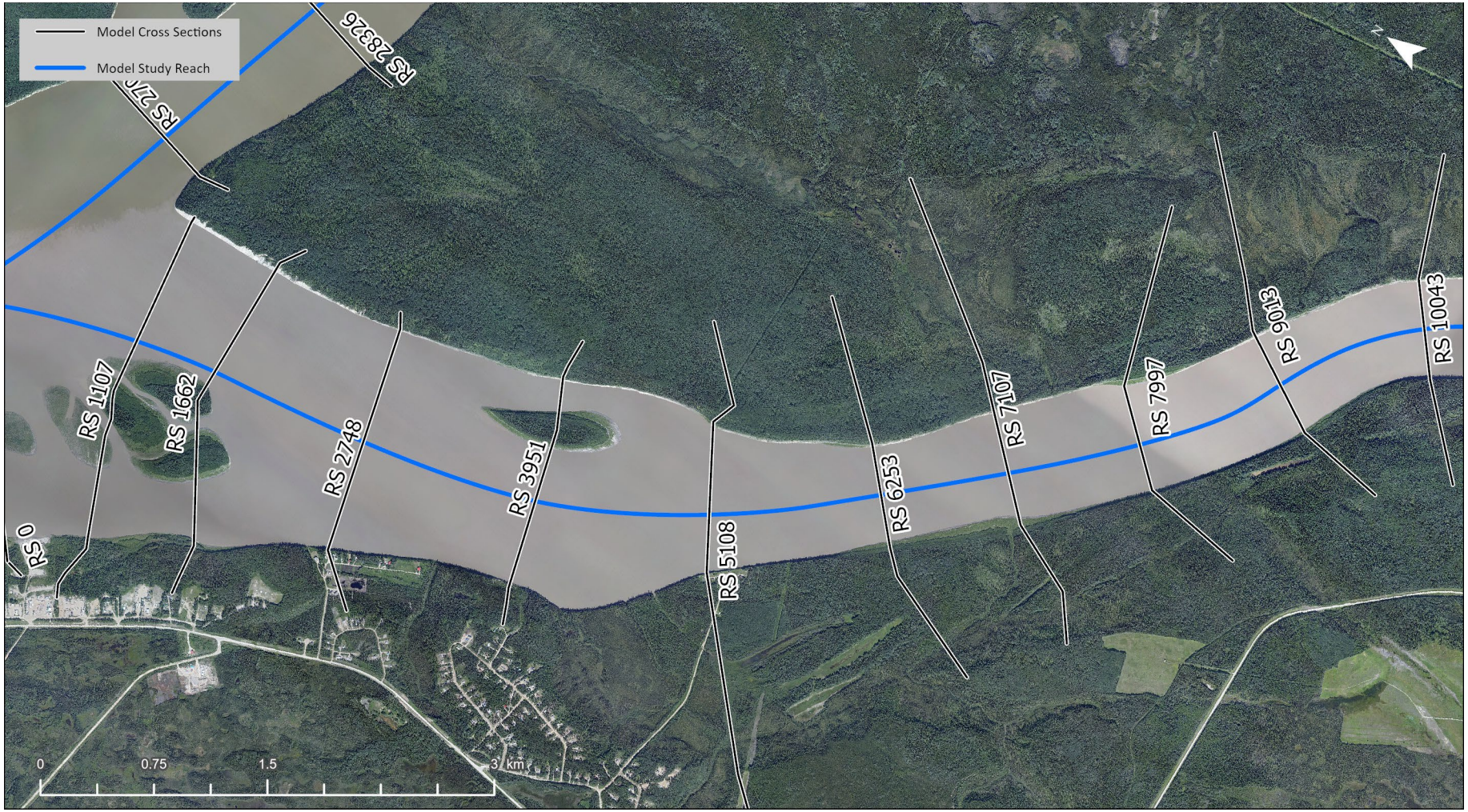

Government of Northwest Territories / Gouvernement des Territoires du Nord-Ouest; Canada; nhc	SCALE – AS SHOWN	FORT SIMPSON FLOOD HAZARD MAPPING STUDY ***RIVER CENTRELINES AND MODEL CROSS SECTIONS LIARD RIVER (REACH 1 OF 2)***
	Job: 1008469 / *Date: APR-2025*	*FIGURE 23*

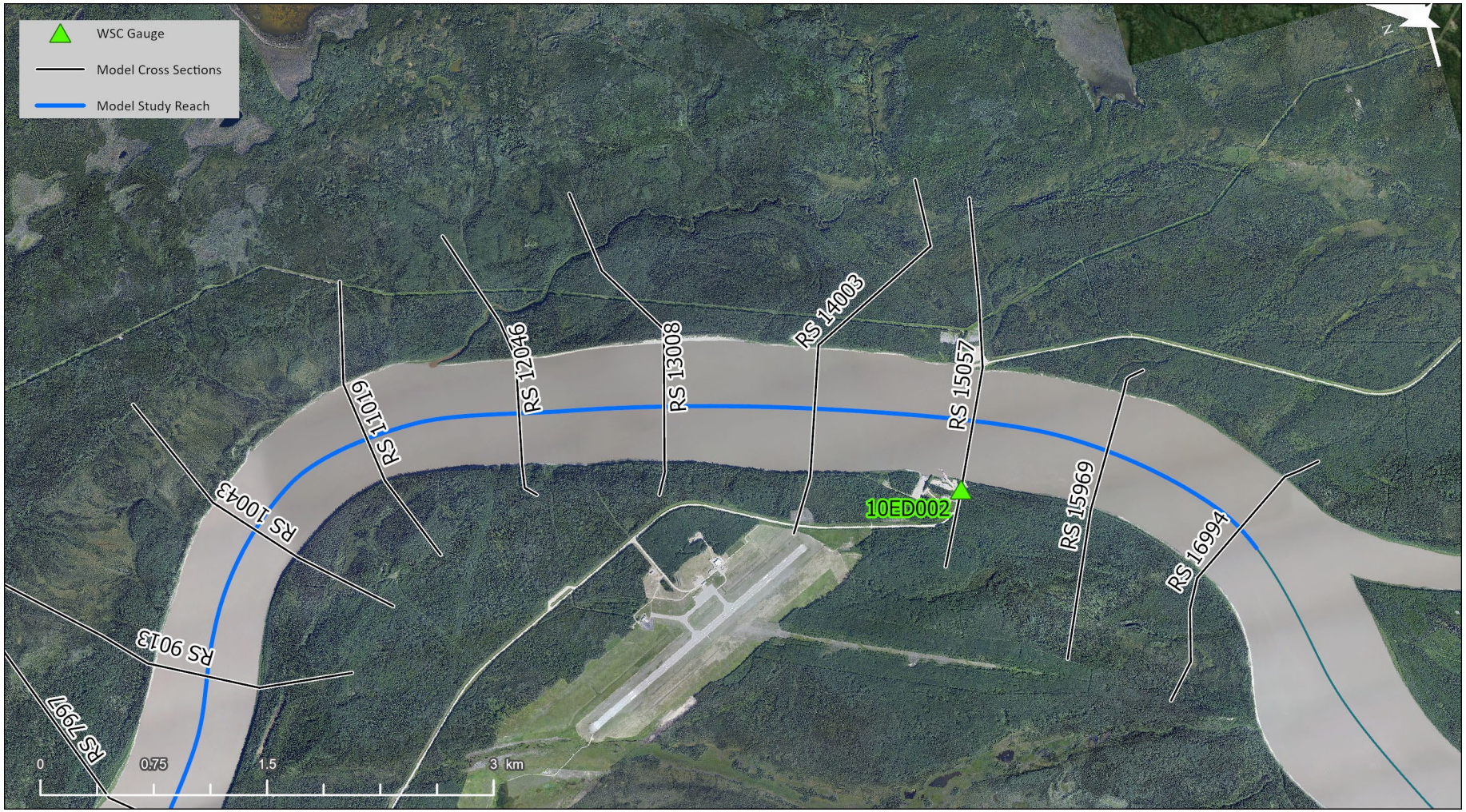

Government of Northwest Territories / Gouvernement des Territoires du Nord-Ouest

Canada

nhc

SCALE – AS SHOWN

FORT SIMPSON FLOOD HAZARD MAPPING STUDY

RIVER CENTRELINES AND MODEL CROSS SECTIONS LIARD RIVER (REACH 2 OF 2)

Job: 1008469

Date: APR-2025

FIGURE 24

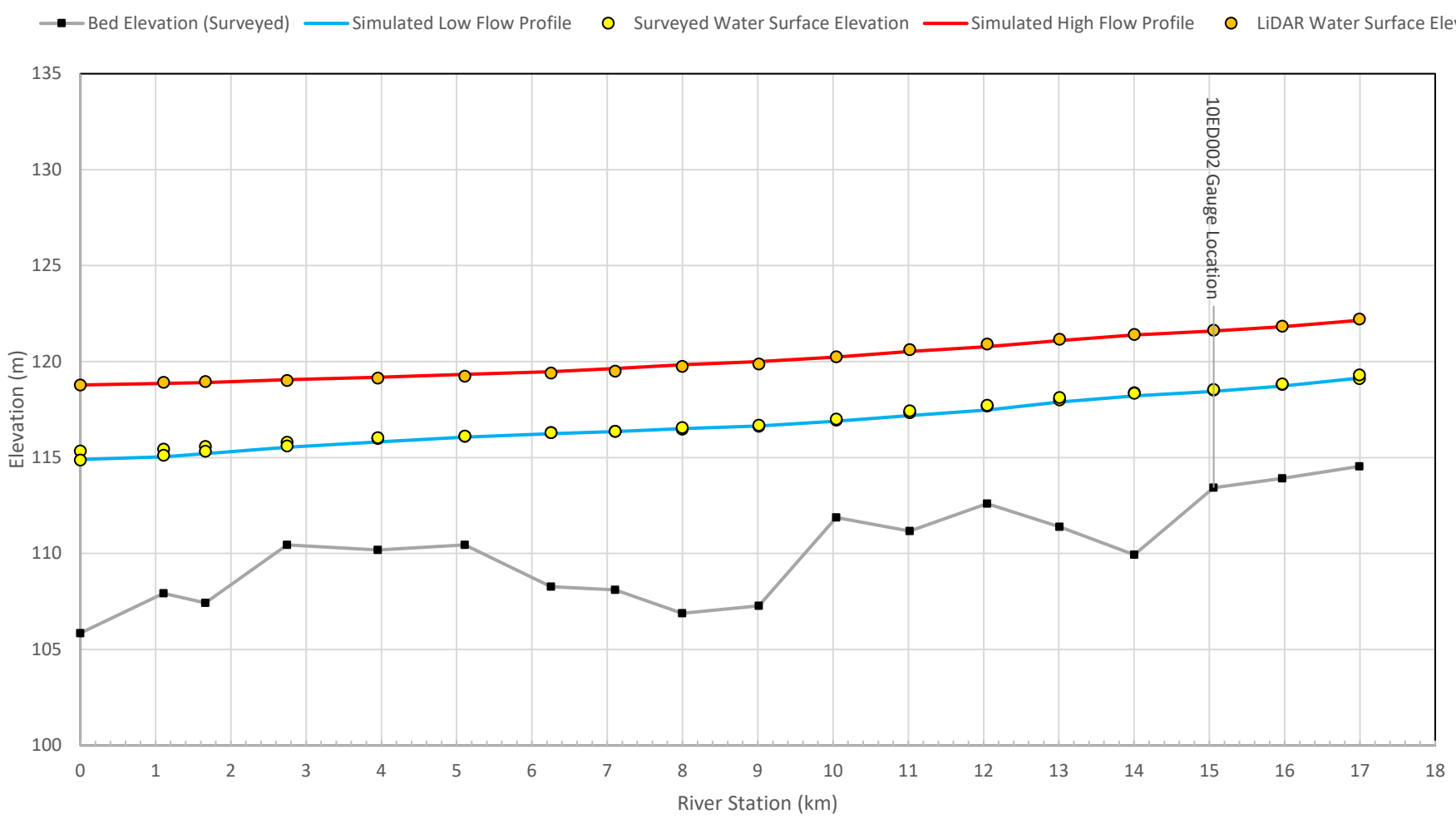

Government of Northwest Territories / Gouvernement des Territoires du Nord-Ouest

Canada

nhc

UNITS – AS SHOWN

VERTICAL ELEVATION DATUM: CGVD2013a

Job: 1008469

Date: APR-2025

FORT SIMPSON FLOOD HAZARD MAPPING STUDY

OPEN WATER CALIBRATION PROFILES
LIARD RIVER

FIGURE 25

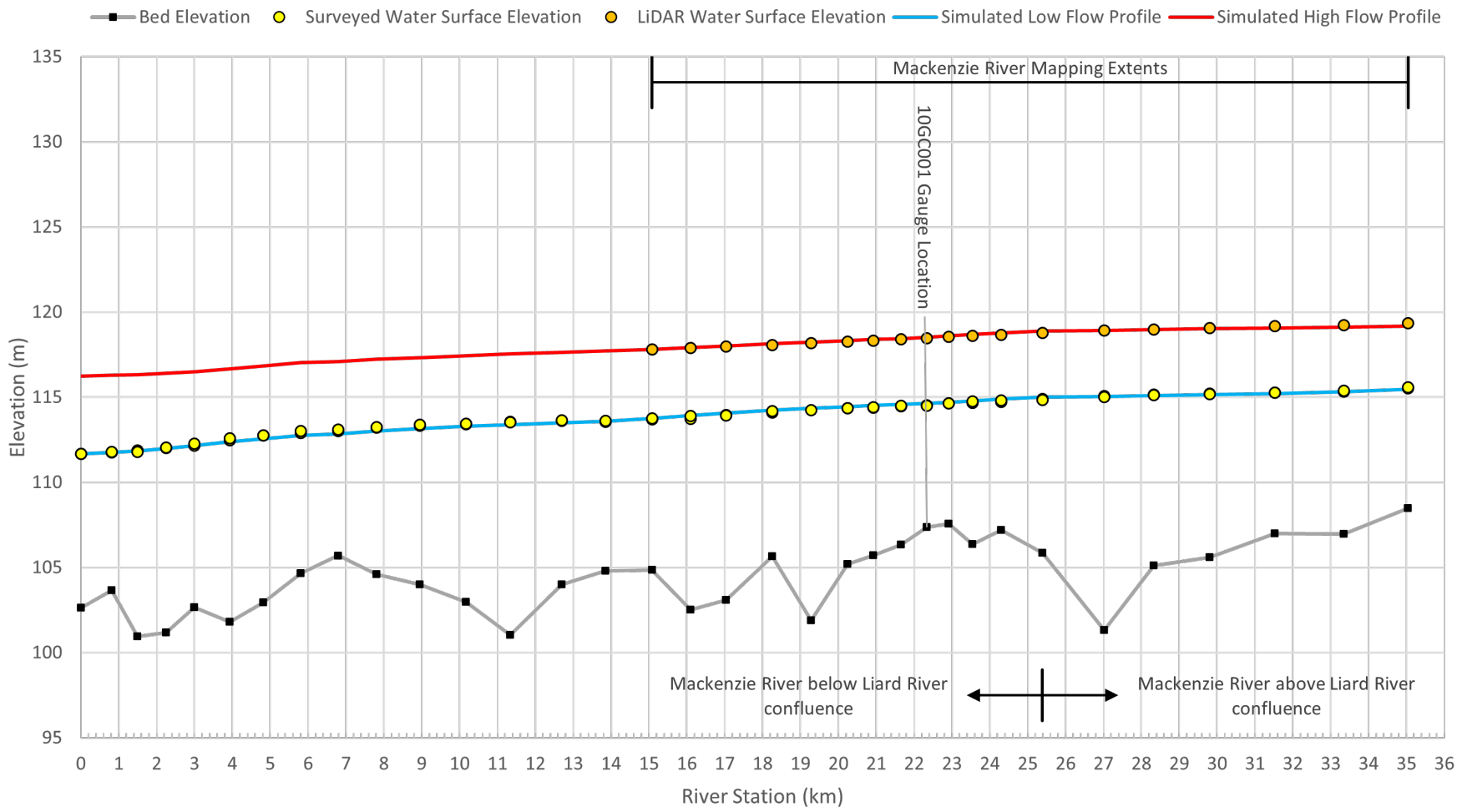

Government of Northwest Territories
Gouvernement des Territoires du Nord-Ouest

Canada

nhc

UNITS – AS SHOWN

VERTICAL ELEVATION DATUM: CGVD2013a

Job: 1008469

Date: APR-2025

FORT SIMPSON FLOOD HAZARD MAPPING STUDY

OPEN WATER CALIBRATION PROFILES MACKENZIE RIVER

FIGURE 26

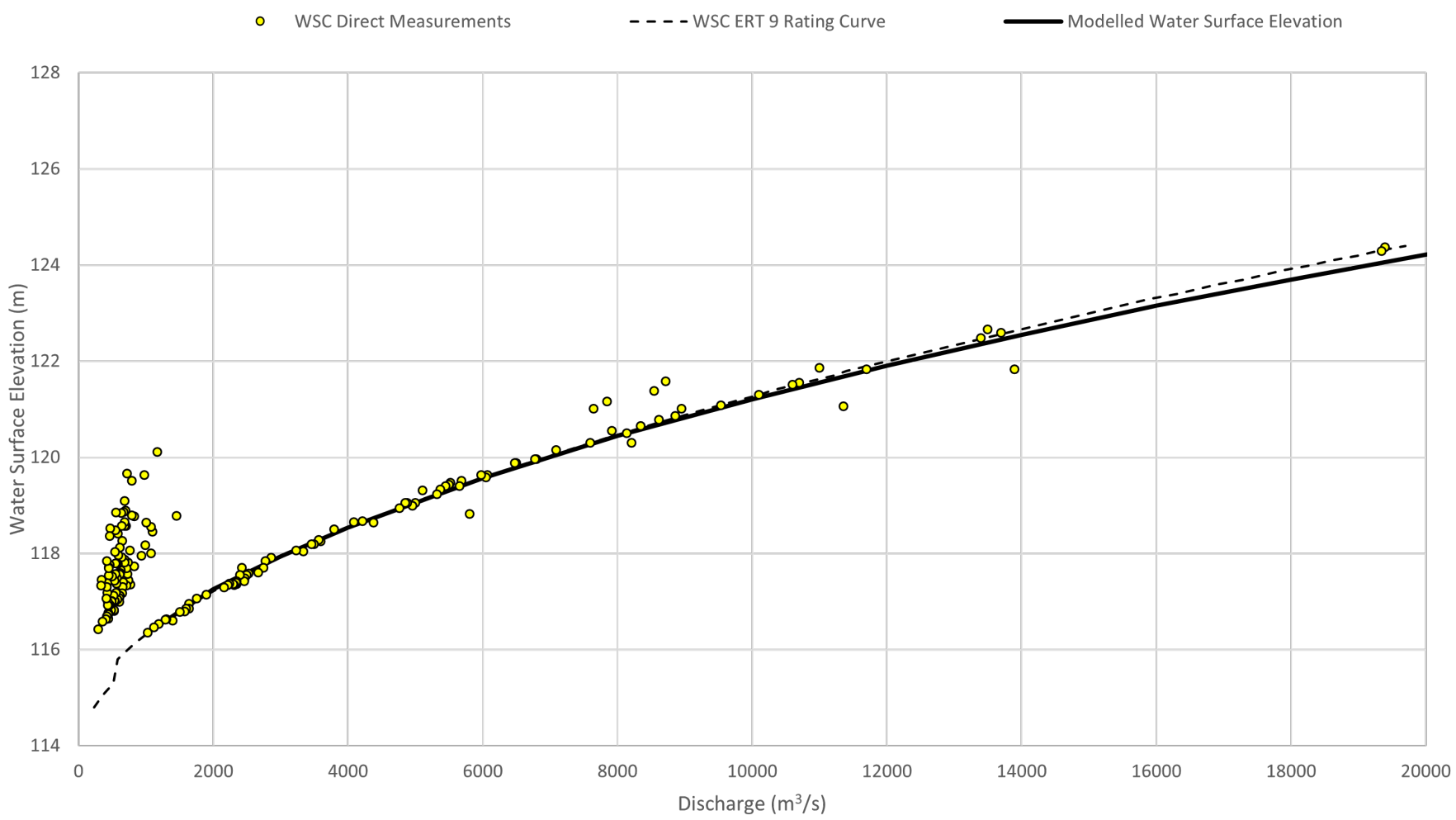

Notes:
1. WSC Direct Measurements and WSC ERT 9 Rating Curve data converted to NHC datum using a conversion of 114.800 m.

Government of Northwest Territories / Gouvernement des Territoires du Nord-Ouest; Canada; nhc		FORT SIMPSON FLOOD HAZARD MAPPING STUDY
	UNITS – AS SHOWN VERTICAL ELEVATION DATUM: CGVD2013a	***OPEN WATER RATING CURVE CALIBRATION RESULTS LIARD RIVER NEAR THE MOUTH (10ED002)***
	Job: 1008469 / *Date: APR-2025*	*FIGURE 27*

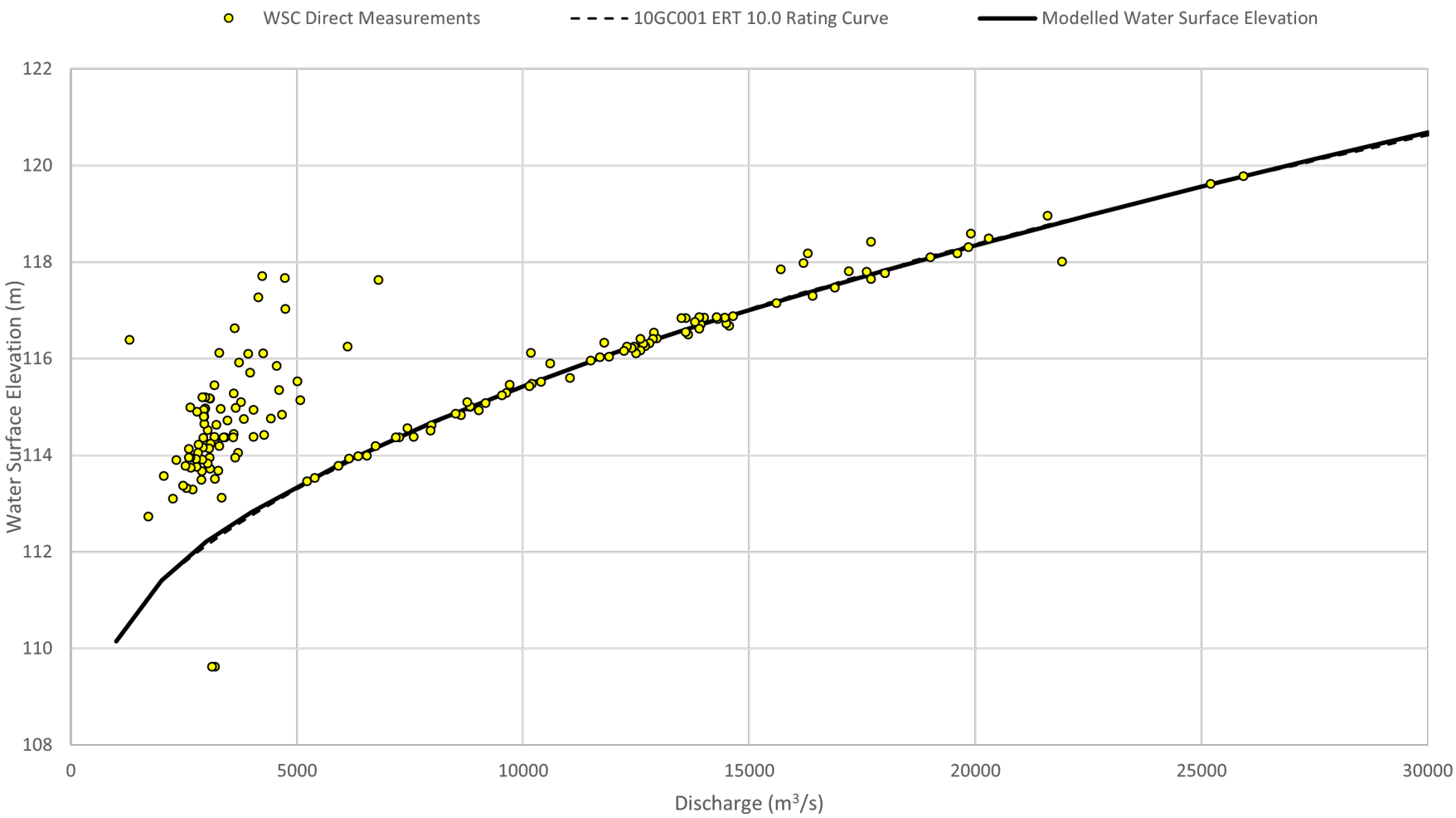

Notes:
1. WSC Direct Measurements and WSC ERT 10.0 Rating Curve data converted to NHC datum using a conversion of 109.623 m.

Government of Northwest Territories / Gouvernement des Territoires du Nord-Ouest; Canada; nhc	UNITS – AS SHOWN VERTICAL ELEVATION DATUM: CGVD2013a	FORT SIMPSON FLOOD HAZARD MAPPING STUDY ***OPEN WATER RATING CURVE CALIBRATION RESULTS MACKENZIE RIVER AT FORT SIMPSON (10GC001)***
	Job: 1008469 / *Date: APR-2025*	*FIGURE 28*

Government of Northwest Territories
Gouvernement des Territoires du Nord-Ouest

Canada

nhc

SCALE – AS SHOWN

FORT SIMPSON FLOOD HAZARD MAPPING STUDY

2021 ICE JAM FLOOD
SURVEYED HIGHWATER MARK LOCATIONS

Job: 1008469

Date: APR-2025

FIGURE 29

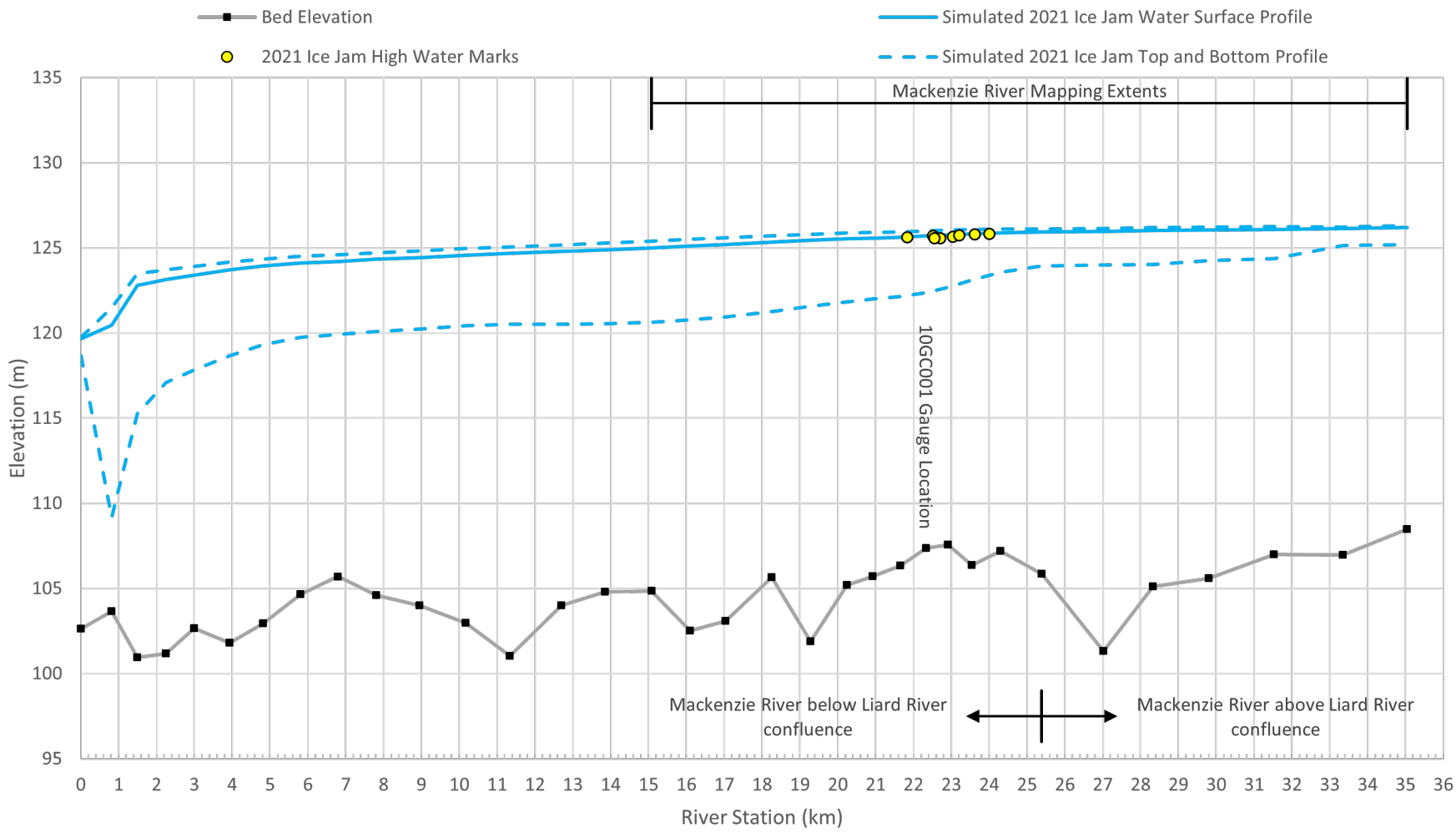

Government of Northwest Territories
Gouvernement des Territoires du Nord-Ouest

Canada

nhc

UNITS – AS SHOWN

VERTICAL ELEVATION DATUM: CGVD2013a

Job: 1008469

Date: APR-2025

FORT SIMPSON FLOOD HAZARD MAPPING STUDY

2021 ICE JAM CALIBRATION PROFILE MACKENZIE RIVER

FIGURE 30

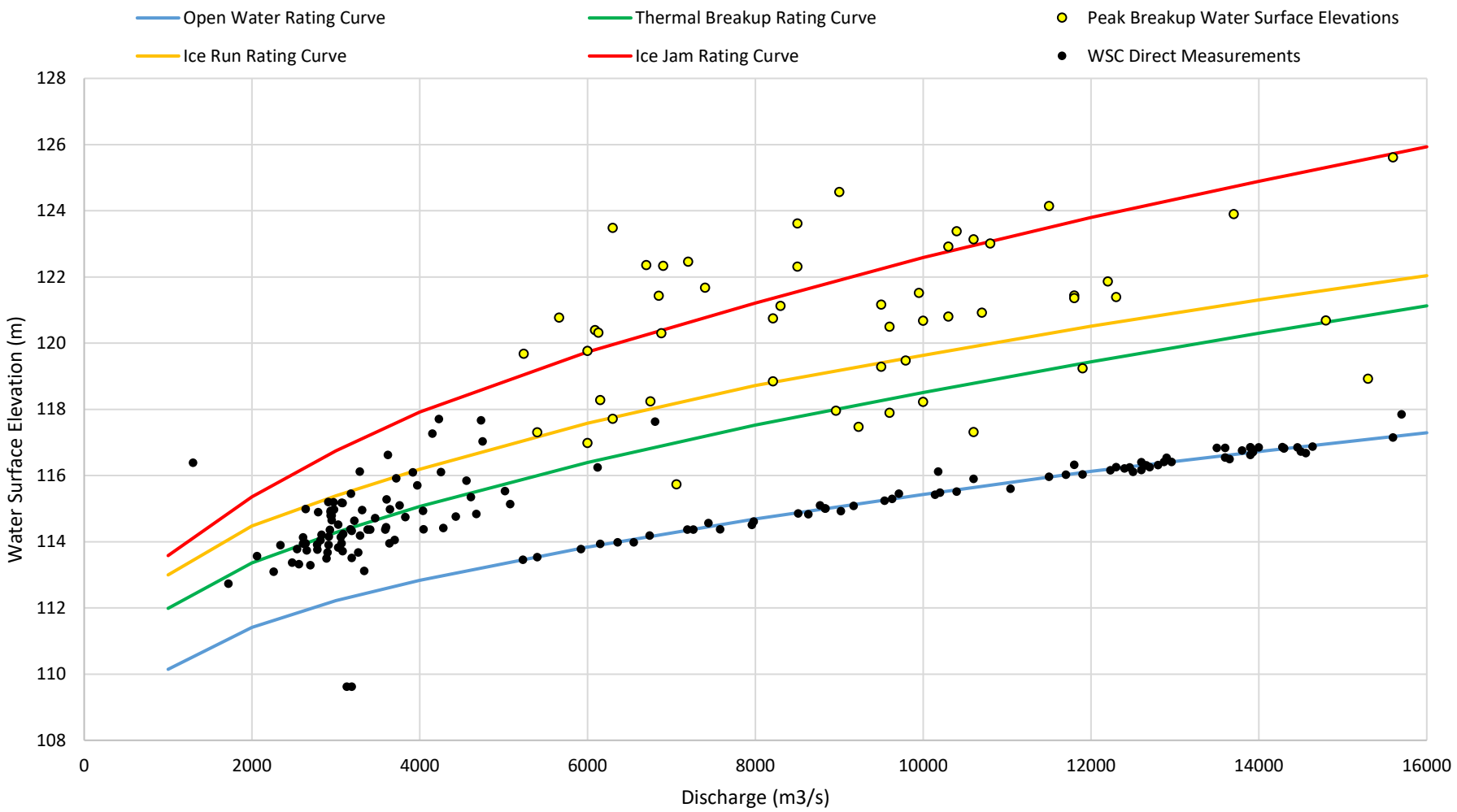

Government of Northwest Territories / Gouvernement des Territoires du Nord-Ouest

Canada

nhc

UNITS – AS SHOWN

VERTICAL ELEVATION DATUM: CGVD2013a

Job: 1008469

Date: APR-2025

FORT SIMPSON FLOOD HAZARD MAPPING STUDY

ICE JAM RATING CURVE CALIBRATION PROFILES MACKENZIE RIVER

FIGURE 31

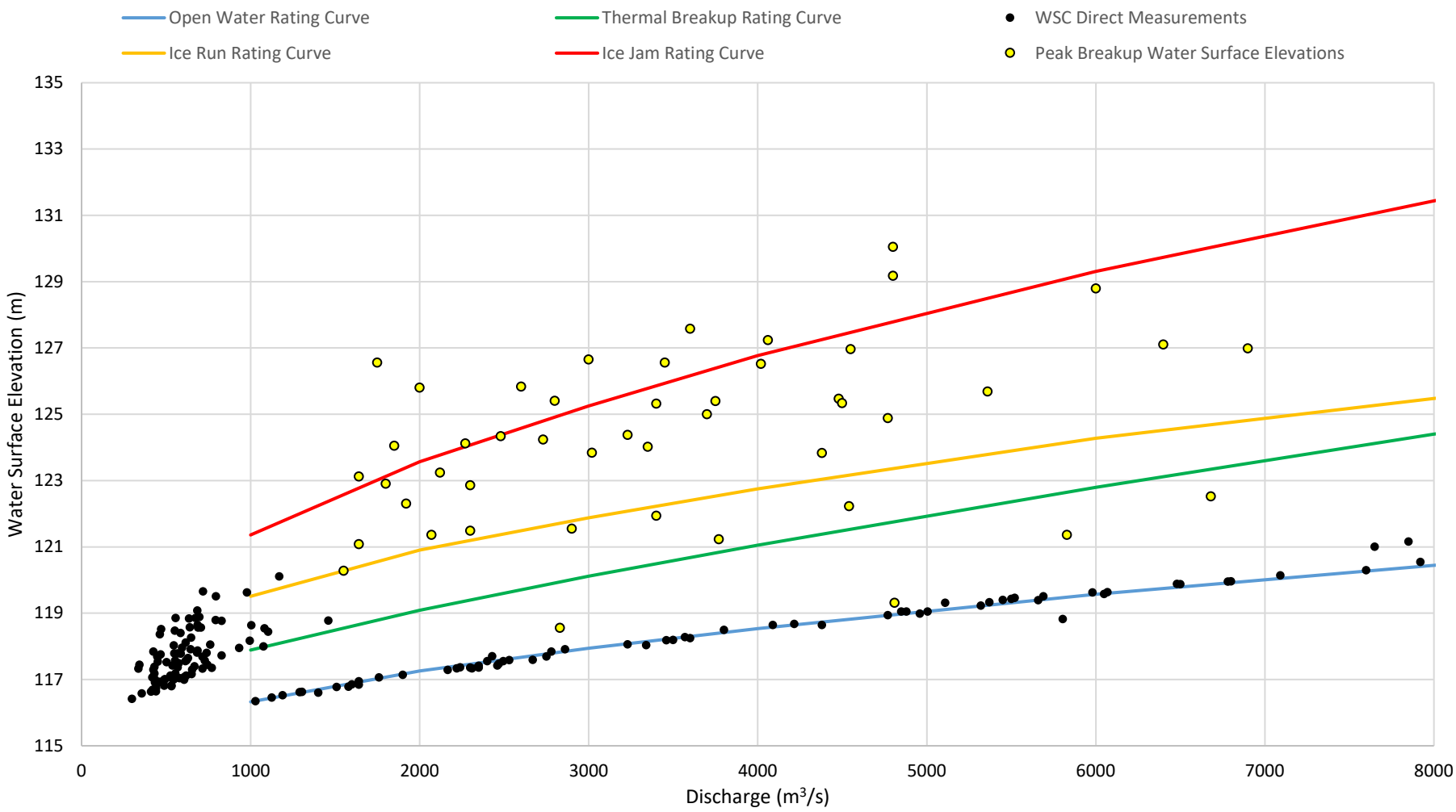

Government of Northwest Territories
Gouvernement des Territoires du Nord-Ouest

Canada

nhc

UNITS – AS SHOWN

VERTICAL ELEVATION DATUM: CGVD2013a

Job: 1008469

Date: APR-2025

FORT SIMPSON FLOOD HAZARD MAPPING STUDY

ICE JAM RATING CURVE CALIBRATION
LIARD RIVER

FIGURE 32

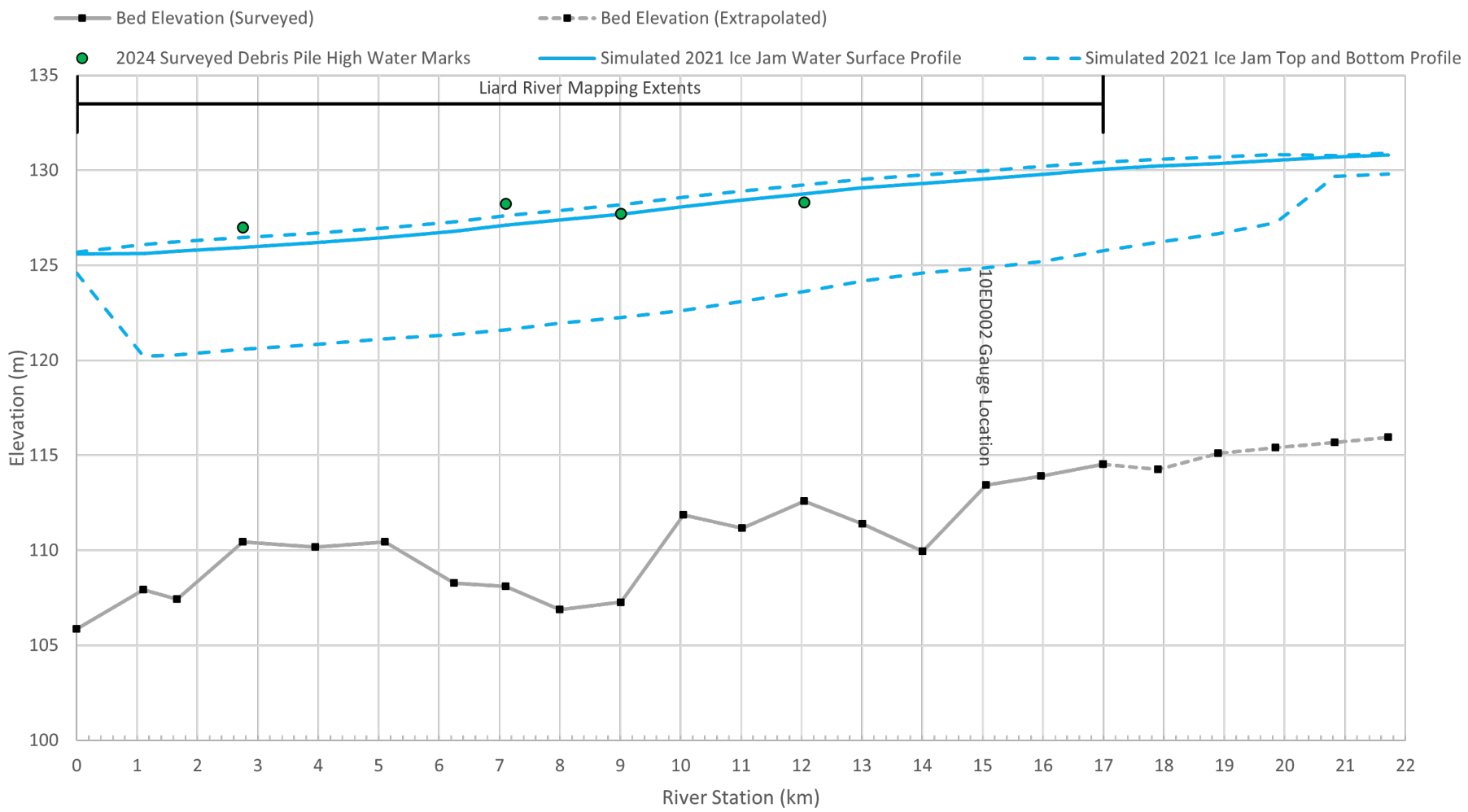

Notes:

1. Profile shown using the estimated 2021 breakup discharge of 6240 m^3/s
2. Surveyed debris pile high water marks are shown for comparison, but are considered inadequate for calibration

Government of Northwest Territories
Gouvernement des Territoires du Nord-Ouest

Canada

nhc

UNITS – AS SHOWN

VERTICAL ELEVATION DATUM: CGVD2013a

Job: 1008469

Date: APR-2025

FORT SIMPSON FLOOD HAZARD MAPPING STUDY

ICE JAM CALIBRATION PROFILE
LIARD RIVER

FIGURE 33

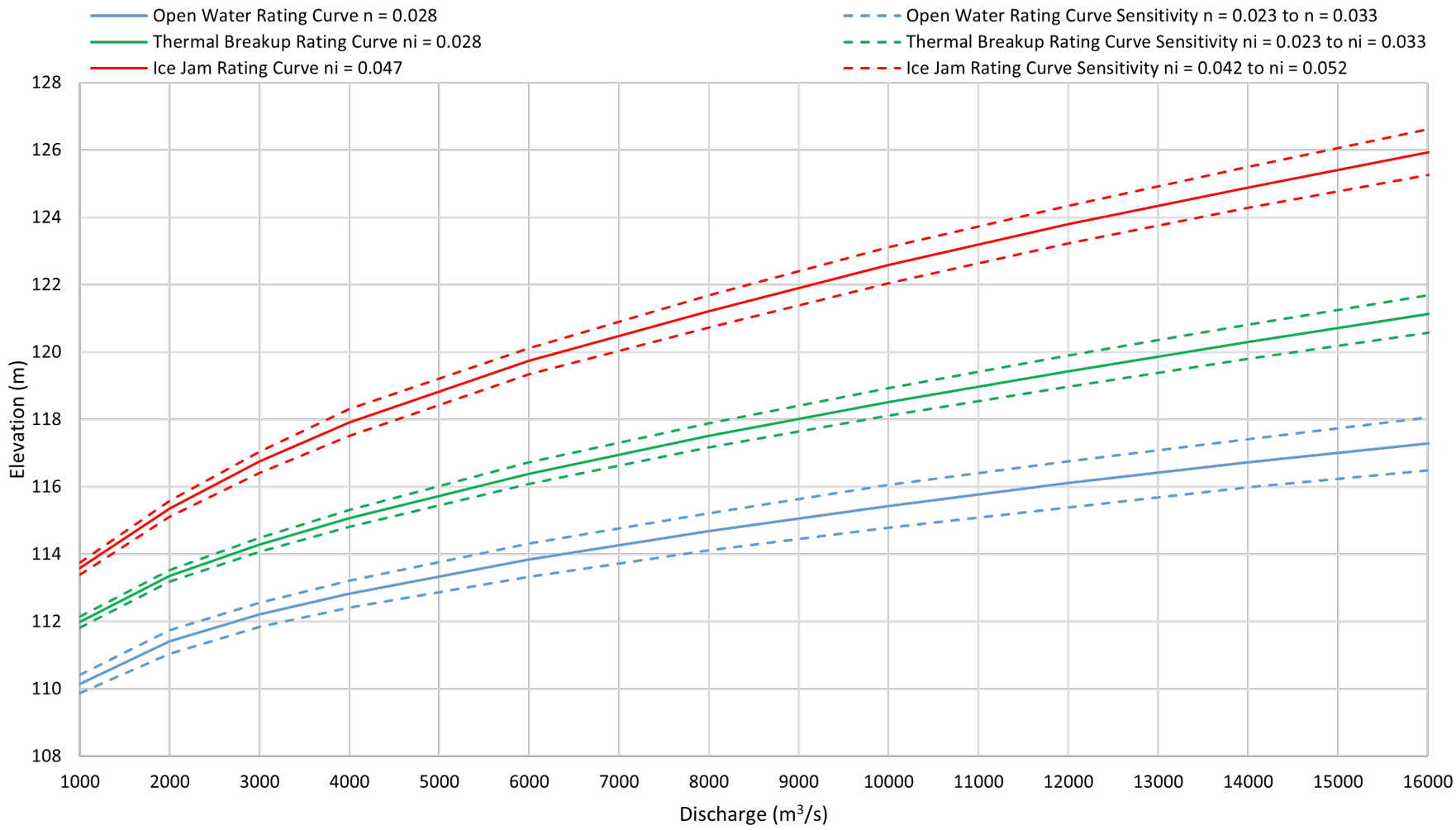

Government of Northwest Territories
Gouvernement des Territoires du Nord-Ouest

Canada

nhc

FORT SIMPSON FLOOD HAZARD MAPPING STUDY

MODEL SENSITIVITY TO CALIBRATED MANNING'S ROUGHNESS: MACKENZIE RIVER

Job: 1008469

Date: APR-2025

FIGURE 34

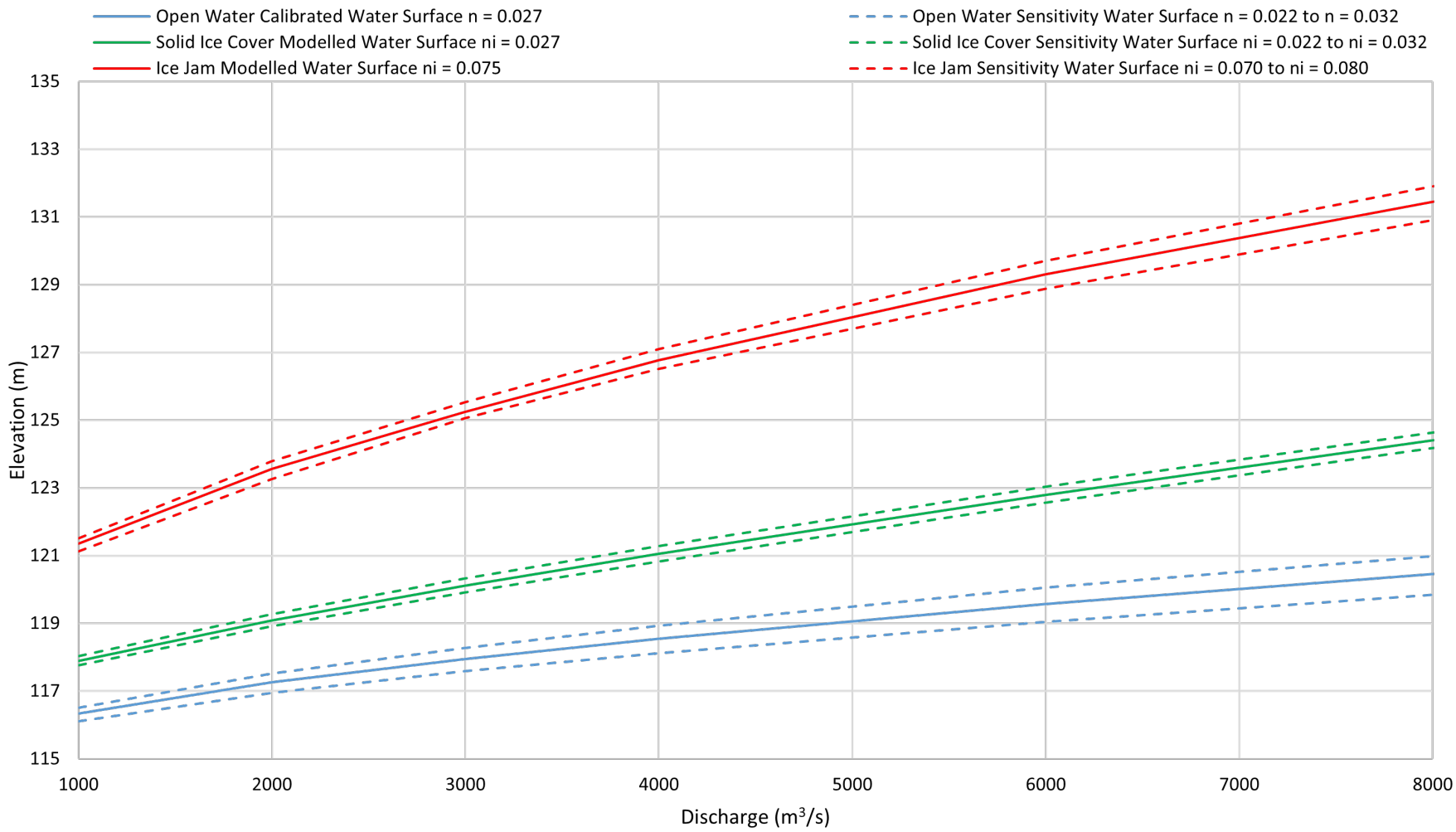

Government of Northwest Territories
Gouvernement des Territoires du Nord-Ouest

Canada

nhc

FORT SIMPSON FLOOD HAZARD MAPPING STUDY

MODEL SENSITIVITY TO CALIBRATED MANNING'S ROUGHNESS: LIARD RIVER

Job: 1008469

Date: APR-2025

FIGURE 35

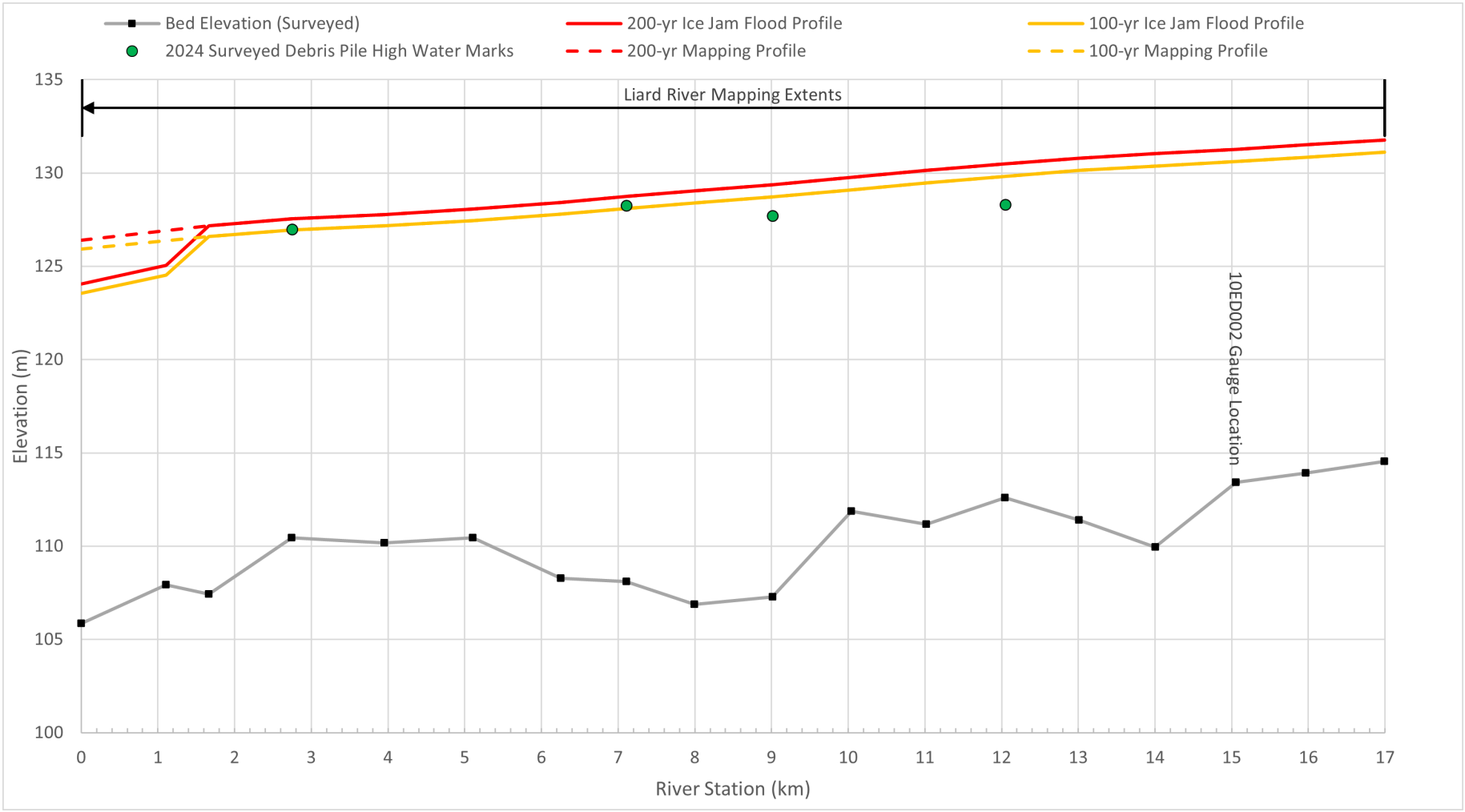

Notes:
1. Mapped water elevations at River Station 0 km were derived from water elevation at Mackenzie River Station 25.386 km. Both the Liard and Mackenzie river station are at the same location.
2. Mapped water elevations between RS 0 km to RS 1.662 km are interpolated.

Government of Northwest Territories / Gouvernement des Territoires du Nord-Ouest

Canada

nhc

UNITS – AS SHOWN

VERTICAL ELEVATION DATUM: CGVD2013a

Job: 1008469

Date: APR-2025

FORT SIMPSON FLOOD HAZARD MAPPING STUDY

FLOOD FREQUENCY PROFILES
LIARD RIVER

FIGURE 36

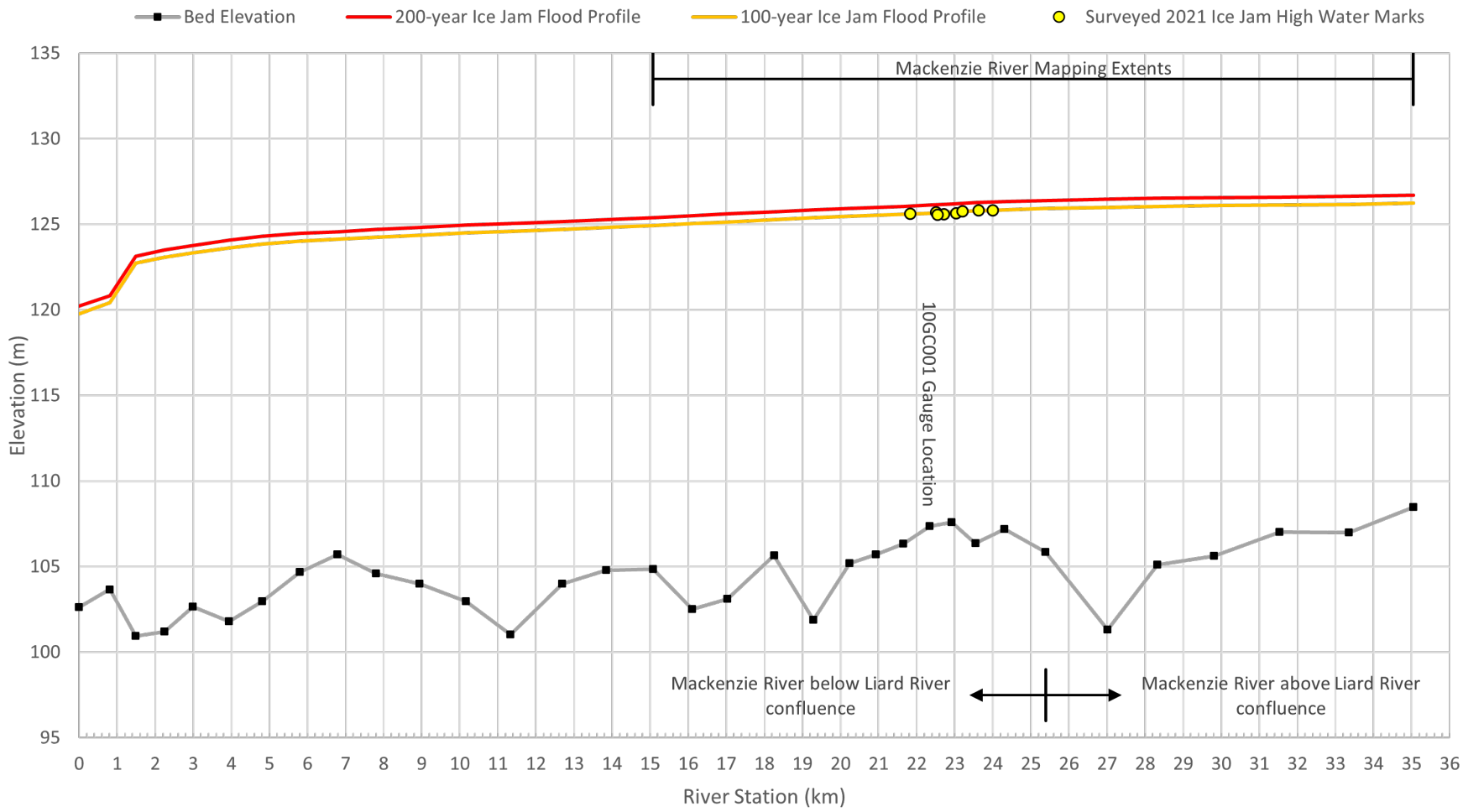

Government of Northwest Territories
Gouvernement des Territoires du Nord-Ouest

Canada

nhc

UNITS – AS SHOWN

VERTICAL ELEVATION DATUM: CGVD2013a

Job: 1008469

Date: APR-2025

FORT SIMPSON FLOOD HAZARD MAPPING STUDY

FLOOD FREQUENCY PROFILES
MACKENZIE RIVER

FIGURE 37

Fall (Sep-Oct-Nov)

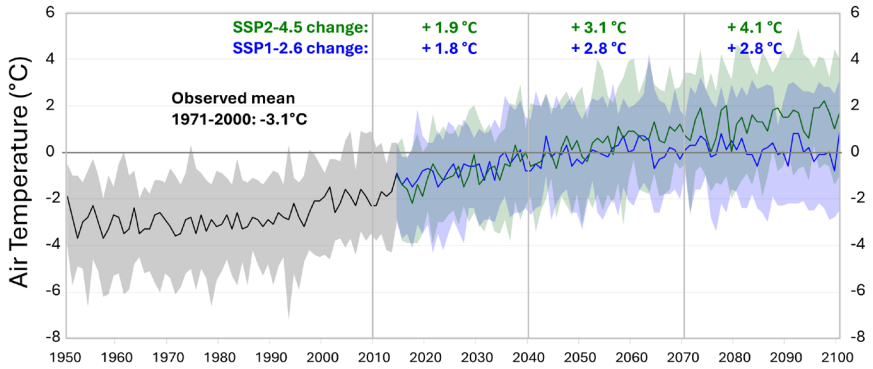

Winter (Dec-Jan-Feb)

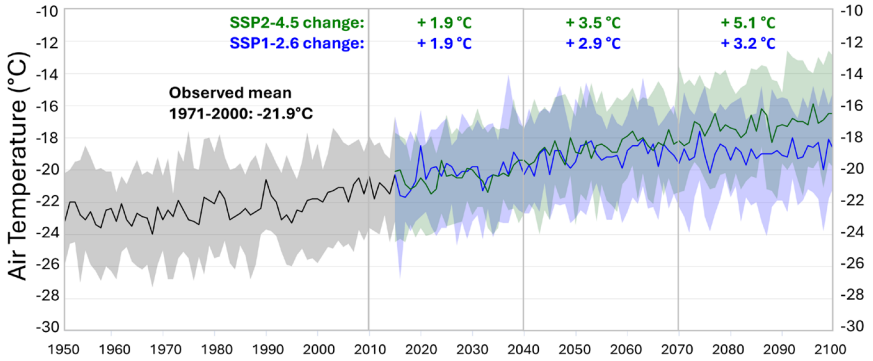

Spring (Mar-Apr-May)

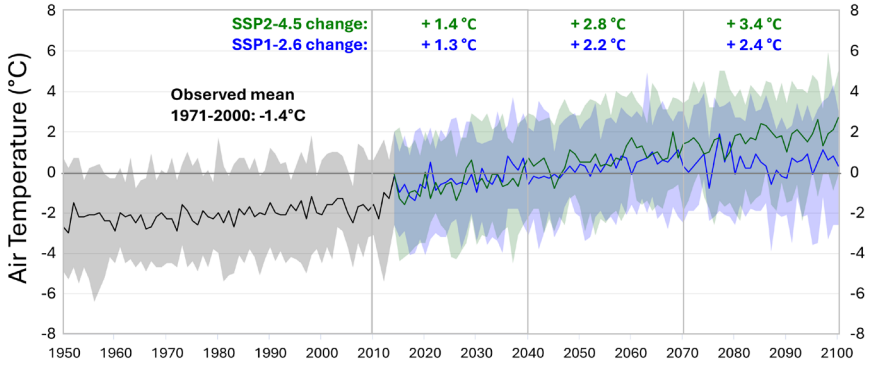

Summer (Jun-Jul-Aug)

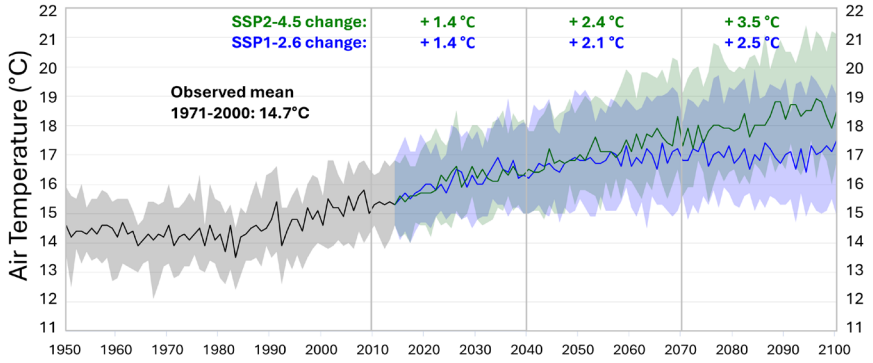

Notes:
1. The values annotated are for periods 2011-2040, 2041-2070 and 2071-2100, relative to 1971-2000

Government of Northwest Territories
Gouvernement des Territoires du Nord-Ouest
Canada
nhc

UNITS – AS SHOWN

Job: 1008469

Date: APR-2025

FORT SIMPSON FLOOD HAZARD MAPPING STUDY

PROJECTED AIR TEMPERATURE RISES FOR THE LOWER LIARD RIVER BASIN

FIGURE 38

Fall (Sep-Oct-Nov)

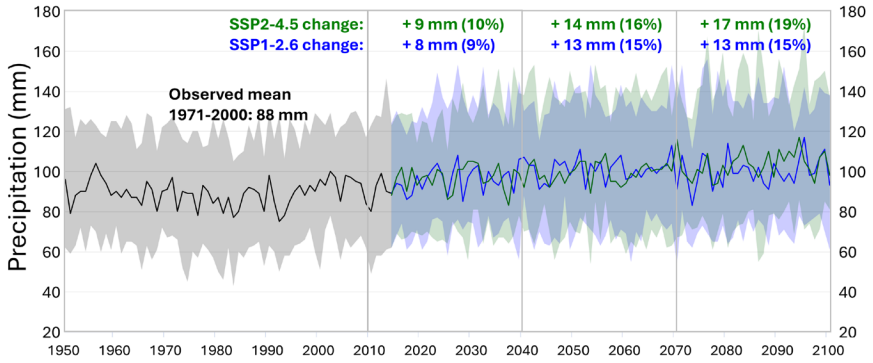

Winter (Dec-Jan-Feb)

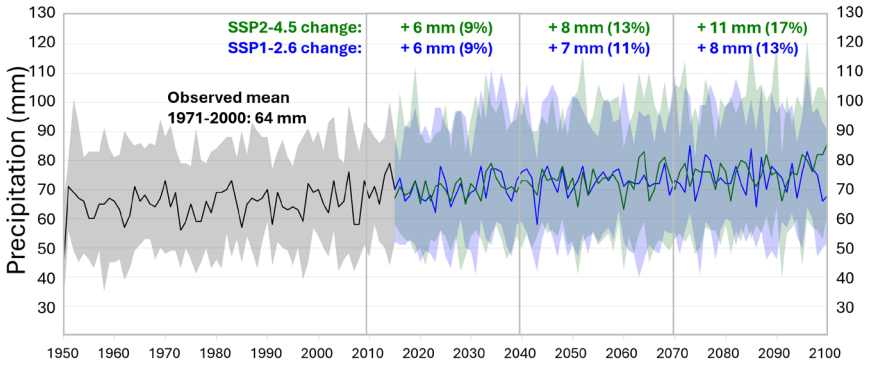

Spring (Mar-Apr-May)

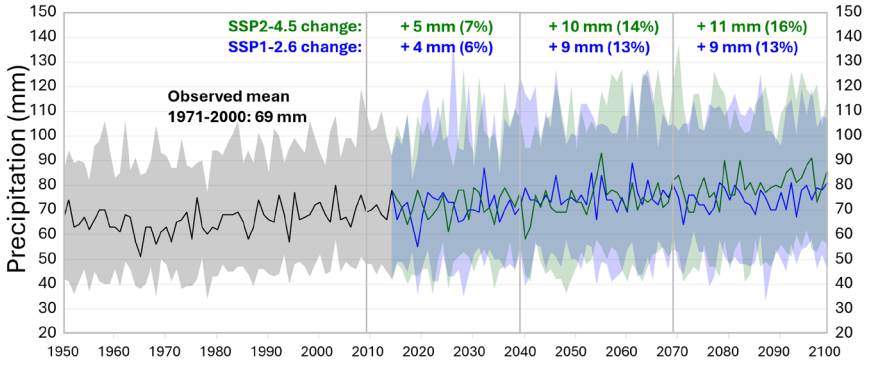

Summer (Jun-Jul-Aug)

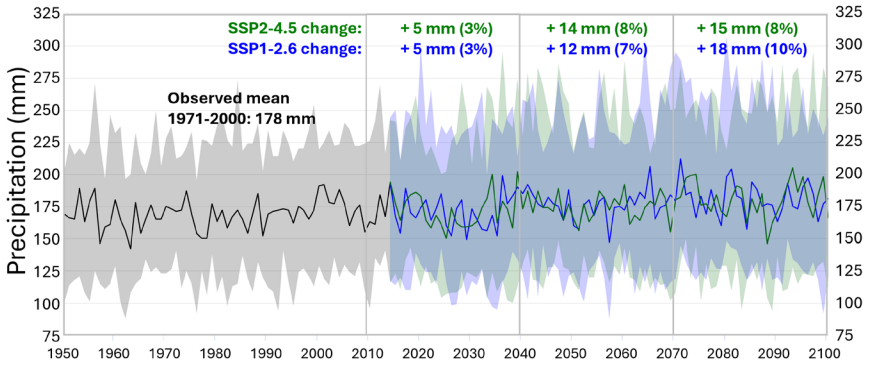

Notes:

1. The values annotated are for periods 2011-2040, 2041-2070 and 2071-2100, relative to 1971-2000

Government of Northwest Territories
Gouvernement des Territoires du Nord-Ouest

Canada

nhc

UNITS – AS SHOWN

FORT SIMPSON FLOOD HAZARD MAPPING STUDY

PROJECTED PRECIPITATION RISES FOR THE LOWER LIARD RIVER BASIN

Job: 1008469

Date: APR-2025

FIGURE 39

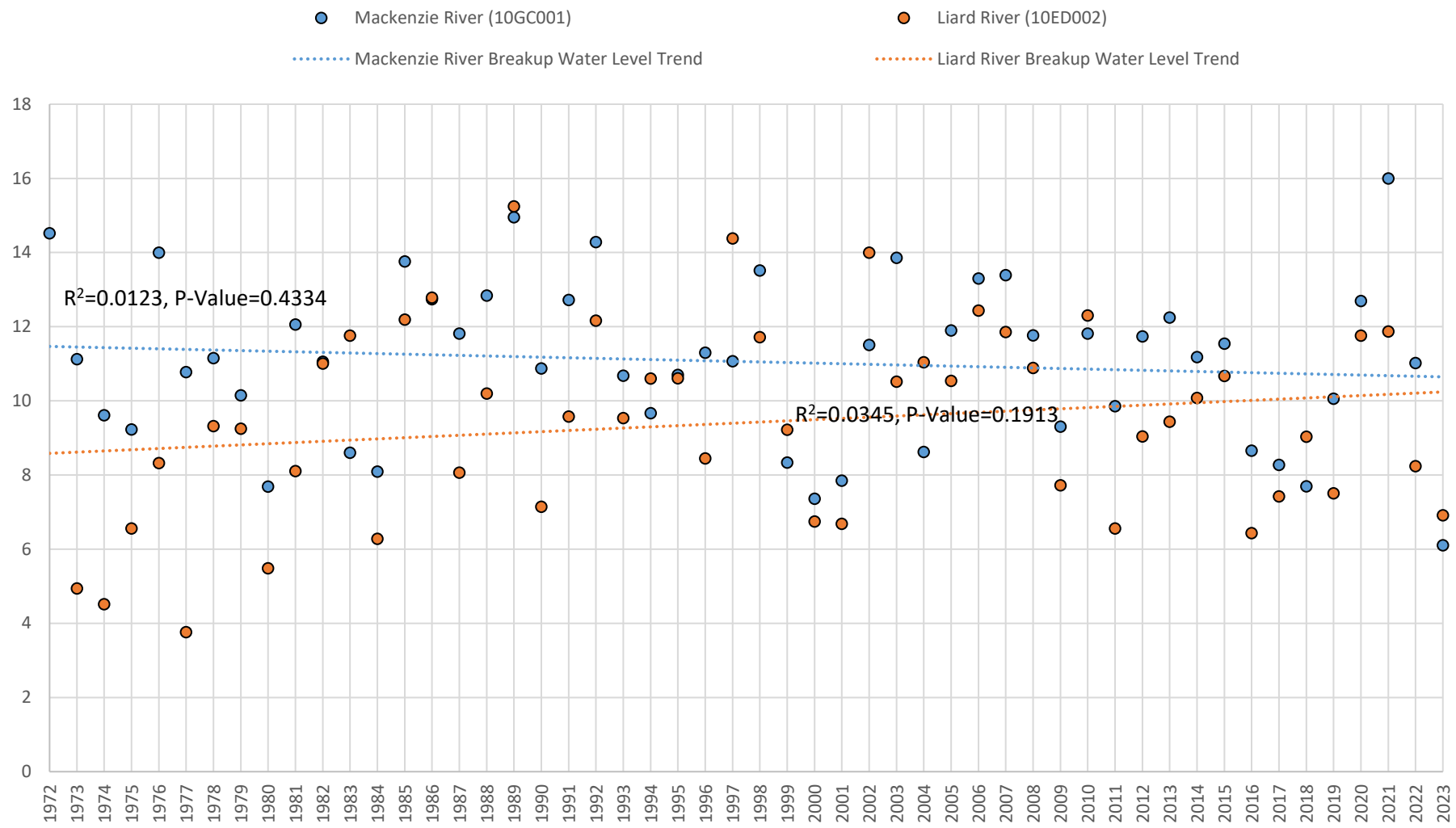

Government of Northwest Territories
Gouvernement des Territoires du Nord-Ouest

Canada

nhc

FORT SIMPSON FLOOD HAZARD MAPPING STUDY

RECORDED PEAK BREAKUP WATER LEVELS AT 10ED002 LIARD RIVER NEAR THE MOUTH AND 10GC001 MACKENZIE RIVER AT FORT SIMPSON GAUGES

Job: 1008469

Date: APR-2025

FIGURE 40

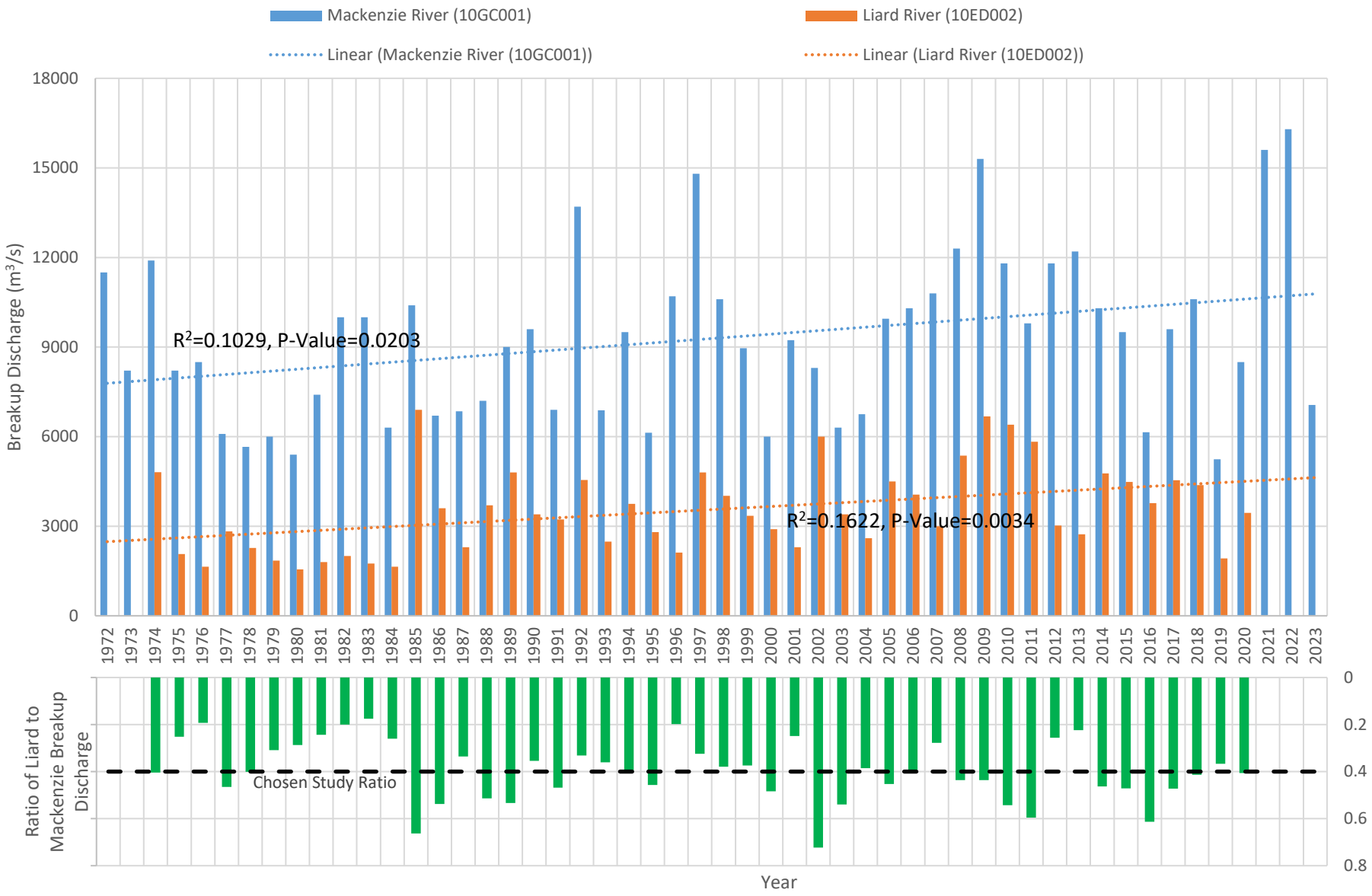

Government of Northwest Territories / Gouvernement des Territoires du Nord-Ouest

Canada

nhc

FORT SIMPSON FLOOD HAZARD MAPPING STUDY

RECORDED PEAK BREAKUP DISCHARGES AT 10ED002 LIARD RIVER NEAR THE MOUTH AND 10GC001 MACKENZIE RIVER AT FORT SIMPSON GAUGES

Job: 1008469

Date: APR-2025

FIGURE 41

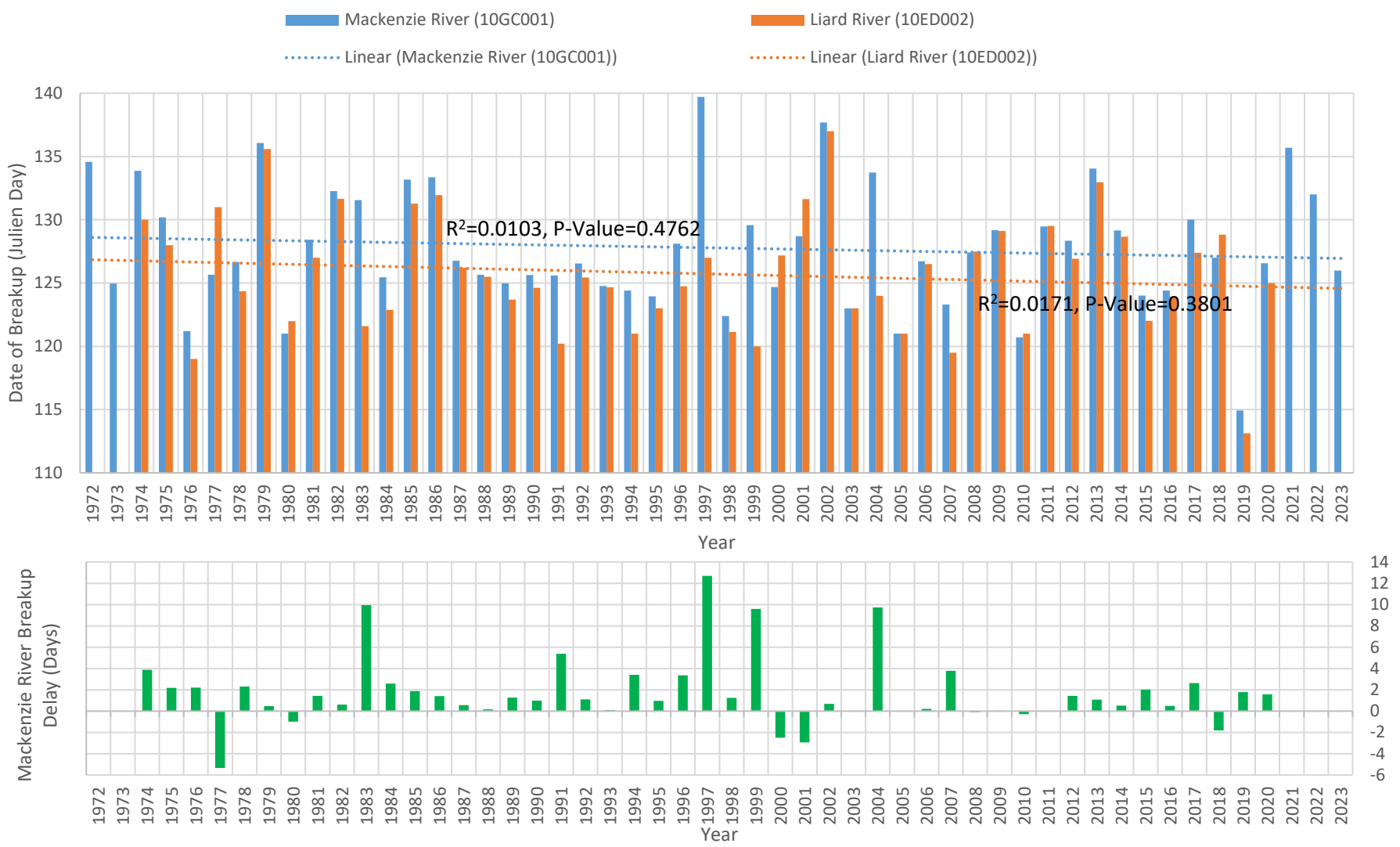

Government of Northwest Territories
Gouvernement des Territoires du Nord-Ouest

Canada

nhc

FORT SIMPSON FLOOD HAZARD MAPPING STUDY

RECORDED PEAK BREAKUP TIMING AT 10ED002 LIARD RIVER NEAR THE MOUTH AND 10GC001 MACKENZIE RIVER AT FORT SIMPSON GAUGES

Job: 1008469

Date: APR-2025

FIGURE 42

APPENDIX A

SURVEY DATA

Provided as an electronic file in ESRI geodatabase format (FortSimpsonSurvey2024.gdb).

APPENDIX B

REACH REPRESENTATIVE PHOTOS

1) Looking upstream from the left bank from PXS-33 (RS 33351).

2) Looking downstream from the right bank from PXS-32 (RS 31527).

3) Looking upstream from the right bank of the north channel along Martin Island from PXS-30 (RS 28326).

4) Looking upstream at the confluence of the Liard and Mackenzie Rivers from PXS-28 (RS 25386).

5) Looking upstream from the left at the Fort Simpson island from PXS-24 (RS 22338).

6) Looking upstream from the right bank from PXS-10 (RS 7807).

Note:

Photos taken by NHC during site visit on June 6 through June 10.

Government of Northwest Territories

FORT SIMPSON FLOOD HAZARD MAPPING STUDY

Reach Representative Photos – Mackenzie River

1008469	April 2025	**B-1**

1) Looking downstream from the left bank from PXS-3 (RS 1492).

2) Looking downstream at the Snye from PXS-26 (RS 23542).

3) Looking upstream at the Snye from PXS-21 (RS 20237) .

4) Looking downstream at the shoals and islands downstream of the Fort Simpson island from PXS-21 (RS 20237).

5) Looking downstream at the side channel from PXS-20 (RS 19285).

6) Looking at the landslide along the left of the Mackenzie River at PXS-14 (RS 12692).

Note:

Photos taken by NHC during site visit on June 6 through June 10

Government of Northwest Territories

FORT SIMPSON FLOOD HAZARD MAPPING STUDY

Reach Representative Photos – Mackenzie River

1008469	April 2025	**B-2**

1) Looking across the channel at the right bank from PXS-49 (RS 15057).

2) Looking upstream from the left bank at PXS-47 (RS 12222).

3Looking downstream from the left bank at PXS-42 (RS 8173) .

4) Looking upstream from the Island at PXS-37 (RS 2927).

5) Looking upstream from the Island at PXS-35 (RS 1218).

6) Looking US from the right bank at the PXS-35 (RS 1218).

Note:

Photos taken by NHC during site visit on June 8 through June 10

Government of Northwest Territories

FORT SIMPSON FLOOD HAZARD MAPPING STUDY

Reach Representative Photos – Liard River

1008469	April 2025	**B-3**

APPENDIX C

COMPUTED REGULATORY FLOOD LEVELS

Table C-1 Liard River computed flood frequency water levels

River Station (m)	Flood Return Period	
	100-year Ice Jam	200-year Ice Jam
	Water Surface Elevation (m)	
0[1]	126.39	125.92
1107[2]	N/A	N/A
1662	127.18	126.60
2748	127.55	126.96
3951	127.77	127.18
5108	128.07	127.46
6253	128.42	127.79
7107	128.74	128.10
7997	129.05	128.40
9013	129.38	128.72
10043	129.77	129.11
11019	130.14	129.48
12046	130.49	129.82
13008	130.80	130.13
14003	131.04	130.38
15057	131.28	130.61
15969	131.51	130.85
16994	131.77	131.11

Notes:

1. Water elevations at River Station 0 are derived from the water elevations at Mackenzie River Station 25386 as both river stations are at the same location.
2. Mapped water elevations at River Station 1107 were interpolated based on water elevations at the surrounding river stations.

Table C-2 Mackenzie River computed flood frequency water levels

River Station (m)	Flood Return Period	
	100-year Ice Jam	200-year Ice Jam
	Water Surface Elevation (m)	
0	120.22	119.79
806	120.82	120.44
1492	123.15	122.73
2249	123.51	123.08
2989	123.76	123.32
3935	124.07	123.63
4812	124.30	123.85
5801	124.48	124.03
6788	124.58	124.13
7807	124.70	124.25
8946	124.82	124.36
10164	124.96	124.50
11331	125.06	124.60
12692	125.17	124.71
13845	125.27	124.81
15077	125.39	124.93
16100	125.51	125.05
17030	125.61	125.15
18254	125.75	125.29
19285	125.85	125.39
20237	125.93	125.47
20927	125.99	125.52
21653	126.05	125.58
22338	126.12	125.65
22915	126.20	125.73
23542	126.27	125.80
24300	126.33	125.86
25386	126.39	125.92
27013	126.47	126.00
28326	126.53	126.06
29806	126.57	126.10
31527	126.59	126.12
33351	126.65	126.18
35042	126.71	126.24

APPENDIX D

100-YEAR ICE JAM FLOOD HAZARD MAP

Provided under separate cover.

APPENDIX E

200-YEAR ICE JAM FLOOD HAZARD MAP

Provided under separate cover.

APPENDIX F

CLIMATE CHANGE SUPPORTING INFORMATION

CLIMATE CHANGE SUPPORTING INFORMATION

GNWT Climate Change Strategic Framework

The Government of the Northwest Territories Climate Change Strategic Framework[1] has three goals: (1) Transition to a strong, healthy economy that uses less fossil fuel, thereby reducing greenhouse gas emissions by 30% below 2005 levels by 2030; (2) Improve knowledge of the climate change impacts occurring in the NWT; and (3) Build resilience and adapt to a changing climate. Goal 2 is most relevant to this work, details on the goal are provided below.

Goal #2- Improve knowledge of the climate change impacts occurring in the NWT

"Improving knowledge of climate change impacts occurring in the NWT is the second goal of the Framework. To address climate change, there is a need for greater understanding of the impacts to the natural environment, residents' health, safety, culture and heritage, and the territory's infrastructure. The integrated use and management of traditional, local and scientific knowledge to determine knowledge gaps, set and implement research and monitoring requirements, and obtain current and timely information, is essential.

"The warming climate is leading to gradual shifts within ecosystems and more extreme events affecting the natural environment. Thawing of permafrost, changes to water quality and quantity, altered forests and tundra vegetation, and impacts on wildlife, fish and marine mammal health and distribution, have been observed for several years and are intensifying.

"The effects of climate change on the natural environment can directly impact the health of NWT residents, both physically (such as increases in respiratory problems due to extreme weather) and mentally (such as stress or effects on well-being due to impacts on traditional harvesting sites and activities).

"Safety of the general public is also a central concern, from erosion of coastlines leading to building instability, to increased flood risks in certain communities, to less predictable winter travel conditions, all leading to a heightened risk of injury and death.

"Effects on the territory's culture and heritage, from risks to heritage resources such as archeological sites due to permafrost thaw and wildland fires, to impacts on traditional economies such as trapping, are evident and will likely continue to intensify. Indigenous people and other residents of the NWT are particularly vulnerable to climate related changes since, for generations, they have depended on the land, water and wildlife for their livelihood and sustenance.

"The NWT's infrastructure (buildings, roads, pipelines, transmission lines, etc.) has been and continues to be impacted by climate change. Permafrost thaw and extreme weather events can have significant effects on infrastructure. Coastal erosion is also a concern in the northern parts of the NWT, threatening important infrastructure such as roads and buildings.

"Developing a better understanding of current and future impacts and opportunities will support informed decision-making on how to build resilience and adapt to a changing climate."

Source: GNWT Climate Change Strategic Framework**Error! Bookmark not defined.**

[1] https://www.gov.nt.ca/ecc/en/services/climate-change/2030-nwt-climate-change-strategic-framework

Available Research and Climate Projection Data

Emission Scenarios

Anthropogenic activities around the globe release greenhouse gases into the earth's atmosphere – CO_2 being the principal one, followed by nitrous oxide – and these interfere with the earth's energy balance creating a trend towards higher air temperatures. At any given geographic location, natural climatic variability continues exhibiting colder years as well as warmer years, but an underlying tendency towards progressively higher mean temperatures over time is projected for the future. A warming trend is found in observational records of recent decades at most global locations.

The magnitude of future global emissions of greenhouse gases cannot be predicted with any certainty, but scientists have developed a number of scenarios for possible future emissions. The ESMs included in the CMIP6 projections dataset were run under these scenarios. However, the IPCC does not attempt to attribute comparative likelihoods to the different scenarios. In this, it follows the tradition established in CMIP3, where the Special Report on Emission Scenarios (Nakićenović, N. et al., 2000) presented all scenarios as *"equally valid with no assigned probabilities of occurrence"*. The scenarios used in CMIP5 were defined on the basis of hypothetical future greenhouse gas concentrations in the earth's atmosphere, i.e., "representative concentrations pathways" (RCPs), where *"no likelihood or preference is attached to any of the individual scenarios in the set"* while they included a very wide range of possibilities described as *"...the full range of emission scenarios available in the current scientific literature, with and without climate policy"* (van Vuuren et al., 2011). No explanations (whether socio-economic, technologic or demographic) were associated with any of the RCPs, until CMIP6.

In CMIP6, explanatory storylines were sought, called "shared socio-economic pathways" (SSPs), and these SSPs were developed to correspond with the RCPs, i.e., a storyline (SSP) was associated with specific greenhouse gas concentrations (RCP). The SSPs represent scenarios of future evolution of human societies and were developed by multidisciplinary teams including economists and energy specialists. Each SSP is based on a storyline of demographic, economic, technological and political evolution involving the world countries.

Five different classes of SSPs were developed with key differences in their narratives (Table 1-1). More complete descriptions are given in Riahi et al. (2017), O'Neill et al. (2014) and van Vuuren et al. (2011). Four of those were used by a large number of ESMs, and SSP4 was used for a smaller number of ESMs and the SSP4 results are not available through the CMIP6 data portals. The main scenario of each SSP is indicated in the last column of Table 1-1.

The numbers in the name of each SSP identify the class as well as the projected global energy imbalance it corresponds to in year 2100. For example, SSP1-2.6 belongs to class SSP1 and corresponds to an energy imbalance of 2.6 Watt per square meter in year 2100. Thus, SSP2-4.5

leads to a higher energy imbalance than SSP1-2.6, therefore more intense warming of the earth's atmosphere, due to higher greenhouse emissions in the course of this century.

Table 1-1 The five classes of SSP global emission scenarios and the main scenario of each class. Class descriptions are repeated from Riahi et al. (2017).

SSP Class	Class Description	Main scenario of each SSP
SSP1 Low emissions	The world shifts gradually, but pervasively, toward a more sustainable path, emphasizing more inclusive development that respects perceived environmental boundaries. Management of the global commons slowly improves, educational and health investments accelerate the demographic transition, and the emphasis on economic growth shifts toward a broader emphasis on human well-being. Driven by an increasing commitment to achieving development goals, inequality is reduced both across and within countries. Consumption is oriented toward low material growth and lower resource and energy intensity.	SSP1-2.6
SSP2 Moderate emissions	The world follows a path in which social, economic, and technological trends do not shift markedly from historical patterns. Development and income growth proceeds unevenly, with some countries making relatively good progress while others fall short of expectations. Global and national institutions work toward but make slow progress in achieving sustainable development goals. Environmental systems experience degradation, although there are some improvements and overall the intensity of resource and energy use declines. Global population growth is moderate and levels off in the second half of the century. Income inequality persists or improves only slowly and challenges to reducing vulnerability to societal and environmental changes remain.	SSP2-4.5
SSP3 High emissions	A resurgent nationalism, concerns about competitiveness and security, and regional conflicts push countries to increasingly focus on domestic or, at most, regional issues. Policies shift over time to become increasingly oriented toward national and regional security issues. Countries focus on achieving energy and food security goals within their own regions at the expense of broader-based development. Investments in education and technological development decline. Economic development is slow, consumption is material-intensive, and inequalities persist or worsen over time. Population growth is low in industrialized and high in developing countries. A low international priority for addressing environmental concerns leads to strong environmental degradation in some regions.	SSP3-7.0
SSP4 Very high emissions	Highly unequal investments in human capital, combined with increasing disparities in economic opportunity and political power, lead to increasing inequalities and stratification both across and within countries. Over time, a gap widens between an internationally-connected society that contributes to knowledge- and capital-intensive sectors of the global economy, and a fragmented collection of lower-income, poorly educated societies that work in a labor intensive, low-tech economy. Social cohesion degrades and conflict and unrest become increasingly common. Technology development is high in the high-tech economy and sectors. The globally connected energy sector diversifies, with investments in both carbon-intensive fuels like coal and unconventional oil, but also low-carbon energy sources. Environmental policies focus on local issues around middle and high income areas.	unavailable

SSP Class	Class Description	Main scenario of each SSP
SSP5 Extreme emissions	This world places increasing faith in competitive markets, innovation and participatory societies to produce rapid technological progress and development of human capital as the path to sustainable development. Global markets are increasingly integrated. There are also strong investments in health, education, and institutions to enhance human and social capital. At the same time, the push for economic and social development is coupled with the exploitation of abundant fossil fuel resources and the adoption of resource and energy intensive lifestyles around the world. All these factors lead to rapid growth of the global economy, while global population peaks and declines in the 21st century. Local environmental problems like air pollution are successfully managed. There is faith in the ability to effectively manage social and ecological systems, including by geo-engineering if necessary.	SSP5-8.5

Figure 1.1 shows the evolution over time of our planet's energy imbalance (known as "radiative forcing") and mean global temperature corresponding to each SSP and RCP. This figure also shows the relationship between the RCP scenarios from CMIP5 and the SSP scenarios of CMIP6.

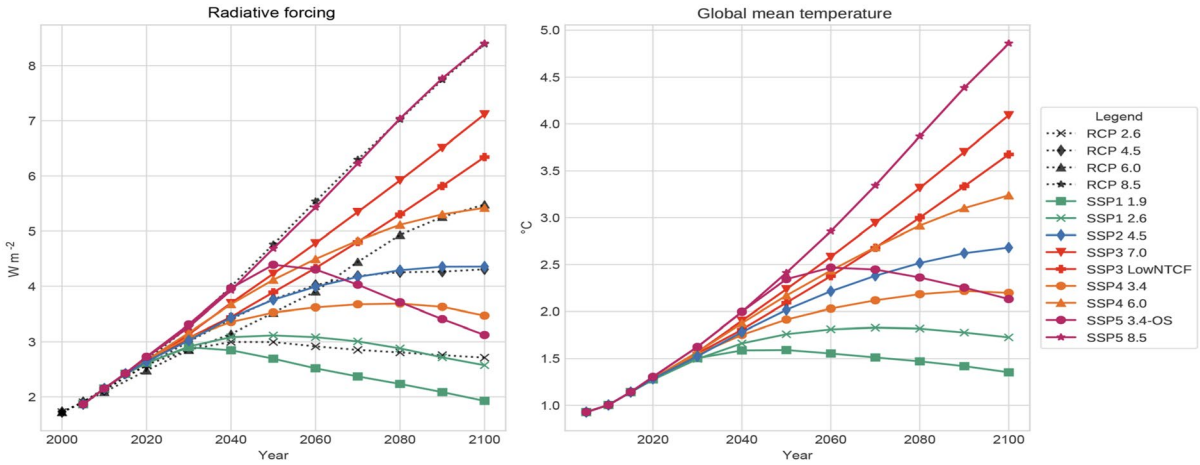

Figure 1.1 Radiative forcing or global energy imbalance (left panel) and global mean temperature (right panel) for each RCP and SSP. Figure source: Gidden et al. (2019).

Downscaled climate projections

The downscaled projections are from an ensemble of 24 earth system models (ESMs) and were made available on the Canadian government data portal[2], for SSP1-2.6, SSP2-4.5 and SSP5-8.5. An empirical-statistical methodology – briefly described below – was used to obtain these projections. Other sources provide downscaled projections in gridded format (e.g., the Pacific

[2] https://climatedata.ca

Climate Impacts Consortium data portal[3]) but, to our knowledge, this one[Error! Bookmark not defined.] is unique in providing projections by watershed.

The outputs from earth system models must undergo a process of "downscaling" before they can be used in impact assessment studies. Downscaling serves two purposes: (1) It provides a higher resolution spatial scale, and (2) it provides climatic values that are in better agreement with observations. The increased spatial resolution is necessary because grid cells of earth system models (ESMs) cover considerably large areas, ranging from a few hundred km^2 in some ESMs to several thousand km^2 in others. Resolutions desired for impact assessment studies are typically in the order of 1/8°x 1/8° (less than 150 km^2) or 1/12°x 1/12° (less than 70 km^2).

The higher spatial resolution may be obtained by statistical methods or dynamical models:

(a) Empirical-statistical downscaling models (ESDMs) establish a statistical relationship between the coarse-resolution ESM output for a historical period for a given geographical region and the finer-resolution observations-based gridded data representing that period over that region. The observations-based gridded data may have been obtained by statistical interpolation of ground observations or using a weather model that assimilates those ground observations to create a "Reanalysis" data set.

(b) Dynamical downscaling uses regional climate models (RCMs), which have higher spatial resolution than ESMs and better represent land topography and coastlines. The output from the RCMs typically needs to be statistically downscaled (as in (a) above) to remove the bias present in most RCM data.

While option (b), dynamical downscaling, is scientifically superior than option (a), empirical-statistical downscaling, it involves computationally (and financially) costly runs of regional climate models. For this reason, dynamically-downscaled projections are not readily available for large ESM ensembles.

Selection of SSP scenarios for this study

Projections for two SSPs are consulted in this study in section 1.3.2. They are SSP1-2.6 and SSP2-4.5. This section explains the reasons for this selection of SSPs instead of others. Similar to previous IPCC assessment reports, no probabilities or relative likelihoods were assigned to the SSPs (Riahi et al., 2017). Thus, the user is to make their own evaluation. Difficulties resulting from this approach have been reviewed e.g. by Huard et al. (2022), however various scientists have argued from early on that it is not possible to assign probabilities to future emissions because

[3] https://www.pacificclimate.org/data/statistically-downscaled-climate-scenarios

they represent "unknowable knowledge" and depend on subjective opinions about future developments which are unpredictable (e.g., Dessai and Hulme, 2004).

Despite the reluctance to assign probabilities to SSPs, the first chapter of the IPCC Sixth Assessment report (Chen et al., 2021) does discuss their likelihood. It concludes that SSP5-8.5 and SSP3-7.0, both of which consider completely unregulated and unabated future emissions (in violation of commitments already in place today), should be considered counter-factual scenarios. It also concludes that policies currently agreed upon would lead to an energy imbalance by year 2100 roughly close to 4.5 Watt/m^2 – thus making SSP2-4.5 a likely scenario.

Concerning SSP3-7.0, Shiogama et al. (2023) warns it is not intended for impact studies. It clarifies that SSP3–7.0 was designed to have different characteristics compared with the other scenarios for purposes of increasing scientific understanding of the impacts of aerosols and land use. SSP3-7.0 assumes high-aerosol emissions incompatible with air quality policies and assumes very large deforestation rates.

Other researchers have tried to independently obtain some approximate answers to the question of SSP probabilities. Huard et al. (2022) presented a methodology that allows calculating SSP probabilities, where the first step involves calculating the greenhouse gas emissions rates compatible with each SSP, and the second step involves "integrated assessment models". Unfortunately, the first step is highly uncertain given the complexity of indirect emissions resulting from carbon cycle feedbacks (for example, the carbon emissions from permafrost thaw). Nevertheless, their estimation of a very low probability for SSP5-8.5 (the most extreme SSP) in the second half of this century appears to be a robust result. Another, more uncertain result of their study is that SSP2-4.5 is the most likely pathway for this century.

The recent work of Venmans and Carr (2024) offered a different approach, which focuses on the emission-reduction policies which have already been approved by different governments around the world. This includes individual policies as well as international accords. Assuming those policies will indeed be implemented, they demonstrate that the most likely energy imbalance reached in year 2100 is close to 4.5 Watt/m^2, making SSP2-4.5 the most likely. This result agrees with that of Huard et al. (2022) mentioned above. They also agree with Huard et al. (2022) in estimating a very low probability for SSP5-8.5, on the basis that the costs of renewable energies have fallen far more rapidly in recent years than had been anticipated; the global coal consumption has stagnated since 2013 (and the International Energy Agency (IEA) projects it will fall by another 25% before year 2050 as a result of policies already agreed on and given the fall in price of shale gas); and the cost of batteries has also dropped, lowering the demand for oil (which the IEA projects will stagnate around year 2030). Moreover, as they point out, the price of carbon in the European Union Emission Trading Scheme increased sharply (from 5/tCO_2 in 2017 to over 80/tCO_2 in 2023); the United States have rejoined the Paris Accord; and in 2021 China launched the largest emission trading scheme of all time so far.

Earlier this year, a publication by Nathan Gillett from ECCC (Gillett, 2024) argued that the uncertainty associated with future greenhouse gas emissions has roughly halved in the past decade, on the basis of their analysis of the progress made in climate policy and climate science. The conclusion presented is that *"…the range of plausible future emissions is now lower and narrower than it was in 2013 … and can reasonably be bracketed by the SSP1-1.9 and SSP2-4.5 scenarios"* (Gillett, 2024).

Uncertainty Associated with Climate Projections

While there is a need to provide climate projections for planning purposes, the underlying projections of climate change are subject to large and unquantifiable uncertainty. The projections of air temperature and precipitation presented below should therefore be considered as plausible representations of the future, given the best current scientific information, and do not represent specific predictions. The actual future realizations of these variables over the areas studied will differ from any of the projections considered here, and their differences compared to historical climate may be greater or smaller than the differences in the projections considered. Uncertainty is particularly great for precipitation projections, where even the sign of change (increase or decrease) often differs between earth system models. Precipitation processes have chaotic behavior and involve multiple spatial scales including scales finer than the resolution of earth system models.

The main sources of uncertainty are unknown future emissions of greenhouse gases (addressed in the preceding section); limitations of current scientific knowledge and the formulation of the earth system models used; and the natural variability of climate, in particular the great variability of precipitation from year to year and at longer scales such as decadal scale. An additional source of uncertainty is the use of spatial downscaling of the precipitation and temperature time series simulated by earth system models. Extreme precipitation additionally depends on a major non-climatic factor, which is the local atmospheric concentrations of different types of aerosols.

Adding to the uncertainty of climate projections, the effects of the Great Slave Lake on regional climate as the lake's ice cover period lengthens are not well represented by CMIP6 earth systems models. The lake's presence, due to its thermal inertial across the seasons, could moderate seasonal climatic changes (Huziy and Sushama, 2017). The lake's presence could also lead to increased snowfall in the ice-free fall season, known as "lake effect snow".

Review of Literature on Ice Jam Flooding Related to the Hay River and Fort Simpson

Ice jams on the lower Hay River have been studied over time, and Burrell et al. (2015) provides a list of 16 different studies, spanning 1959 to 2012. Notable from this list are theses and peer-reviewed publications by students of Prof. Faye Hicks at University of Alberta, dating from 2011 and 2012. NHC consulted these studies for the present assessment, having found that the doctoral thesis by Zhao (2012) contains important observations-based interpretation of the

hydro-climatic factors associated with ice jam flooding on the Hay River, which will be reviewed in section 1.4.

A good number of peer-reviewed publications address specifically the effects of climate change on ice jam flooding frequency and severity. A selection of key publications were reviewed for the present assessment in section 1.4. Some of these publications themselves represent literature reviews, including Turcotte et al. (2019), while others focus on particular aspects of river ice formation, thickening, ice break, ice jams, etc., most of them with a focus on tributaries of the Mackenzie River.

Climate change will impact ice jam flooding risk through a number of processes that this section attempts to separate into subsections.

Thresholds Between Mechanical and Thermal Breakup of River Ice Cover

Due to the clarity of its exposition, Beltaos (2003) is quoted directly below:

"The breakup of river ice is triggered by mild weather and encompasses a variety of processes associated with thermal deterioration, initial fracture, movement, fragmentation, transport, jamming, and final clearance of the ice. Though several or all of these processes may be occurring simultaneously within a given reach, it is convenient to visualize the breakup period as a succession of distinct phases such as ***pre-breakup, onset, drive, wash****. During the pre-breakup phase, the ice cover becomes more susceptible to fracture and movement via thermally induced reductions in thickness and strength (excepting premature breakup events, as discussed later). At the same time, the warming weather brings about increased flow discharges, due to snowmelt or rainfall or both. The increasing hydrodynamic forces and rising water levels fracture the ice cover and reduce its attachment to the riverbanks while the increased flow velocities cause it to move and break down into relatively small blocks. This is the onset of breakup, and is followed by the drive, that is, the transport of ice blocks and slabs by the current.*

"The onset is governed by many factors, including channel morphology, which is highly variable along the river. It is thus typical to find reaches where breakup has started alternating with reaches where the winter ice cover has not yet moved. This configuration is the almost exclusive cause of breakup jamming: ice blocks moving down the river eventually encounter stationary ice cover and begin to pile up behind it, initiating a jam. In this case, the upstream drive has been stalled at a reach that is still in the pre-breakup phase, and which may well be followed by another that is in the drive, or even wash, phase. As the flow continues to increase and thermal deterioration advances, ice jams release, thus generating major ice runs and surging flows. The wash may begin after the passage of an ice run and typically involves re-floating and transporting ice blocks that may have been left stranded on shallow areas near the banks or mid-channels bars and islands.

"Depending on hydrometeorological conditions, the severity of a breakup event can vary between two extremes, those of the thermal or overmature breakup and the premature breakup. The former type occurs when mild weather is accompanied by low runoff, due to gradual slow melt and lack of

rain. The ice cover deteriorates in place and eventually disintegrates under the limited forces applied by the modest current. Ice jamming is minimal, if any, and water levels remain low. Premature breakup on the other hand, is associated with rapid runoff, usually due to a combination of rapid melt and heavy rain. The hydrodynamic forces are sufficient to lift and break segments of the ice cover before significant thermal deterioration can occur. Ice jams are now the most persistent because they are held in place by sheet ice that retains its strength and thickness. This is aggravated by the high river flows caused by the intense runoff, rendering premature events the most severe in terms of flooding and damages. Usually, a breakup event falls somewhere between these two extremes, and involves a combination of thermal effects and mechanical fracture of the ice. The term mechanical breakup is used herein to denote all nonthermal events because they are 'at least partly' governed by the mechanical properties of the ice cover.

"The conditions that determine whether a breakup event will be thermal or mechanical have never been examined or quantified, despite their practical significance in flood forecasting and warning, and in hydroclimatic studies of river ice processes. Using current understanding of breakup initiation mechanisms, a first attempt to develop physics-based criteria for this threshold has been carried out and is presented herein. The resulting relationships are tested with case studies in three different rivers, and their practical implications are discussed.

"Onset of mechanical breakup:

"Defining the onset of the breakup event at any particular location along a river as the time when the winter ice cover is set in sustained motion, a number of onset criteria have been formulated in the past few decades (e.g. see Beltaos, 1995). Most are completely empirical, relying on various combinations of water level, ice thickness, freeze-up conditions, and air temperature indices such as degree-days of thaw. A common criterion that incorporates past empirical findings (...) is:

$$H_B - H_F = k \cdot h_0 - F(S) \qquad (1)$$

in which H_B = water surface elevation at which the ice cover starts to move; H_F = water surface elevation at which the ice cover formed during the preceding freeze-up event = freeze-up level; h_0 = ice cover thickness prior to the start of melt, or ''initial'' thickness for the pre-breakup period; F = a site-specific function of S, the latter being an index of thermal effects on the ice cover, often taken as the cumulative heat flux to the ice or simply the accumulated degreedays of thaw; and k = site-specific coefficient, so far known to take on values between 2 and 10. Note that this type of criterion does not apply to thermal breakup events.

"Eq. (1) and others like it do not explicitly account for hydrodynamic or morphological effects; hence, they can only be applied to the particular river site at which they have been calibrated, i.e. they are site-specific."

Snow Accumulation and Snowmelt

Future warming leads to the **shortening of the snow accumulation period**. However, winter temperatures will remain well below freezing throughout this century (Figure 1.2) and **winter precipitation is projected to increase** (Figure 1.3). There will be a possible increase in snowfall as the Great Slave Lake experiences a shortening of its ice cover period. The known **"lake effect snow"** refers to the enhancement of snowfall after a cold air mass passes through open water and becomes saturated with moisture. Rühland et al. (2023) presented a recent account of the climatic changes affecting the Great Slave Lake.

Snow falling in river water frequently leads to the formation of slush, later resulting in thicker river ice cover (Turcotte et al., 2012). A thicker and denser snowpack promotes the formation of thicker river ice due to higher albedo (Bush and Lemmen, 2019).

Streamflow Hydrograph

As a result of warming in the fall and spring, seasonal flows throughout the southern Mackenzie River upstream of Fort Simpson, including the Hay River, will experience changes in their seasonal means and seasonal peak flow frequencies. Warming of the fall season, where the average air temperature is crossing above 0°C (as seen in Figure 1.2 for the lower Liard River), implies a progressive transition from snowfall to rainfall and higher mean seasonal flows and peak flows in this season. A trend toward earlier arrival of the spring freshet was detected throughout the Mackenzie River basin (Von de Wall et al., 2010).

The progressive thawing of permafrost will increase infiltration capacity and amplify the subsurface component of the hydrograph (e.g., St. Jacques and Sauchyn, 2009), which may augment minimum flows in winter. An observed decline in minimum flows in the Liard River basin was detected already 20 years ago (Burn et al., 2004). It also has potential implications for channel stability (addressed in section 1.2.3.4). However, permafrost thaw can also amplify surface runoff response and therefore peak flows, due to increased surface connectivity. This phenomenon was studied specifically for the Liard River basin by Connon et al. (2014), and this publication is reviewed in section1.2.3.10.

Land cover changes may occur as a result of permafrost thaw and warming, including not only a shift in tree species (see section 1.2.3.10) but also an increased incidence of forest fires instigated by pine beetle infestations that kill trees, producing fuel for fires. The proliferation of pine beetles is inhibited by very low minimum air temperatures. Strong rains in the years following a fire can produce exceptional runoff peaks, due to hydrophobic soils in addition of lesser canopy interception. Such runoff peaks may lead to dynamic ice breakup (section 1.2.3.7).

Streamflow changes have important consequences for channel morphology, ice formation and ice break-up, as highlighted in each of the subsections below.

Channel Morphology

Most geomorphological change occurs during the dynamic periods of freezup and breakup. Pulses of high sediment concentration typically peak shortly after the arrival of the peak surface concentration of ice. An increase in frequency and magnitude of ice jams, associated with a changing climate, will tend to intensify erosion and sedimentation processes.

The thawing of permafrost as well as possible increases in the frequency of freeze-thaw cycles are expected to decrease bank resistance (Ettema and Daly, 2004), increasing erosion and sediment supply to the channel. Increased sediment transport is expected to lead to morphological changes (Turcotte et al., 2011), but the impact of such changes on ice jams is uncertain and site specific. Turcotte et al. (2019) writes: *"A modification of any channel geometry parameter (i.e., channel avulsion, channel widening, bank incision), alignment (i.e., meander migration acceleration) or profile (i.e., increased spacing between pools) could either reinforce or reverse the intensity and frequency of the [ice] generating process through an alteration of ice-cover or ice-jam mobilization resisting and driving forces. The location of ice jams could also be impacted."*

Ice Formation

Freeze-up conditions in a warmer climate are important to study because they help determine ice cover thickness and ice resistance at breakup, thereby influencing ice jam flood risk. Future changes in air temperature will influence freeze-up conditions through multiple avenues:

(a) Higher flows in late autumn and early winter (see section 1.2.3.1) **delay and prolong the river freezing-over process and the development of a consolidated river ice cover** by preventing ice congestion and slowing down progression of the ice front (e.g., Prowse et al., 2007; Burrell et al., 2023). Prowse et al. (2007) indicates that higher streamflows during freeze-up could translate into an increased initial ice thickness, promoting addition of ice vertically instead of horizontally in the upstream direction, thus delaying the upstream advance of the freeze-up front. According to Prowse et al. (2007), this would result in a **heterogeneous ice cover thickness from upstream to downstream**, which could **lower the thresholds for ice breakup** (Burrell et al., 2023).

(b) Because freeze-up time is prolonged, there is **more formation of frazil ice** instead of an ice layer. Higher flows are more turbulent – which promotes mixing and precludes thermal stratification of the water column, thereby requiring that a larger volume of water be cooled before ice can be produced (e.g., Prowse et al., 2007; Beltaos and Prowse, 2009).

(c) Beltaos and Prowse (2009) suggest that higher streamflows can also lead to more frequent occurrence of a process (termed "**telescoping**") where the initial ice cover undergoes a process of collapsing, thickening and shortening; and that he combination of higher flows with higher air temperatures can increase the severity of **freeze-up**

jamming.

(d) Importantly, higher streamflows cause ice to be formed at higher stage levels in the stream channel. The **higher freeze-up stage** will require a higher streamflow threshold capable of initiating ice breakup in the spring (section 1.2.3.6). This higher threshold can **potentially reduce the frequency of ice jams during break-up** (Beltaos et al., 2006; Turcotte et al., 2019), especially if spring flows are reduced due to lesser snow accumulation given a shorter cold season. On the other hand, the higher threshold does ensure that **an ice jam flood, if it does occur, will be of significant magnitude.**

Ice Thickness

After ice formation, which in this region historically occurs in the fall, ice continues to grow during the winter but at declining rates. This is because the ice sheet itself, and the snow cover, provide thermal insulation. Beltaos and Burrel (2002) remark that *"In the colder parts of Canada, ice thickness hardly changes during the latter part of the winter. A general rise in air temperatures would then produce a relatively small reduction in the pre-breakup ice thickness, which is the value that influences the breakup process."* Burrell et al. (2023), citing studies by Brown and Duguay (2010) and Dibike et al. (2011), indicates that trends in ice thickness are associated not only with air temperature but also snow cover, with the thickest ice corresponding to the smallest snow depth, and vice versa.

The simplest established approach for representing the dependence of maximum ice thickness (Z_{ice}) on air temperature is the Stefan equation (Stefan, 1891; Jumikis, 1977), which represents a linear dependence on the square root of the accumulated freezing degree days ($AFDD$). The Stefan equation is $Z_{ice} = \alpha\sqrt{AFDD}$. The multiplication factor (α) is to be obtained empirically for the specific site of interest, and is sometimes called the "insulation coefficient". Its values have been found to vary between 7 and 27 (according to Turcotte et al., 2019 citing Michel, 1971, and Beltaos, 1995b). Factor α depends on the conditions of snowpack and wind as well as characteristics of the water body. While additional factors, such as streamflow and latent heat fluxes, also influence Z_{ice}, their effect is much smaller (Beltaos and Prowse, 2009). The Stefan equation was used e.g. by Das et al. (2020) for obtaining Z_{ice} projections for the Athabasca River at Fort McMurray, Alberta, under future climate conditions.

For the lower Peace River, Beltaos and Bonsal (2021) obtained an empirical relationship between Z_{ice} and $AFDD$ that differed from the Stefan equation by having an $AFDD$ exponent of 0.59 (instead of 0.5). The empirical value of α was a non-linear function of total winter snowfall. Based on this equation, they used projected $AFDD$ and projected snowfall to obtain projected ice thickness, which indicated a reduction of about 0.2 meters between the 1980s and 2050s and by an additional 0.1 m by the 2080s under the RCP8.5 emissions scenario.

Ice growth in southern rivers of the pan-Arctic domain depends more strongly on air temperature, while in more northern rivers snowpack depth plays a more important role (Burrell

et al., 2023, citing the work of Park et al., 2016). In the southern Mackenzie River basin, air temperature is expected to dominate, hence ice is likely to become thinner, regardless of the uncertain future of snow accumulation. Beltaos (2007) showed a reduction by about 10 cm in the maximum ice thickness on the Peace River in the period 1962-2006 – a finding in line with separate studies at a few other North American locations and Russia. As ice thickness declines, the volume of ice available for forming a jam is smaller, reducing the flood risk it poses (Rokaya et al., 2022).

Ice Breakup

The initiation of ice breakup results when the driving force is greater than the resisting force of the ice. In a "dynamic breakup", the driving force is provided by the moving water under the ice cover, while the resistance force depends on the ice cover strength in the downstream direction. In a "thermal breakup", the driving force is a strong radiative balance, brought by increasing air temperature and sunlight in spring. Broken ice may get washed out of the reach and may form an ice jam farther downstream. The warming projected for spring does suggest that rain on snow might become a common occurrence in future, with runoff peaks occurring while the ice still maintains its thickness due to the relatively early date in the year.

Turcotte et al. (2019) provides conceptual graphic representations (reproduced in Figure 1.4) of the evolution of driving and resisting forces from fall to spring, for (a) a cold winter, (b) a less cold and shorter winter, and (c) a very mild winter. As the winter season warms and shortens, the number of ice-jam events may increase due to higher streamflows but cold enough temperatures for ice cover to regrow and regain strength (Figure 1.4b). As warming continues, multiple mid-winter runoff events may break the ice, while air temperatures are insufficiently cold to build a resistance ice cover – resulting in a single and minor ice-jam event in spring (Figure 1.4c). Mid-winter breakup events may occur more frequently as a result of higher peak flows in winter – see e.g. evidence from (Beltaos, 2002).

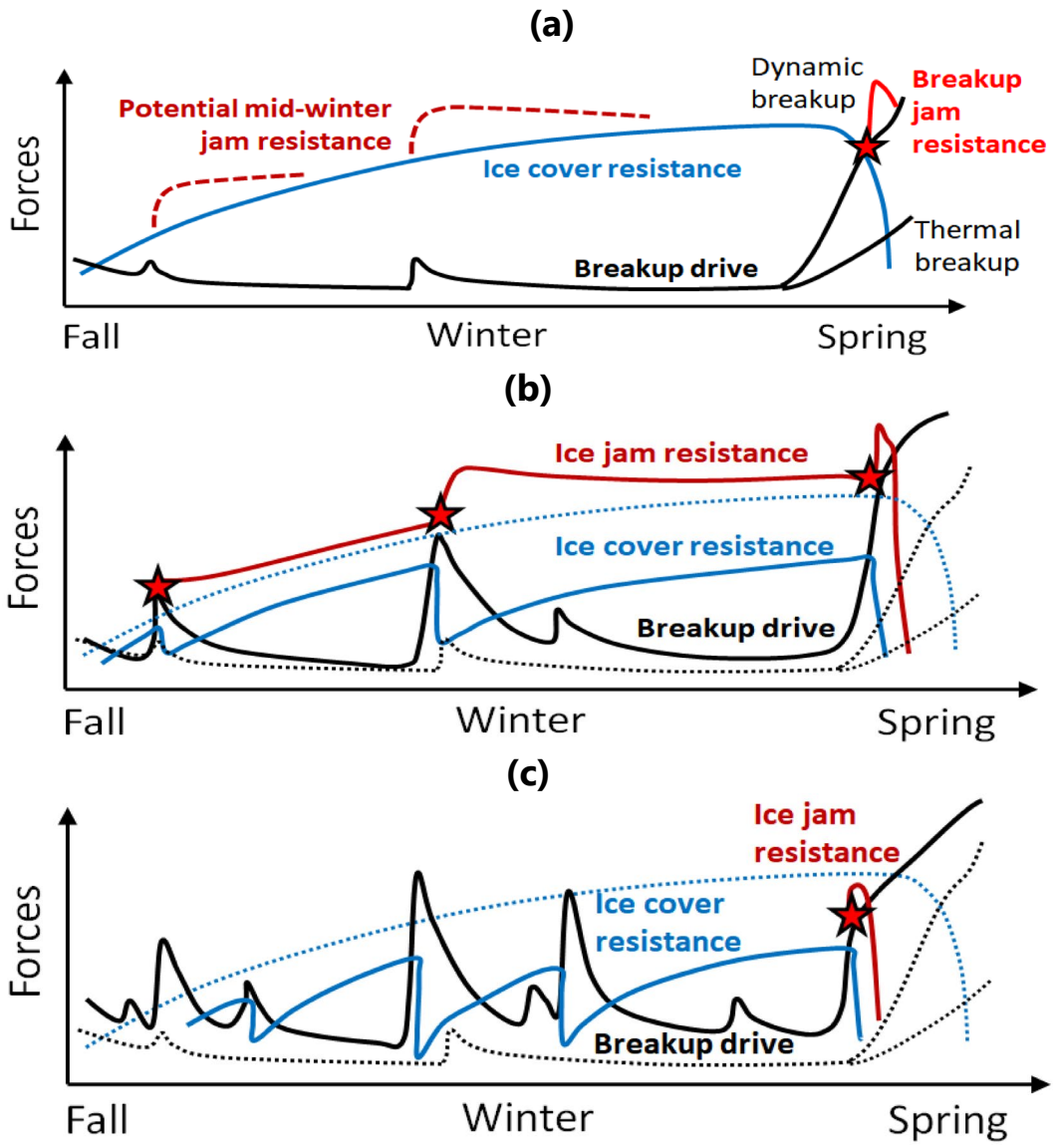

Figure 1.2 Conceptual graphs showing how resisting forces (blue for intact ice cover, red for ice jams) and driving forces (black lines) may evolve under climate warming. The figure panels are reproduced from Turcotte et al. (2019) and they show:

(a) A specific winter scenario characterized by minor mid-winter runoff events.

(b) A shorter winter characterized by major mid-winter runoff events and cold enough temperatures, followed by a dynamic spring breakup event. Three ice-jam events are represented by red stars. Compare to dotted lines from panel a.

(c) A very mild winter characterized by multiple mid-winter runoff events and air temperatures too mild to generate a resistant ice cover. Only one minor ice-jam event is represented by a red star. Compare to dotted lines from panel a.

Turcotte et al. (2019) recommends to use **streamflow** as the best single indicator of the driving forces. He admonishes against using **degree days of thaw (DDT)** as an indicator of high streamflow from spring snowmelt because DDT's strongest effect is through the weakening of the ice cover. In other words, DDT is best used as an indicator of (weakened) resisting forces, though it may also enhance the driving force.

Approaches to Determine Climate Change Impacts on Ice Jam Flooding

Turcotte et al. (2019) describes five different approaches:

1. Statistical analysis of historical water-level trends during the presence of ice
2. Climate-simulation outputs, hydrological models, and river-ice-jam models
3. Climate-simulation outputs and hydromorphologic-climatic transfer
4. Climate-simulation outputs and river ice-jam parameters
5. Climate-simulation outputs and conceptual river ice-jam models

Rather than repeat the descriptions here, we can refer directly to Turcotte et al. (2019).

Liard River Study by Connon et al. (2014)

The intense rate of warming experienced by this region has led to widespread permafrost thaw and the southern limit of discontinuous permafrost in the Mackenzie River valley has migrated progressively to the north, a process already underway 30 years ago (Kwong and Gan, 1994, cited by Connon et al., 2014).

The progressive thawing of permafrost increases infiltration capacity and amplifies the subsurface component of the hydrograph (e.g., St. Jacques and Sauchyn, 2009), which may augment minimum flows in winter. It also has implications for channel stability (addressed in section 1.2.3.4). However, permafrost thaw can also amplify surface runoff response and therefore peak flows, due to increased surface connectivity. This phenomenon was studied specifically for the Liard River basin by Connon et al. (2014). The following is excerpted from Connon et al. (2014):

"The loss of permafrost often leads to the complete conversion of forest ecosystems to wetlands (Quinton et al., 2011). Vitt et al. (1994) show that vegetation on undisturbed peat plateaus exerts a control on the supra-permafrost water table. The combination of canopy transpiration and an unsaturated organic layer keeps the water table at a sufficient depth to allow for the establishment of rooting zones. In areas experiencing permafrost degradation, lateral thawing of permafrost results in ground subsidence, bringing the water table closer to the ground surface (Jorgenson and Osterkamp, 2005). Permafrost significantly influences the partitioning of precipitation into infiltration and runoff and influences drainage patterns because the surface of the permafrost bodies rise above adjacent permafrost-free terrains, thereby impounding or redirecting water.

"In the lower Liard River valley, permafrost exists predominantly below treed peat plateaus, which are surrounded by adjacent wetlands (i.e. flat bogs and channel fens). Quinton et al. (2003) suggested that each of these three land-cover types has a unique function in the basin hydrological cycle: Peat plateaus act as runoff generators owing to their small storage capacity (Wright et al., 2009) and higher elevation relative to the adjacent wetlands, flat bogs are primarily storage features and channel fens convey water to the basin outlet. Given the contrasting hydrological functions of bogs, fens and plateaus, permafrost-thaw-induced changes to the landscape therefore have the potential to influence the hydrograph response of basins (Quinton et al., 2003).

"Image analysis of time-separated aerial photos and/or satellite images is commonly used to estimate the rate and pattern of permafrost loss using forest loss as a proxy method of estimating permafrost loss (Tutubalina and Rees, 2001; Beilman and Robinson, 2003; Chasmer et al., 2010). Quinton et al. (2011) analysed images from a 1 km^2 area of interest (AOI) spanning from 1947 to 2008 at Scotty Creek, NWT, situated in the lower Liard River valley. Over this period, they found that the area underlain by permafrost decreased from 70% to 43%. Permafrost-free areas were shown to be expanding and coalescing as permafrost thaw became more prevalent. The majority (72%) of the permafrost-free area lost since 1947 transformed from wooded peat plateaus to flat bogs, indicating the importance of understanding the influence of bogs on the basin hydrograph as permafrost thaw proceeds."

Connon et al. (2014) conclude as follows from their study, with text in bold added by NHC for emphasis:

"Stream flow has increased in the lower Liard River valley in the NWT as a result of climatic drivers. Although precipitation has increased in the region, this does not entirely explain the observed increases in stream flow. ***The current paradigm in the literature suggests that the opening of groundwater pathways resulting from permafrost thaw is a primary driver behind increasing stream flows. We show that in the lower Liard River valley, increasing groundwater inputs are a relatively small component. Here, we have outlined a number of alternative mechanisms, induced by land-cover change via long-term permafrost thaw, which may better explain the magnitude of these increases****. These land-cover changes have the potential to fundamentally alter the hydrology of a basin as the relationship between bogs and peat plateaus changes with ongoing permafrost thaw. Bogs that were formerly isolated are now becoming incorporated into the basin drainage network. This is shown by a strong correlation between increased stream flow and the per cent cover of bogs in a basin, indicating potential areas of vulnerability. As permafrost thaws, surficial pathways for water become more direct as runoff-generating land-cover types coalesce. Increases to the size of the basin drainage network allow for more channel precipitation and increased runoff from adjacent plateaus. We have shown that surface pathways have opened up at a rate disproportionate to permafrost thaw and can therefore be viewed as a nonlinear response to warming. Further work is necessary (…)."*

Fort Simpson Study by Turcotte (2021)

Turcotte (2021) the water stage records of a few rivers of northwest Canada, including the Mackenzie River at Fort Simpson. (Above, the results for Hay River were presented.) Figure 1.10 plots stage against estimated discharge. The highest stage peaks are break-up peaks (red squares). Turcotte (2021) conveys the difficulty in estimating discharge during ice breakup, especially in the presence of ice jams, and which may explain the poor x-y correlation seen for the red squares plotted in the figure.

Figure 1.11 shows these data plotted chronologically. The variability and auto-correlation clearly exhibited by the data, and the relatively short duration of this record, give insufficient confidence to the trend estimates represented by the dashed lines.

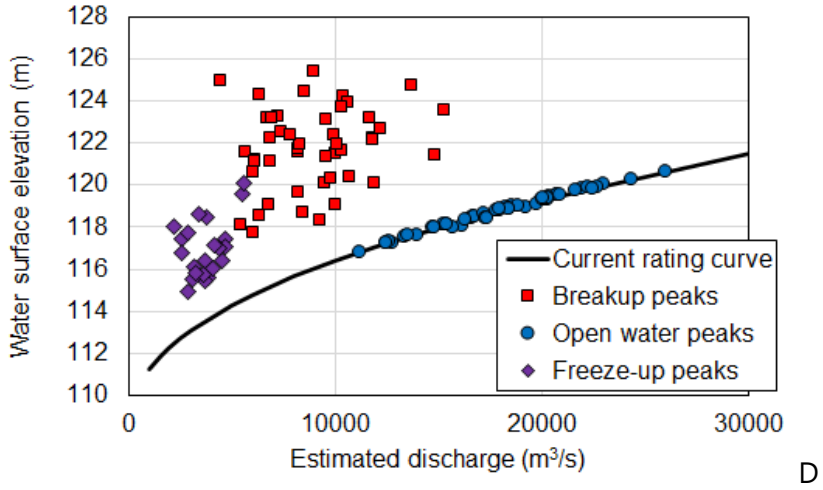

D

Figure 1.3 Approximate current rating curve, maximum breakup water levels, maximum open water levels and maximum freeze-up water levels between 1972 and 2021 (starting in 1996 for freeze-up) expressed as a function of the estimated discharge at station 10GC001 on the Mackenzie River at Fort Simpson, Northwest Territories. This figure and legend are reproduced from Turcotte (2021).

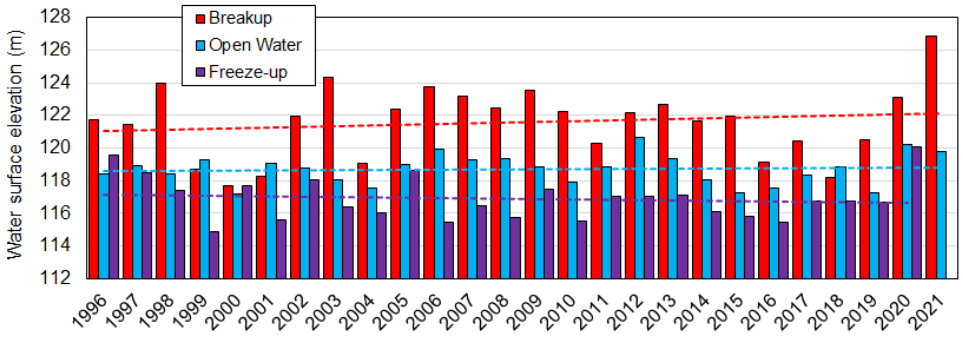

Figure 1.4 Historical annual maximum water levels at breakup, during the open water season, and at freeze-up between 1996 and 2021 at station 10GC001 on the Mackenzie River at Fort Simpson, Northwest Territories. This figure and legend are reproduced from Turcotte (2021).